European Journal of Medicinal Chemistry 297 (2025) 117936

Contents lists available at ScienceDirect

European Journal of Medicinal Chemistry

journal homepage: www.elsevier.com/locate/ejmech

Research paper

Targeting voltage-gated proton channel H_V1: Optimised 5-phenyl-2-aminoimidazoles with anticancer potential

Martina Piga [a], Geraldo Jorge Domingos [b], Adam Feher [b], Ferenc Papp [b], Kavya C. Bangera [b], Zoltan Varga [b], Florina Zakany [b], Tamas Kovacs [b], Jaka Dernovšek [a], Tihomir Tomašič [a], Nace Zidar [a,*]

[a] Faculty of Pharmacy, University of Ljubljana, Aškerčeva cesta 7, Ljubljana, 1000, Slovenia
[b] Faculty of Medicine, Department of Biophysics and Cell Biology, University of Debrecen, Egyetem tér 1, Debrecen, H-4032, Hungary

ARTICLE INFO

Keywords:
Anticancer
H_V1
Inhibitor
5-phenyl-2-aminoimidazole
Voltage-gated proton channel

ABSTRACT

The voltage-gated proton channel (H_V1) has been linked to the development of tumours, neuroinflammatory diseases, immune disorders and infertility, making H_V1 inhibitors promising candidates for therapeutic development. In this study, we designed and synthesized an optimised series of 5-phenyl-2-aminoimidazole-based H_V1 inhibitors, with the most potent compounds exhibiting low micromolar IC_{50} values. Structural analysis highlighted the importance of an unsubstituted 2-aminoimidazole core and flexible linkers for optimal ligand-channel binding, driven by hydrogen bonding and hydrophobic interactions. Antiproliferative assays showed that the most potent H_V1 inhibitors had IC_{50} values in the low micromolar range, with greater efficacy against THP-1 cells (human monocytic leukaemia), which express H_V1 at high levels, compared to MCF-7 cells (human breast cancer) with lower H_V1 expression. The type II compounds exhibited superior drug-like properties, including improved solubility, plasma protein binding and permeability compared to previous 5-phenyl-2-aminoimidazole-based H_V1 inhibitors, as well as robust metabolic stability. However, selectivity over the $K_V1.3$ and $Na_V1.5$ channels remained limited. This work advances the development of H_V1 inhibitors. It provides valuable chemical tools to study the role of H_V1 in disease pathogenesis and lays the foundation for new therapeutic strategies targeting H_V1-mediated signalling pathways.

1. Introduction

Voltage-gated proton channel 1 (H_V1) is a proton-selective transmembrane protein expressed in various cell types, including immune cells, skeletal muscle, blood cells, spermatozoa, oocytes and osteoclasts [1–4]. H_V1 regulates intracellular pH by facilitating H^+ efflux along an electrochemical gradient [4], a process that is critical for immune responses, cell proliferation, motility and sperm capacitation [5]. It also supports the production of reactive oxygen species (ROS) by NADPH oxidase (NOX) through charge balancing and proton removal [6–9].

Structurally, H_V1 consists of a voltage-sensing domain (VSD) with four transmembrane segments (S1–S4) that lack the pore-forming S5–S6 domains typical of other voltage-gated ion channels [3,4]. In most species, it functions as a homodimer, with each subunit having an independent voltage sensor, pH sensor and proton permeation pathway. The voltage sensitivity results from the arginine residues of the S4 segment (Arg205, Arg208, Arg211), which shift outward upon depolarisation, enabling proton conduction [10–13].

Aberrant expression of H_V1 has been associated with neuroinflammatory diseases, immune disorders and infertility [1,2,14,15], while increased levels of the channel have been reported in colorectal tumours, glioblastoma, leukaemia and breast cancer [16–20]. Overexpression of H_V1 disrupts pH homeostasis and is closely associated with cancer progression, making it a marker of malignancy [4,18,21,22]. Under physiological conditions and at resting membrane potential, H_V1 remains closed but metabolic dysfunction under pathological conditions activates it and promotes an acidic microenvironment that facilitates tumour survival and suppresses immune function [22–25].

Given its role in pH regulation and its involvement in various diseases, H_V1 is an attractive target for drug development [2,26,27]. However, the development of selective inhibitors is hampered by the limited mechanistic understanding of its activation and proton

* Corresponding author.
E-mail address: nace.zidar@ffa.uni-lj.si (N. Zidar).

https://doi.org/10.1016/j.ejmech.2025.117936
Received 17 April 2025; Received in revised form 1 July 2025; Accepted 3 July 2025
Available online 7 July 2025

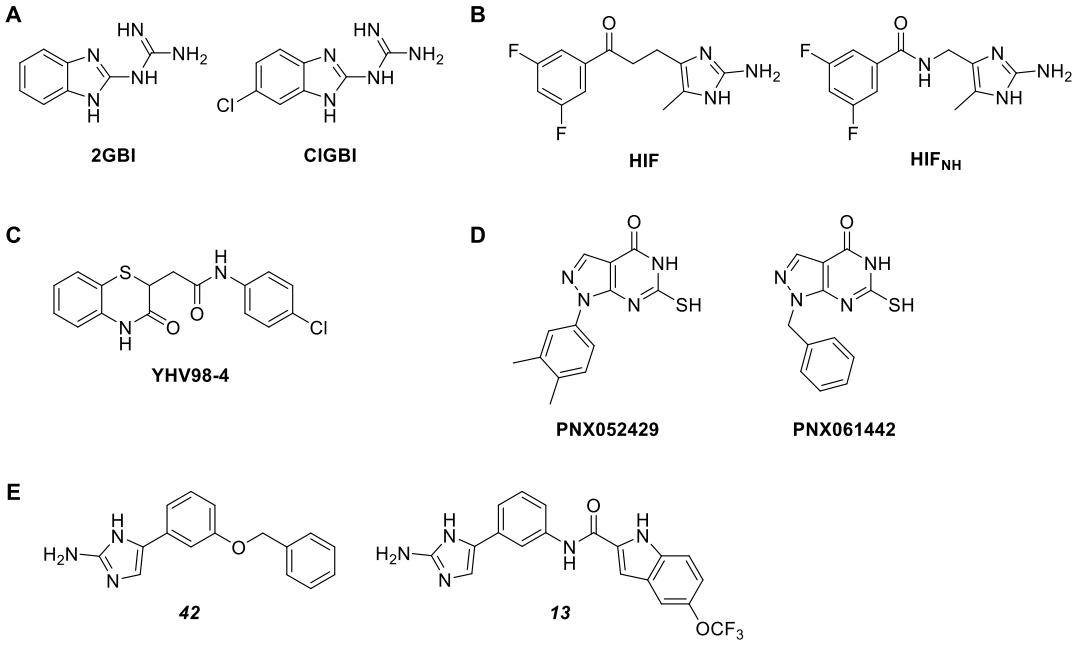

Fig. 1. Structures of the known H_V1 inhibitors. A) Guanidine derivatives 2-guanidinobenzimidazole (2GBI) and 5-chloro-2-guanidinobenzimidazole (ClGBI) [30,31]. B) "H_V1 inhibitor flexible" compounds (HIFs) [32,33]. C) YHV98-4 [2]. D) PNX52429 and PNX61442 [27]; (E) 5-phenyl-2-aminoimidazoles ***13*** and ***42*** [26].

permeation [2,26,27]. Early inhibitors, such as zinc ions, bind to extracellular histidine residues and act as proton competitors that stabilize the resting state at micromolar concentrations [27–29]. However, the involvement of Zn^{2+} in numerous physiological processes limits its utility as a selective H_V1 inhibitor [1]. Guanidine derivatives, such as 2-guanidinobenzimidazole (2GBI) and 5-chloro-2-guanidinobenzimidazole (ClGBI) (Fig. 1), act as reversible open-state inhibitors targeting the intracellular side of the voltage-sensing domain (VSD) [30,31]. Based on these scaffolds, the "H_V1-Inhibitor-Flexible" (HIF) compounds were subsequently developed [32,33] (Fig. 1). However, these inhibitors lack specificity for proton channels and may also interact with other voltage-gated ion channels. In addition, they often exhibit poor membrane permeability. [34,35]. Recently, novel inhibitors such as the small molecule YHV98-4, identified by structure-based design, have shown promising results in alleviating chronic pain and inflammation at micromolar concentrations [2] (Fig. 1). In addition, high-throughput screening has led to the discovery of PNX52429 and PNX61442, which represent valuable scaffolds for the further development of new, more selective H_V1 inhibitors [27] (Fig. 1). In a recent study, we identified 5-phenyl-2-aminoimidazoles as a new structural class of H_V1 based on a virtual screening (VS) performed on an open-conformation model of human H_V1 at the 2GBI binding site [26] (Fig. 1). These compounds inhibit proton currents at low micromolar concentrations and show antiproliferative effects in MDA-MB-231 (breast cancer) and THP-1 (monocytic leukaemia) cell lines.

Building on this foundation, we aimed to optimise the 5-phenyl-2-aminoimidazole scaffold to improve H_V1 inhibition and antiproliferative activity. In addition, we systematically investigated their key physicochemical and pharmacological properties such as solubility, plasma protein binding, partition coefficient, metabolic stability and permeability as well as their selectivity towards the $K_V1.3$ and $Na_V1.5$ channels and compared them with previous inhibitors.

2. Results and discussion

2.1. Design

Based on our previous research on this structural class, we have designed a new series of 5-phenyl-2-aminoimidazole-based H_V1 channel inhibitors [26] (Fig. 2). Compounds ***13*** (H_V1 $IC_{50} = 8.5$ μM) and ***42*** (H_V1 $IC_{50} = 12.0$ μM, Fig. 2) were selected as lead structures for optimisation due to their promising inhibitory and antiproliferative activities. In particular, ***13*** showed strong growth inhibition in the MDA-MB-231 and THP-1 cell lines (IC_{50} = 9.0 μM and 8.1 μM, respectively), while ***42*** showed moderate activity (IC_{50} = 29 μM and 32 μM, respectively) but exhibited better drug-like properties due to the incorporation of a flexible oxomethylene linker. Guided by docking studies that emphasised the importance of the 5-phenyl-2-aminoimidazole core in H_V1 binding [26], we retained this pharmacophoric scaffold while systematically modifying the peripheral regions to improve potency and physicochemical properties.

Two types of inhibitors were prepared, differing mainly in the groups attached to the right-hand side of the molecules (Fig. 2). In the type I compounds, various aromatic heterocycles (e.g. substituted pyrrole, imidazole, pyridine or oxazole; R^2) are linked to the central benzene ring via an amide bond. In addition, some of the type I compounds contain pyridinyl, oxazole or *tert*-butoxycarbonyl (Boc) groups on the imidazole N-1 (R^1). Most type II compounds contain substituted benzyloxy groups in the *meta*- or *para*-position of the central phenyl ring. In some type II compounds, the central oxomethylene linker has been extended by one carbon atom to obtain the phenethyloxy derivatives (n = 2, Fig. 2). Various substituents such as fluorine, chlorine, trifluoromethyl, methyl

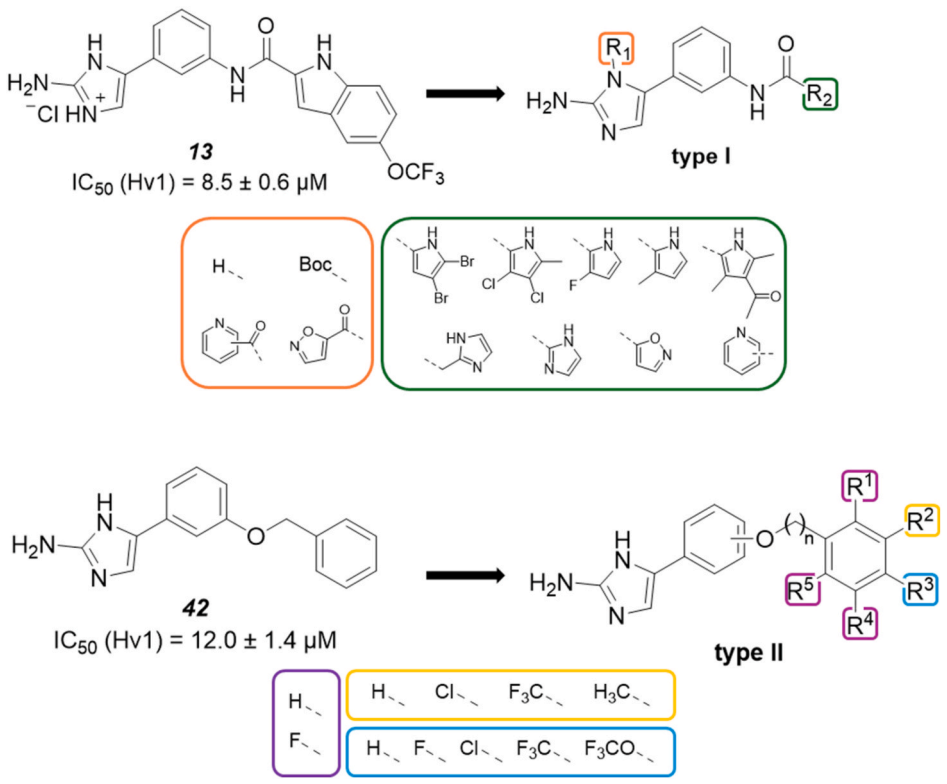

Fig. 2. Design of two types of 5-phenyl-2-aminoimidazoles as inhibitors of human voltage-gated proton channels H_V1 based on previously published inhibitors ***13*** and ***42*** [26].

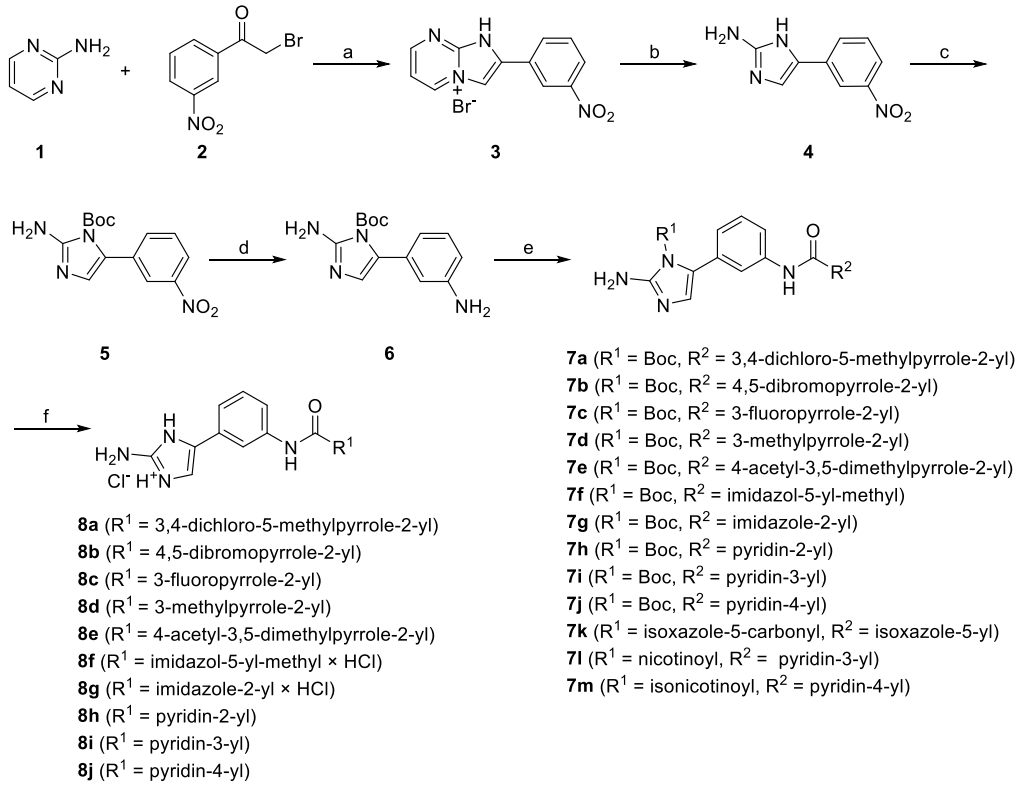

Scheme 1. Reagents and experimental conditions for the synthesis of type I compounds: (a) DMAP, acetonitrile (CH_3CN), 85 °C, 5 h; (b) hydrazine hydrate, abs. EtOH, microwave irradiation: 120 °C, 40 min; (c) Boc_2O, 2:1 MeOH/H_2O, room temperature (rt), 15 h; (d) H_2/Pd–C, 4:1 anhydrous tetrahydrofuran (THF)/ anhydrous MeOH, rt, 4 h; (e) carboxylic acid, TBTU, *N*-methylmorpholine, anhydrous dichloromethane (DCM), 40 °C, 15 h (for the synthesis of **7a-d** and **7k**) or carboxylic acid, HATU, *N*,*N*-diisopropylethylamine, DMAP, anhydrous *N*,*N*-dimethylformamide (DMF), 50 °C, 15 h (for the synthesis of **7e-j**, **7l-m**); (f) 4 M HCl in 1,4-dioxane, 1,4-dioxane, rt, 3 d (for the synthesis of **8a-d**) or trifluoroacetic acid (TFA), anhydrous DCM, rt, 2d (for the synthesis of **8e-j**).

or trifluoromethoxy were attached to the benzyloxy or phenethyloxy aromatic rings in order to modulate both the inhibitory activity and the physicochemical parameters of the inhibitors.

These structural variations were designed to elucidate the structure-activity relationship (SAR) within this series while addressing key limitations of the previous analogues. The focus was on optimising the biological activity of the compounds and improving their physicochemical properties by introducing different functionalities and steric/electronic tuning of substituents.

2.2. Chemistry

The synthesis of type I compounds (**7a-m**, **8a-j**) is shown in Scheme 1. In the first step, condensation of 2-aminopyrimidine (**1**) and 2-bromo-3-nitroacetophenone (**2**) in the presence of 4-dimethylaminopyridine (DMAP) gave the 1*H*-imidazo[1,2-*a*]pyrimidin-4-ium salt **3**. Hydrazinolysis of **3** in ethanol under microwave irradiation (120 °C, 40 min) afforded the 2-aminoimidazole **4** [36]. Subsequent Boc protection of the imidazole N-1 nitrogen of **4** with Boc anhydride in a methanol/water mixture gave the intermediate **5**. Catalytic hydrogenation of **5** with Pd/C under a hydrogen atmosphere reduced the nitro group to an amine and gave **6**. The amine **6** was coupled with various carboxylic acids (e.g. substituted pyrrole-2-carboxylic acids, imidazole-2-carboxylic acid or pyridine carboxylic acids) using 1-[bis(dimethylamino)methylene]-1*H*-benzotriazolium 3-oxide tetrafluoroborate (TBTU) or 1-[bis(dimethylamino)methylene]-1*H*-1,2,3-triazolo[4,5-*b*]pyridinium 3-oxide hexafluorophosphate (HATU) reagent to obtain the amides **7a-j**. Interestingly, couplings with isoxazole-5-carboxylic acid, nicotinic acid or isonicotinic acid simultaneously led to Boc cleavage and acylation of the 2-aminoimidazole N-1 nitrogen, resulting in **7k-m** (Scheme 1). The final Boc cleavage of **7a-j** with 4 M hydrochloric acid (HCl) in 1, 4-dioxane or trifluoroacetic acid in dichloromethane gave the target compounds **8a-j**.

The synthesis of type II compounds **14a-t** began with the alkylation of 3- or 4-hydroxyacetophenone (**10a/b**) with substituted benzyl or phenethyl bromides (**9a-t**) in the presence of potassium carbonate in acetonitrile (70 °C, 15 h), which gave the intermediates **11a-t** (Scheme 2). Bromination of **11a-t** with bromine (Br_2) in a mixture of dichloromethane and methanol (0 °C to rt) gave the α-bromoacetophenones **12a-t**. Cyclocondensation of **12a-t** with 2-aminopyrimidine and DMAP in acetonitrile under reflux (85 °C, 15 h) formed 1*H*-imidazo[1,2-*a*]pyrimidin-4-ium salts **13a-t**, which were finally hydrazinolysed to **14a-t** under microwave irradiation (120 °C, 80 min).

2.3. Biological evaluation

2.3.1. Inhibition of H_V1 channels

The inhibitory effects of the synthesized compounds on H_V1 channels were investigated using manual patch-clamp electrophysiology in Chinese hamster ovary (CHO) cells transiently expressing human H_V1. Ionic currents were recorded using the standard whole-cell patch-clamp method [37]. As certain inhibitors may shift the opening threshold of

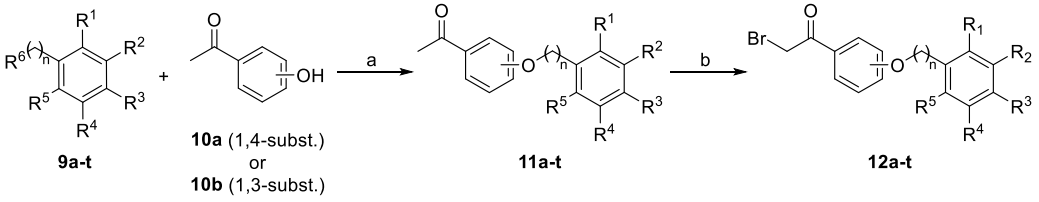

9a (R^1, R^2, R^3, R^4, R^5 = H, R^6 = Br, n = 1)
9b (R^1, R^2, R^4, R^5 = H, R^3 = CF_3, R^6 = Br, n = 1)
9c (R^1, R^3, R^4, R^5 = H, R^2 = CF_3, R^6 = Cl, n = 1)
9d (R^1, R^2, R^4, R^5 = H, R^3 = OCF_3, R^6 = Br, n = 1)
9e (R^1, R^2, R^4, R^5 = H, R^3 = Cl, R^6 = Cl, n = 1)
9f (R^1, R^3, R^4, R^5 = H, R^2 = Cl, R^6 = Br, n = 1)
9g (R^1, R^5 = F, R^2, R^3, R^4 = H, R^6 = Br, n = 1)
9h (R^1, R^3, R^4 = F, R^2, R^5 = H, R^6 = Br, n = 1)
9i (R^1, R^2, R^4, R^5 = H, R^3 = F, R^6 = Br, n = 1)
9j (R^1, R^2, R^4, R^5 = H, R^3 = CF_3, R^6 = Br, n = 1)
9k (R^1, R^3, R^4, R^5 = H, R^2 = CF_3, R^6 = Cl, n = 1)
9l (R^1, R^2, R^4, R^5 = H, R^3 = OCF_3, R^6 = Br, n = 1)
9m (R^1, R^3, R^4, R^5 = H, R^2 = Cl, R^6 = Br, n = 1)
9n (R^1, R^3, R^4, R^5 = H, R^2 = CH_3, R^6 = Br, n = 1)
9o (R^1, R^5 = F, R^2, R^3, R^4 = H, R^6 = Br, n = 1)
9p (R^1, R^3, R^4 = F, R^2, R^5 = H, R^6 = Br, n = 1)
9q (R^1, R^4, R^5 = H, R^2 = CF_3, R^3 = Cl, R^6 = Br, n = 1)
9r (R^1, R^2, R^3, R^4, R^5 = H, R^6 = Br, n = 2)
9s (R^1, R^2, R^3, R^4, R^5 = H, R^6 = Br, n = 2)
9t (R^1, R^2, R^3, R^5 = H, R^4 = F, R^6 = Br, n = 2)

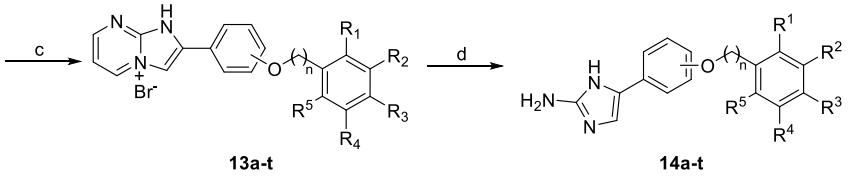

11-14a (R^1, R^2, R^3, R^4, R^5 = H, n = 1, 1,4-subst.)
11-14b (R^1, R^2, R^4, R^5 = H, R^3 = CF_3, n = 1, 1,4-subst.)
11-14c (R^1, R^3, R^4, R^5 = H, R^2 = CF_3, n = 1, 1,4-subst.)
11-14d (R^1, R^2, R^4, R^5 = H, R^3 = OCF_3, n = 1, 1,4-subst.)
11-14e (R^1, R^2, R^4, R^5 = H, R^3 = Cl, n = 1, 1,4-subst.)
11-14f (R^1, R^3, R^4, R^5 = H, R^2 = Cl, n = 1, 1,4-subst.)
11-14g (R^1, R^5 = F, R^2, R^3, R^4 = H, n = 1, 1,4-subst.)
11-14h (R^1, R^3, R^4 = F, R^2, R^5 = H, n = 1, 1,4-subst.)
11-14i (R^1, R^2, R^4, R^5 = H, R^3 = F, n = 1, 1,3-subst.)
11-14j (R^1, R^2, R^4, R^5 = H, R^3 = CF_3, n = 1, 1,3-subst.)
11-14k (R^1, R^3, R^4, R^5 = H, R^2 = CF_3, n = 1, 1,3-subst.)
11-14l (R^1, R^2, R^4, R^5 = H, R^3 = OCF_3, n = 1, 1,3-subst.)
11-14m (R^1, R^3, R^4, R^5 = H, R^2 = Cl, n = 1, 1,3-subst.)
11-14n (R^1, R^3, R^4, R^5 = H, R^2 = CH_3, n = 1, 1,3-subst.)
11-14o (R^1, R^5 = F, R^2, R^3, R^4 = H, n = 1, 1,3-subst.)
11-14p (R^1, R^3, R^4 = F, R^2, R^5 = H, n = 1, 1,3-subst.)
11-14q (R^1, R^4, R^5 = H, R^2 = CF_3, R^3 = Cl, n = 1, 1,3-subst.)
11-14r (R^1, R^2, R^3, R^4, R^5 = H, n = 2, 1,4-subst.)
11-14s (R^1, R^2, R^3, R^4, R^5 = H, n = 2, 1,3-subst.)
11-14t (R^1, R^2, R^3, R^5 = H, R^4 = F, n = 2, 1,3-subst.)

Scheme 2. Reagents and experimental conditions for the synthesis of type II compounds: (a) K_2CO_3, CH_3CN, 70 °C, 15 h; (b) Br_2, anhydrous DCM/anhydrous MeOH, 0 °C → rt, 3 h; (c) 2-aminopyrimidine, DMAP, CH_3CN, 85 °C, 15 h; (d) hydrazine hydrate, abs. EtOH, microwave irradiation: 120 °C, 80 min.

Table 1
Inhibitory activities of type I 5-phenyl-2-aminoimidazoles on human voltage-gated proton channels H_V1.

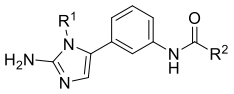

Comp.	R^1	R^2	RCF [%][a]
7f			0.83 ± 0.07
7k			1.07 ± 0.03
7l			0.99 ± 0.04
7m			0.95 ± 0.02
8a		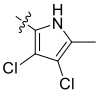	0.66 ± 0.07
8b		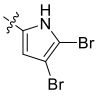	0.39 ± 0.06
8c			1.03 ± 0.25
8d			1.36 ± 0.04
8e		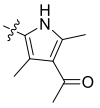	0.95 ± 0.14
8f			1.03 ± 0.03
8g			0.92 ± 0.02
8h			0.68 ± 0.07
8i			0.98 ± 0.07
8j			0.95 ± 0.11

[a] Remaining H_V1 current fraction (RCF) measured at +60 mV in the presence of 50 μM of the compounds. ClGBI was used as a positive control. IC_{50} value for ClGBI was determined to be 15.9 ± 2.0 μM. All measurements were performed in at least three independent experiments.

voltage-gated channels, in most cases we applied voltage ramps from −60 to +60 mV, as this protocol allows both the measurement of the peak current at +60 mV and assessment of the activation threshold voltage of the channels. Inhibition was quantified by calculating the remaining current fraction (RCF) measured at +60 mV in the presence of 50 μM of the compounds. The RCF (=I/I_0) was defined as the ratio of the peak current at equilibrium inhibition (at 50 μM compound concentration, I_0) to the peak current measured in the absence of the compound (I). Compounds exhibiting an RCF ≤0.30 were subjected to dose-response experiments to determine their half-maximal inhibitory concentrations (IC_{50}).

As summarised in Table 1, the type I 5-phenyl-2-aminoimidazole derivatives did not exceed the inhibitory activity of the reference compound ***13*** (RCF = 0.19 at 50 μM [26]). The most active type I analogues, **8a** (5-methyl-3,4-dichloropyrrol-2-yl substituent at R^2; RCF = 0.66), **8b** (4,5-dibromopyrrol-2-yl substituent at R^2; RCF = 0.39) and **8h** (pyridin-2-yl substituent at R^2; RCF = 0.68), showed modest but reduced activity compared to ***13***. According to the predicted binding modes, the type I analogues were found to have a similar orientation to 2GBI and form interactions with many of the residues involved in the binding of 2GBI and its analogues [38], as shown for compound **8b** (Fig. 3). Nevertheless, their lower activity suggests that the indole moiety in ***13***, which contains an additional phenyl ring compared to the pyrrole (**8a-b**) and pyridine (**8h**) derivatives, may be involved in hydrophobic or π-stacking interactions within the H_V1 binding pocket. This highlights the potential role of extended aromatic systems in stabilising ligand-channel interactions.

The R^1-substituted derivatives (**7f**, **7k-m**) and the R^2-modified analogues bearing oxazole, imidazole or pyridine groups (**7k-m**, **8f-j**) exhibited negligible inhibition of H_V1 channels (RCF >0.90). The most important structural element for H_V1 inhibition was predicted to be the 2-aminoimidazole ring, which forms ionic interactions and hydrogen bonds with the Asp112 and Asp185 side chains. It also formed a π-stacking with the Phe150 side chain and a cation-π-stacking with Arg211 (Fig. 3). In the R^1-substituted derivatives, these critical hydrogen bonds are disrupted, weakening the ligand binding. These results emphasise the importance of retaining hydrogen bond donor functionalities at key positions to preserve interactions with residues important for proton conduction of H_V1.

As summarised in Table 2, type II 5-phenyl-2-aminoimidazoles bearing benzyloxy or phenethyloxy substituents at the *meta*- or *para*-positions of the central phenyl ring exhibit significantly more potent H_V1 inhibitory activity compared to type I analogues. The most potent molecules cause nearly complete inhibition, reducing proton current by up to approximately 90 % at 50 μM (Fig. 4). Structural analysis suggests that the increased conformational flexibility mediated by oxomethylene or oxoethylene linkers enhances ligand-channel binding, while terminal aromatic moieties stabilize interactions via hydrophobic contacts and aromatic π-stacking. These differences were also observed in the docking studies. For example, the 4,5-dibromopyrrole moiety of **8b** was predicted to have the same orientation as 2GBI [26], forming cation-π-stacking with Lys157 and hydrogen bonding with Arg223. In contrast, the hydrophobic groups of the type II compounds were oriented in the opposite direction and formed mainly hydrophobic interactions in the binding site, as shown for compound **14c** (Fig. 5).

Among the type II derivatives, benzyloxy-substituted compounds (**14a-q**) generally showed slightly higher potency than their phenethyloxy counterparts (**14r-t**), as evidenced by the comparison of compound ***42*** (RCF = 0.25) and compound **14a** (RCF = 0.20) with their phenethyloxy analogues, **14s** (RCF = 0.34) and **14r** (RCF = 0.50), respectively. These results suggest that shorter alkyl spacers favour optimal pharmacophore positioning. Substituents attached to the benzyloxy/phenethyloxy groups – including fluoro, chloro, trifluoromethyl, methyl or trifluoromethoxy substituents – had only marginal effects on inhibitory activity, suggesting limited structure-activity relationships (SARs) within these peripheral regions. However, this moiety has been shown to

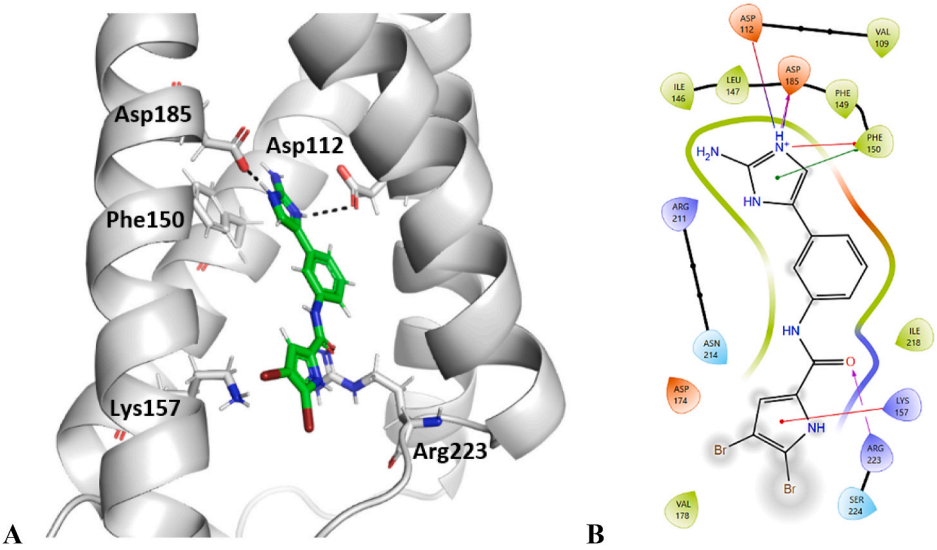

Fig. 3. Binding mode of **8b** in the proposed binding pocket in the H_V1 VSD, predicted by docking with Glide. A) The ligand (in green) and the neighbouring protein side chains are shown as stick models, coloured according to the chemical atom type. For clarity, only key amino acids are shown. H-bonds are indicated by black dotted lines. B) In the schematic representations of protein-ligand interactions, hydrogen bonds are shown as arrows (in magenta), cation-π-stacking as a red line, π-π interaction as a green line, ionic interactions as red-blue lines and hydrophobic contacts as grey spheres. (For interpretation of the references to colour in this figure legend, the reader is referred to the Web version of this article.)

tolerate a wide range of substitutions, including single atoms or small lipophilic groups, as well as modifications at multiple positions. Notably, the *para*-substituted derivatives (**14a-h**) exhibited slightly improved potency over the meta-isomers (**14i-q**), likely due to improved complementarity with the hydrophobic subpocket of the H_V1 channel. The dose-response curves for the three representative H_V1 inhibitors from the type II series are shown in Fig. 6.

Several H_V1 inhibitors are described here that are structurally related but may differ, for example, in their lipophilicity or binding orientation. As a result, they may exhibit different characteristics of inhibition. Indeed, when investigating selected inhibitors, we observed some variability in inhibitory potency, rate and reversibility of inhibition (Fig. 7).

To confirm that the observed effects on H_V1 activity were due specifically to compound-mediated inhibition and not to unintended changes in pH across the cell membrane, we performed experiments to determine the reversal potential in the absence and presence of the compound. We selected one of the most potent compounds, **14c**, at a concentration of 5 μM, which produces strong inhibition (>50 %) while preserving sufficient residual current for accurate determination of E_{rev}. For current activation, we used both 1000-ms ramps, which were used for the inhibition experiments presented in the manuscript, and 1000-ms steps before stepping to tail voltages (Fig. 8). The step protocol allows for greater overall charge movement and is more susceptible to depletion artefacts. However, the two protocols produced identical results and we found no significant difference in reversal potentials. Control: $E_{rev} = -49.4 \pm 1.8$ mV, blocked: -51.9 ± 3.6 mV, ($n = 5$, paired *t*-test, $p = 0.368$). Prior to the measurements, we also tested the pH of the extracellular solution before and after the addition of 50 μM of the compounds (the highest concentration used in the study). We tested five active (**14c**, **14e**, **14h**, **14k** and **14q**) and two inactive (**7m** and **8f**) compounds on H_V1 and found no change in the pH of the extracellular solution (paired *t*-test: control: 7.414 ± 0.0001, drug: 7.420 ± 0.0002, $p = 0.321$).

We performed experiments with different voltage protocols with one of the most potent compounds, **14c**, to investigate its binding properties. We recorded I–V protocols with voltage steps from −60 to +100 mV in 10 mV increments and constructed G-V curves both under control conditions and in the presence of 2 μM of **14c** (RCF = 0.46 ± 0.09, $n = 5$, Fig. 9). The two curves completely overlapped, indicating that there was no shift in the voltage dependence of the conductance: control: $V_{1/2} = 13.1$ mV, $k = 14.5$ mV, **14c**: $V_{1/2} = 14.1$ mV, $k = 14.3$ mV.

We also tested intracellular application of **14c** using excised inside-out patches (Fig. S1, Supplementary Information), which resulted in inhibition with similar kinetics and magnitude to extracellular application. This suggests that its binding site may be accessible from the intracellular side or via the membrane.

2.3.2. Antiproliferative activity

To assess the antiproliferative activity of our compounds, we selected twelve H_V1 inhibitors based on their activity on H_V1 channels (**8b**, **14a**, **14c**, **14e**, **14g**, **14h**, **14i**, **14k**, **14l**, **14m**, **14s** and **14t**) and evaluated their effect using the MTS assay in two cancer cell lines: MCF-7 (human breast cancer) and THP-1 (human monocytic leukaemia). Statistical comparisons of the effects of the compounds at each concentration (0.2–50 μM) are shown in Fig. 10 (for **14c**, **14e**, **14h** an **14l**) and Fig. S2 (Supplementary Information, for **8b**, **14a**, **14g**, **14i**, **14k**, **14m**, **14s** and **14t**).

THP-1 cells are known to overexpress H_V1, a property associated with invasion, metastasis and sustained ROS production, as well as a role in phagosomal acidification and pH oscillations [39–42]. In contrast, H_V1 expression is significantly lower in MCF-7 cells, which have a weak metastatic potential [21]. Consistent with this expression pattern, statistical analysis revealed that our compounds exerted a significantly stronger antiproliferative effect on THP-1 cells than on MCF-7 cells at most concentrations tested, suggesting a correlation between their antiproliferative activity and H_V1 inhibition. Of the compounds tested, the benzyloxy analogues **14c**, **14e**, **14h** and **14l** showed the strongest antiproliferative activity. Notably, these same compounds exhibited the strongest H_V1 inhibition, further supporting the link between H_V1 inhibition and reduced proliferation of cancer cells.

2.3.3. Physicochemical profiling

We analysed the main physicochemical properties – including thermodynamic solubility, plasma protein binding (unbound fraction) and distribution coefficients (LogD at pH 7.4) – for seven selected H_V1 inhibitors (**8b**, **14c**, **14h**, **14l**, **14m**, **14s**, **14t**) and compared them with the starting compounds ***13*** and ***42*** [26] (Table 3). The selection of the seven compounds was based on their activity on H_V1 channels and the desire

Table 2
Inhibitory activities of type II 5-phenyl-2-aminoimidazoles on human voltage-gated proton channels H_V1.

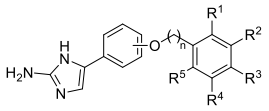

Comp.	R^1	R^2	R^3	R^4	R^5	n	Subst.	RCF [%] [a]	IC_{50} [μM] [b]
14a	H	H	H	H	H	1	1,4	0.20 ± 0.01	14.0 ± 17.0
14b	H	H	CF_3	H	H	1	1,4	0.27 ± 0.03	16.0 ± 3.0
14c	H	CF_3	H	H	H	1	1,4	0.19 ± 0.04[c]	2.14 ± 2.0
14d	H	H	OCF_3	H	H	1	1,4	0.39 ± 0.07	n.d.[d]
14e	H	H	Cl	H	H	1	1,4	0.13 ± 0.03	2.15 ± 1.1
14f	H	Cl	H	H	H	1	1,4	0.31 ± 0.04[c]	9.0 ± 6.0
14g	F	H	H	H	F	1	1,4	0.21 ± 0.03	15.0 ± 3.0
14h	F	H	F	F	H	1	1,4	0.13 ± 0.02[c]	1.6 ± 0.6
14i	H	H	F	H	H	1	1,3	0.19 ± 0.01	19.0 ± 4.5
14j	H	H	CF_3	H	H	1	1,3	0.41 ± 0.07[c]	n.d.
14k	H	CF_3	H	H	H	1	1,3	0.15 ± 0.03	7.7 ± 0.8
14l	H	H	OCF_3	H	H	1	1,3	0.25 ± 0.04[c]	2.45 ± 0.8
14m	H	Cl	H	H	H	1	1,3	0.25 ± 0.04	13.9 ± 4.3
14n	H	CH_3	H	H	H	1	1,3	0.52 ± 0.04[c]	n.d.
14o	F	H	H	H	F	1	1,3	0.38 ± 0.06	n.d.
14p	F	H	F	F	H	1	1,3	0.35 ± 0.05	n.d.
14q	H	CF_3	Cl	H	H	1	1,3	0.28 ± 0.04[c]	13.7 ± 2.3
14r	H	H	H	H	H	2	1,4	0.50 ± 0.05[c]	n.d.
14s	H	H	H	H	H	2	1,3	0.34 ± 0.06[c]	n.d.
14t	H	H	H	F	H	2	1,3	0.29 ± 0.05[c]	21.3 ± 4.3

ClGBI was used as a positive control. IC_{50} value for ClGBI was determined to be 15.9 ± 2.0 μM. All measurements were performed in at least three independent experiments.

[a] Remaining H_V1 current fraction (RCF) measured at +60 mV in the presence of 50 μM of the compounds.

[b] Half maximal inhibitory concentration.

[c] Not saturated values due to cell loss.

[d] n.d. – not determined.

to represent a broad spectrum of structural features within the inhibitor series. Of the two starting compounds, ***42***, which has a *meta*-benzyloxy substituent on the central phenyl ring, showed significantly better drug-like properties with a thermodynamic solubility of 5.57 μM, an unbound fraction of 1.5 % and a LogD of 3.02. In contrast, ***13*** showed poor solubility (<0.03 μM), no detectable unbound fraction (0 %), and a higher LogD (>4.56).

The most active type I analogue, **8b**, which contains a 4,5-dibromopyrrol-2-yl substituent at the R^2 position, showed slightly improved properties compared to ***13***. This improvement is likely due to the lower lipophilicity of the dibromopyrrole ring compared to the indole moiety in ***13***, highlighting the potential of heteroaromatic substitutions to fine-tune physicochemical profiles. Within the type II series, compounds **14s** and **14t**, which bear phenethyloxy substituents on the central phenyl ring, stood out. They showed the best solubility (0.92 μM and 8.99 μM, respectively) and the highest unbound fractions (0.9 % and

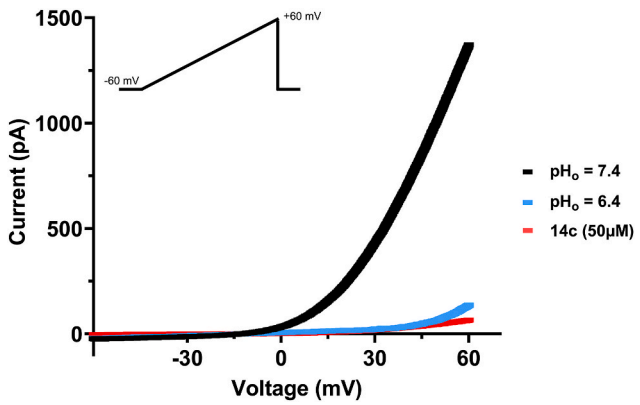

Fig. 4. Inhibition of the hH$_V$1 current by 50 μM of **14c**. Peak currents were determined as the current amplitudes at the end of the ramps at the highest applied voltage of +60 mV. The pH values refer to external (pH$_o$) conditions. The switch to pH$_o$ = 6.4 confirms the proper operation of the perfusion system as the opening threshold is right-shifted and the current is significantly reduced. The details of the protocols and experimental conditions are described in Experimental section.

0.6 %, respectively). These results underline the importance of molecular flexibility for optimising drug-like properties. Notably, while **14s** and **14t** showed improvements, their unbound fractions remained low, suggesting opportunities for further optimisation.

Overall, these results emphasise the crucial role of molecular flexibility and substituent-driven modulation of lipophilicity in improving drug-like properties. The type II 5-phenyl-2-aminoimidazoles, exemplified by ***42***, **14s** and **14t**, offer a good balance between solubility, reduced LogD and structural adaptability for targeted H$_V$1 inhibition. The phenethyloxy analogues **14s** and **14t**, designed with key structural modifications to enhance their reduced activity compared to oxymethylene derivatives, are therefore promising candidates for further development into H$_V$1 inhibitors.

2.3.4. *Metabolic stability in human and mouse liver microsomes*

The metabolic stability of compounds ***13***, ***42*** [26], **8b**, **14c**, **14h**, **14l**, **14m**, **14s** and **14t** was investigated using human and mouse liver microsomes (Table 4). The selection criteria were the same as for the antiproliferative assays. This assay evaluates phase I metabolic conversion mediated by cytochrome P450 (CYP) and flavin-containing monooxygenase (FMO) enzymes. The main pharmacokinetic parameters – including the *in vitro* half-life ($t_{1/2}$), the microsomal intrinsic clearance ($CL_{int(mic)}$) and the intrinsic hepatic clearance *in vivo* ($CL_{int(liver)}$) – were determined using established methods [43,44].

All nine compounds showed favourable metabolic stability with $t_{1/2}$ values of over 54 min in human liver microsomes. In particular, type I compound **8b**, which has a 4,5-dibromopyrrol-2-yl substituent at the R^2 position, showed the highest metabolic stability in human liver microsomes with $t_{1/2}$ values of 99 min. Throughout the series, metabolic stability was generally slightly higher in human liver microsomes than in mouse liver microsomes. The robust metabolic stability observed for these compounds suggests that they are not rapidly metabolised by liver enzymes, which is a strong indicator of favourable bioavailability *in vivo*.

2.3.5. *Bi-directional permeability across the Caco-2 cell monolayer*

To evaluate the potential for *in vivo* absorption, we performed Caco-2 permeability assays for two previously reported inhibitors, ***13*** and ***42*** [26], and for a representative compound from the new series, **14h** (Table 5). Compound **14h** was selected as the representative of the newly synthesized series because it showed the lowest residual current fraction (RCF) at 50 μM among all compounds tested. The results showed different permeability profiles between the type I and type II inhibitors. In particular, the type I compound ***13*** showed a significantly lower apparent permeability (P_{app}) than the type II compounds ***42*** and **14h**, which showed moderate P_{app} values. However, the low recoveries require cautious interpretation of these results and further confirmation by additional *in vitro* and/or *in vivo* data is warranted.

Of note, ***13*** has a high efflux ratio (ER = 320), suggesting that it may be a substrate for efflux transporters such as P-glycoprotein (P-gp). This efflux activity likely contributes to its poor permeability and poses a potential challenge for oral bioavailability. In contrast, the moderate permeability and lower efflux ratios of ***42*** and **14h** suggest a more favourable absorption profile, consistent with their improved physicochemical properties.

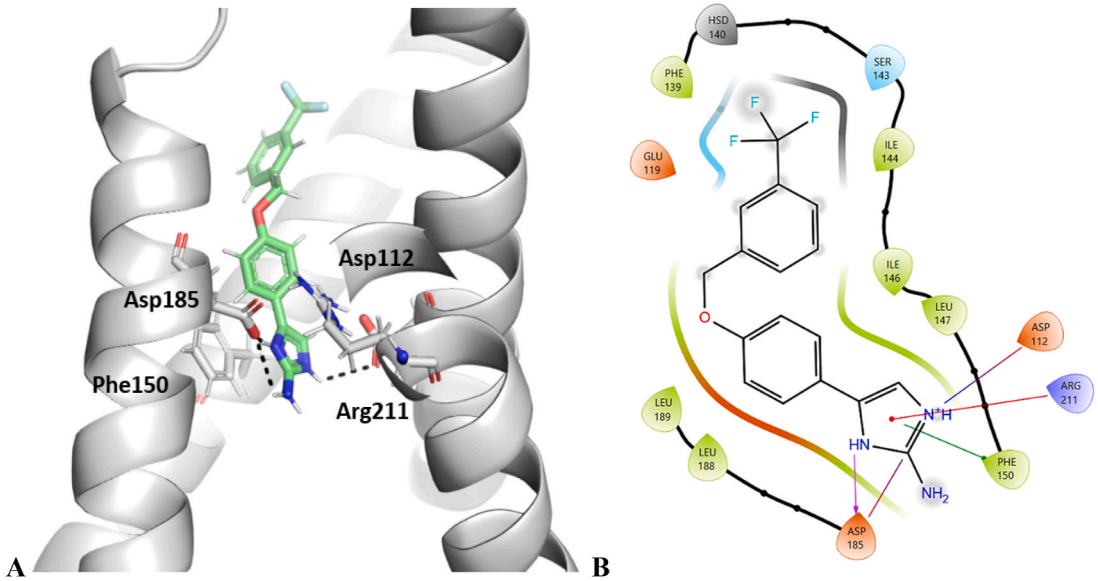

Fig. 5. Binding mode of **14c** in the proposed binding pocket in the H$_V$1 VSD, predicted by docking with Glide. A) The ligand (in green) and the neighbouring protein side chains are shown as stick models, coloured according to the chemical atom type. For clarity, only key amino acids are shown. H-bonds are indicated by black dotted lines. B) In the schematic representations of protein-ligand interactions, hydrogen bonds are shown as arrows (in magenta), cation-π-stacking as a red line, π-π interaction as a green line, ionic interactions as red-blue lines and hydrophobic contacts as grey spheres. (For interpretation of the references to colour in this figure legend, the reader is referred to the Web version of this article.)

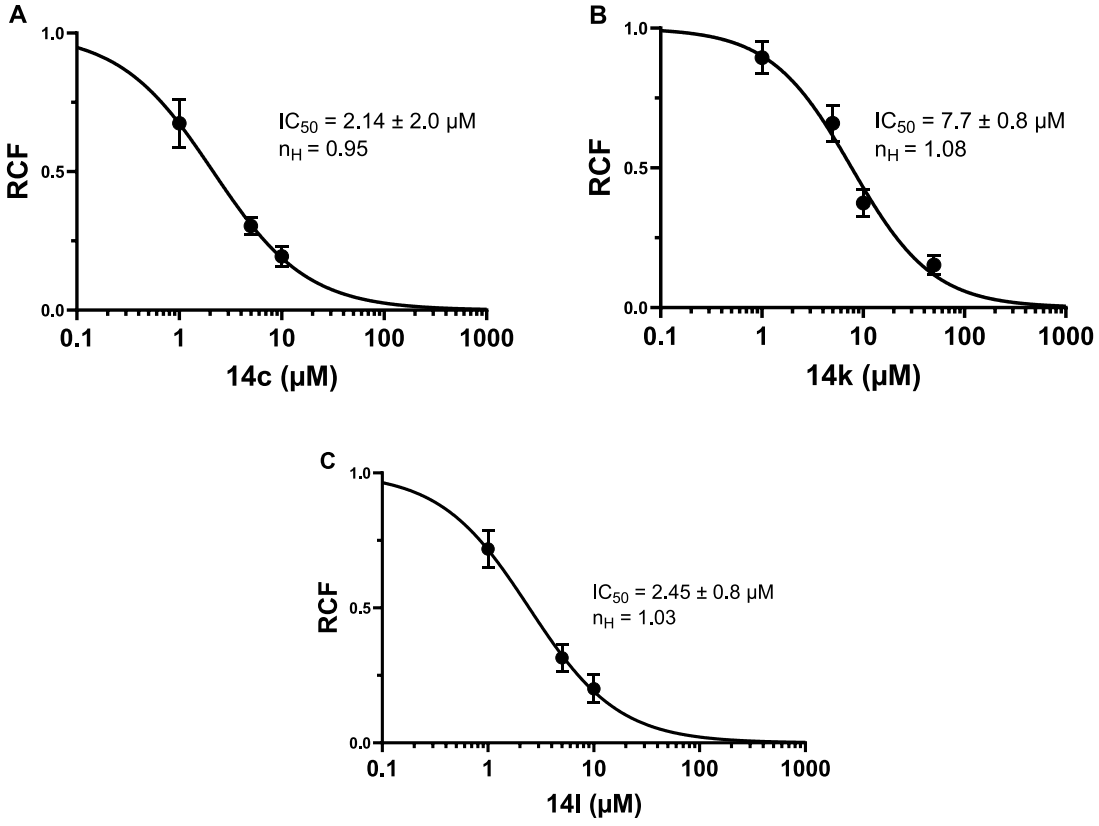

Fig. 6. Dose-response curves for the three representative H_V1 inhibitors **14c** (A), **14k** (B) and **14l** (C). The points on the dose-response curves represent the mean of 3–4 independent measurements (10, 5, 1 μM concentration or 50, 10, 5 and 1 μM concentration). The data points were fitted using a two-parameter Hill equation (see Experimental section). The Hill coefficient is labelled as n_H. The error bars represent the SEM.

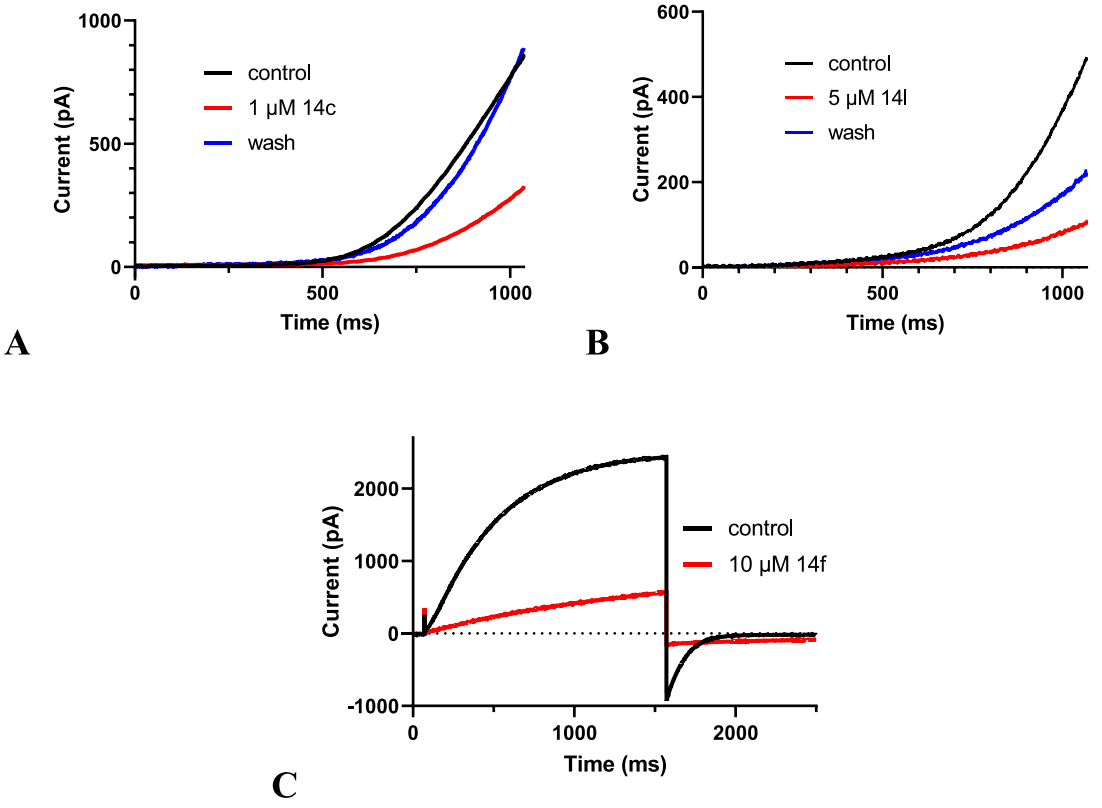

Fig. 7. Representative traces of H_V1 inhibition by various compounds. (**A**, **B**): Current traces recorded with voltage ramps from −60 to +60 mV show no significant shift in activation threshold voltage. Inhibition by 1 μM **14c** is fully reversible, while inhibition by 5 μM **14l** is only partially reversible. (**C**): Current traces recorded during a voltage step to +60 mV followed by a step back to −80 mV show a significant slowing of the opening and closing of the channel together with the current reduction in the presence of 10 μM **14f**.

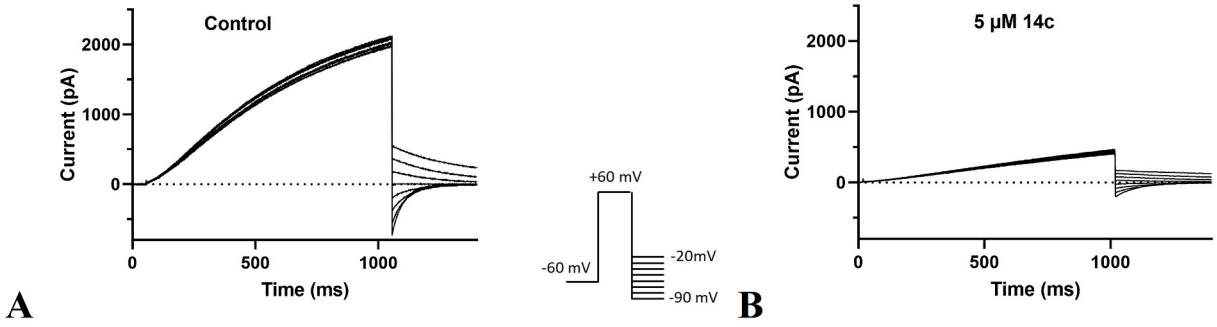

Fig. 8. Tail current protocol: Cells were depolarized to +60 mV for 1 s and then stepped back to tail voltages from −90 to −20 mV in +10 mV increments (inset). Currents recorded in control conditions (**A**) and after reaching equilibrium inhibition with 5 μM compound **14c** (**B**). Tail amplitudes were plotted as a function of voltage and fitted with a straight line, with the intercept taken as the reversal potential.

2.3.6. Membrane fluidity measurements

Hydrophobic compounds can induce cellular toxicity and anti-proliferative effects through large-scale disruption of the structural organization of membranes, and alterations in membrane fluidity can affect the function of various ion channels [45]. Similar effects have also been suggested for H_V1 channel [46]. Therefore, we investigated the effects of compounds ***13***, ***42*** [22], **8b**, **14c**, **14h**, **14l**, **14m**, **14s** and **14t** on membrane fluidity. The compounds were selected on the basis of their activity on H_V1 channels and their coverage of a wide range of structural features. For this purpose, we performed fluorescence anisotropy measurements using the hydrophobic fluorescent membrane probe 4'-(trimethylammonio)-diphenylhexatriene (TMA-DPH). CHO cells were treated with 10 μM of each test compound, labelled with TMA-DPH, and fluorescence intensities were measured by spectrofluorometry. Fluorescence anisotropy (*r*) was calculated for each compound and compared to the control using established protocols [47–49] (Fig. 11).

Fluorescence anisotropy is inversely proportional to membrane fluidity, which means that a decrease in anisotropy corresponds to an increase in membrane fluidity and vice versa. As shown in Fig. 11, compounds ***13***, **14h** and **14l** caused a statistically significant change in fluorescence anisotropy compared to the control, while the other compounds did not cause significant changes. However, the magnitude of the changes, although statistically significant, was notably smaller than the changes previously observed with an identical experimental setup following lipid treatments such as loading and depletion of membrane

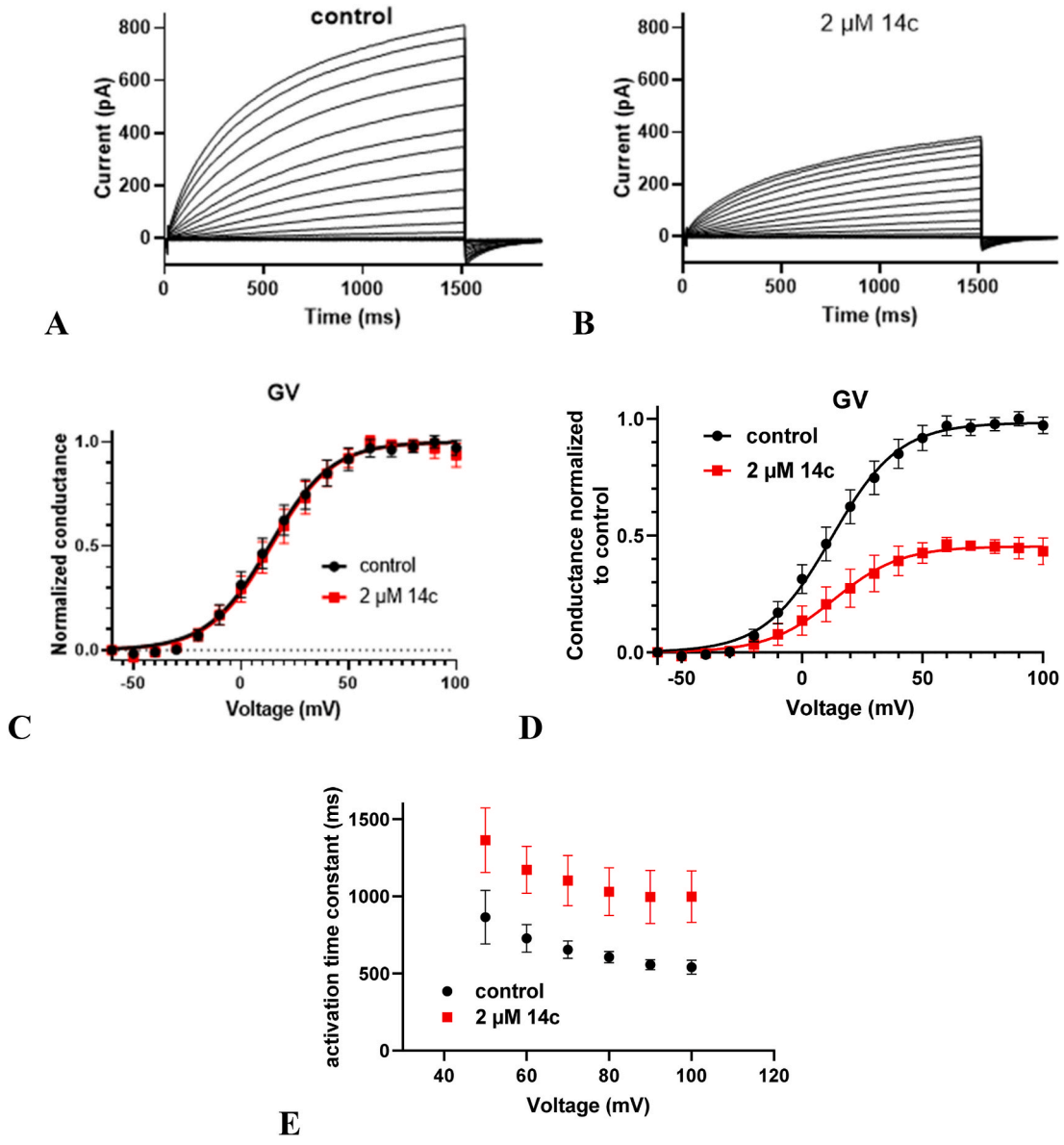

Fig. 9. Representative traces of current families recorded with step depolarizations from −60 to +100 mV in 10 mV increments in the absence (**A**) and presence (**B**) of 2 μM of compound **14c**. The G-V curves (**C**) constructed from the I–V protocols show a close overlap, indicating that the drug has no effect on the voltage-dependence of steady-state channel activation. (**D**): G-V curves normalised to the maximum control conductance. (**E**): Activation time constants as a function of membrane potential, determined by single exponential fits to the current traces under control conditions and in the presence of 2 μM compound **14c** (n = 4).

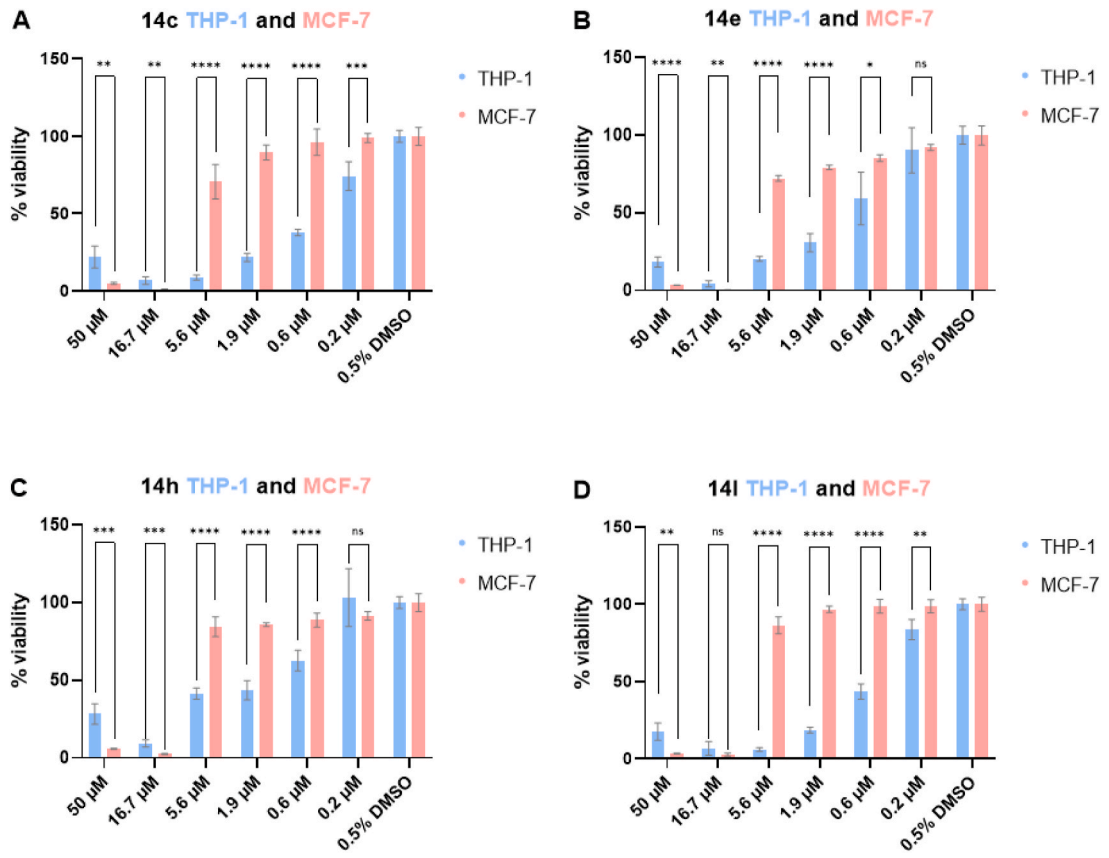

Fig. 10. Statistical comparison of the effect of **14c**, **14e**, **14h** and **14l** on the THP-1 and MCF-7 cell lines at each tested concentration (0.2–50 µM). Cell viability was determined using the MTS assay. DMSO (0.5 %) was used as a control. Data represent mean ± SD of two independent experiments, each performed in triplicate. Statistical significance was determined using an unpaired *t*-test with Welch's correction (*p < 0.05, **p < 0.01, ***p < 0.001, ****p < 0.0001, ns – not significant).

Table 3
Thermodynamic solubility, plasma protein binding and distribution coefficient of selected H_V1 inhibitors.

Comp.	Therm. solubility [µM][a]	PPB (mouse),[b] unbound fraction [%]	LogD[c]
13[d]	<0.03	0.0 ± 0.0	>4.56
42[d]	5.57	1.5 ± 0.0	3.02
8b	0.09	0.2 ± 0.0[e]	3.70
14c	0.10	0.1 ± 0.0[e]	4.44
14h	<0.1	0.3 ± 0.0	3.45
14l	0.06	0.1 ± 0.0	>4.89
14m	0.04	0.3 ± 0.0[e]	4.08
14s	0.92	0.9 ± 0.0	3.43
14t	8.99	0.6 ± 0.1	3.64
warfarin	–	4.4 ± 0.3	–

[a] Thermodynamic solubility.
[b] Plasma protein binding in mice.
[c] Distribution coefficient (octanol/buffer) at pH 7.4.
[d] Previously published compound [26].
[e] The results should be interpreted carefully due to low recovery.

Table 4
Metabolic stability of selected H_V1 inhibitors in human and mouse liver microsomes.

Comp.	HLM[a]			MLM[b]		
	$t_{1/2}$ [min][c]	$CL_{int(mic)}$ [µL min^{-1} mg^{-1}][d]	CL_{int} (liver) [mL min^{-1} kg^{-1}][e]	$t_{1/2}$ [min]	CL_{int} (mic) [µL min^{-1} mg^{-1}]	CL_{int} (liver) [mL min^{-1} kg^{-1}]
13[f]	75.0	18.5	16.6	66.7	20.8	82.3
42[f]	76.9	18.0	16.2	8.3	168	665
8b	98.6	14.1	12.6	26.9	51.6	204
14c	57.7	24.0	21.6	16.6	83.6	331
14h	69.9	19.8	17.8	16.0	86.8	344
14l	81.2	17.1	15.4	50.8	27.3	108
14m	82.7	16.8	15.1	13.8	101	398
14s	57.6	24.1	21.7	15.8	87.6	347
14t	54.4	25.5	22.9	16.6	83.6	331
testosterone	17.0	81.4	73.2	9.0	153	607
diclofenac	6.10	226	203	38.4	36.1	143
propafenone	5.80	238	215	4.60	301	1190

[a] Human liver microsomes.
[b] Mouse liver microsomes.
[c] *In vitro* half-life, time for 50 % disappearance of the parent compound.
[d] Microsomal intrinsic clearance, $CL_{int(mic)} = 0.693/t_{1/2}$/mg microsome protein per mL.
[e] *In vivo* intrinsic (hepatic) clearance, $CL_{int(liver)} = CL_{int(mic)} \times$ (mg microsomal protein/g liver weight) × (g liver weight/kg body weight).
[f] Previously published compound [26].

cholesterol [48,49] or glucosylceramide accumulation [50,51]. Therefore, the small changes in fluidity rule out the possibility that the compounds studied exert antiproliferative effects through large-scale alterations in membrane structure and not via inhibiting H_V1. Overall, the fluidity measurements argue against a significant contribution of indirect effects of the tested compounds on H_V1 and support the specific effect of the inhibitors.

2.3.7. *Selectivity towards the $K_V1.3$ and $Na_V1.5$ channels*

The selectivity of the most potent H_V1 inhibitors (**14a**, **14b**, **14c**,

Table 5
Bi-directional permeability across the Caco-2 cell monolayer of the three selected H_V1 inhibitors.

Comp.	Mean P_{app} [10^{-6} cm/s][a]		Efflux ratio	Mean solution recovery [%]		Rank P_{app}
	A to B	B to A		A to B	B to A	
13[b]	0.013	4.1	320	22	15	Low
42[b]	3.5	3.4	0.95	18	40	Moderate
14h	0.87	0.97	1.1	7.3	25	Moderate
nadolol[c]	0.024	ND[f]	–	93	ND	Low
metoprolol[d]	23	ND	–	97	ND	High
digoxin[e]	0.15	27	180	87	110	Low

The results for **13**, **42** and **14h** should be interpreted carefully due to low recovery.
[a] Apparent permeability coefficient.
[b] Previously published compound [26].
[c] Low permeability marker.
[d] High permeability marker.
[e] P-gp substrate.
[f] Not determined.

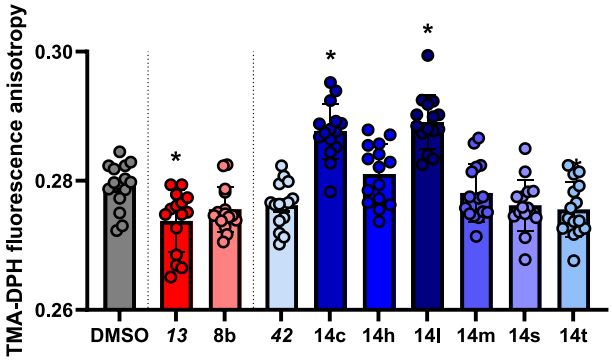

Fig. 11. The effects of 10 μM test compounds on the fluorescence anisotropy of TMA-DPH, as determined by spectrofluorometry, which is inversely related to membrane fluidity. Data are presented as mean ± SD from n = 15 biological replicates across three independent experiments. Asterisks (*) indicate significant differences compared to DMSO-treated control samples ($p < 0.05$, ANOVA followed by Dunnett's multiple comparison test).

Table 6
Inhibitory activities of type II 5-phenyl-2-aminoimidazoles on human voltage-gated proton channels H_V1, human voltage-gated potassium channels $K_V1.3$ and voltage-gated sodium channels $Na_V1.5$.

Comp.	RCF[a] [50 μM]		
	H_V1	$K_V1.3$	$Na_V1.5$
14a	0.20 ± 0.01	0.25 ± 0.04	0.25 ± 0.08
14b	0.27 ± 0.03	0.25 ± 0.03	0.12 ± 0.06
14c	0.19 ± 0.04[b]	0.23 ± 0.14[b]	0.08 ± 0.03
14e	0.13 ± 0.03	0.15 ± 0.02	0.19 ± 0.01
14f	0.31 ± 0.04[b]	0.26 ± 0.08	0.15 ± 0.03
14g	0.21 ± 0.03	0.29 ± 0.15	0.27 ± 0.10
14h	0.13 ± 0.02[b]	0.08 ± 0.02	0.22 ± 0.11
14i	0.19 ± 0.01	0.37 ± 0.02	0.12 ± 0.05
14k	0.15 ± 0.03	0.41 ± 0.03[b]	0.06 ± 0.02
14l	0.25 ± 0.04[b]	0.42 ± 0.06[b]	0.05 ± 0.01
14m	0.25 ± 0.04	0.27 ± 0.07	n.d[c]
14q	0.30 ± 0.04	0.52 ± 0.05	0.40 ± 0.0
14s	0.34 ± 0.06[b]	0.31 ± 0.02	n.d.

[a] Remaining H_V1, $K_V1.3$ and $Na_V1.5$ current fraction (RCF) measured at +60, +40 and 0 mV, respectively, in the presence of 50 μM of the compounds.
[b] Not saturated values due to cell loss.
[c] n.d. – not determined. 10 mM tetraethyl-ammonium and Na^+-free solutions were used for verifying the correct operation of the perfusion system. All measurements were performed in at least three independent experiments.

14e, **14f**, **14g**, **14h**, **14i**, **14k**, **14l**, **14m**, **14q** and **14s**) was investigated on human $K_V1.3$ and $Na_V1.5$ channels expressed natively in peripheral blood lymphocytes or transiently in Chinese hamster ovary (CHO) cells, respectively, using manual patch-clamp electrophysiology. Inhibition was quantified by calculating the remaining current fraction (RCF) at +40 mV with $K_V1.3$ and at 0 mV with $Na_V1.5$ channels in the presence of 50 μM of the compounds (Table 6). The RCF values for Hv1 channels are included in the table for comparison. Unfortunately, selectivity towards the $K_V1.3$ and $Na_V1.5$ channels was limited as the compounds were active in the same concentration range as for the H_V1 channels.

3. Conclusion

In this study, we designed and synthesized an improved series of 5-phenyl-2-aminoimidazoles as inhibitors of the human voltage-gated proton channel (H_V1). Two classes of inhibitors were developed: Type I with aromatic heterocycles linked to the central benzene ring via an amide bond, and type II with benzyloxy or phenethyloxy substituents in the *meta*-or *para*-position of the phenyl core. The most potent compounds exhibited IC_{50} values in the low micromolar range against H_V1. SAR analysis emphasised the critical role of the unsubstituted 2-aminoimidazole core – particularly the NH_2 group and the N-1 nitrogen – in forming a hydrogen bond network with key amino acids in the binding region. The type II inhibitors showed significantly better H_V1 inhibition compared to the type I analogues, probably due to the increased conformational flexibility mediated by oxomethylene or oxoethylene linkers. These linkers facilitate optimal positioning of terminal aromatic groups and promote hydrophobic interactions or π-stacking, which have been shown to contribute significantly to improved ligand-channel binding.

The antiproliferative activity of selected potent H_V1 inhibitors was evaluated against MCF-7 (human breast cancer) and THP-1 (human monocytic leukaemia). Compounds displayed a significantly stronger antiproliferative effect on THP-1 cells expressing high levels of H_V1 than on MCF-7 cells with limited H_V1 expression. The antiproliferative activity corresponds well with the H_V1 inhibition and it underscores the anticancer potential of these inhibitors. Particularly in H_V1-over-expressing malignant tumours the effect of inhibitors appears to be more pronounced and supports further investigation of their therapeutic applications.

Physicochemical profiling showed that the type II compounds possess better drug-like properties, including improved thermodynamic solubility, plasma protein binding and partition coefficients, making them promising candidates for further development. Fluorescence anisotropy measurements using TMA-DPH confirmed that the compounds did not exert substantial, large-scale changes in membrane structure. Selectivity towards $K_V1.3$ and $Na_V1.5$ channels was limited, indicating low specificity for H_V1.

This work advances the development of H_V1 inhibitors with optimised pharmacological profiles and elucidates important structure-activity relationships by highlighting the importance of linker flexibility and aromatic stacking in H_V1 inhibition. These findings provide valuable chemical tools to study the role of H_V1 in tumour progression and other disease states, while providing the basis for new therapeutic strategies.

4. Experimental section

4.1. Chemistry - general information

Chemicals were purchased from Apollo Scientific (Stockport, UK), TCI (Tokyo, Japan), Sigma-Aldrich (St. Louis, USA), and Acros Organics (Geel, Belgium). Thin-layer chromatography (TLC) was performed on Merck 60 F254 silica gel plates (0.25 mm) under visualization with UV light and spray reagents. Flash column chromatography was performed using Kieselgel 60, with a granulometry of 0.040–0.063 nm (230–400

mesh ASTM), supplied by Merck, as stationary phase. ^{1}H and ^{13}C NMR spectra were recorded at 400 and 100 MHz, respectively, on a Bruker Avance III NMR spectrometer (Bruker, MA, USA) at 295 K. The chemical shifts (δ) are reported in ppm and are referenced to the deuterated dimethyl sulfoxide (DMSO-d_6), with tetramethylsilane (TMS) as internal standard. Mass spectrometry (MS) measurements were performed on an Expression CMSL mass spectrometer (Advion, NY, USA). High resolution mass spectrometry (HRMS) measurements were performed on a HPLC–MS/MS system (Q Executive Plus; Thermo Scientific, MA, USA). Analytical reversed-phase UPLC analyses were performed using a modular system (Thermo Scientific Dionex UltiMate 3000 modular system; Thermo Fisher Scientific Inc., MA, USA). Method: Waters Acquity UPLC® HSS C18 SB column (2.1 × 50 mm, 1.8 μm), T = 40 °C; injection volume = 1.750 μL (0.20–0.30 mg of sample, dissolved in 100 μL of DMSO and 900 μL of MeOH); flow rate = 0.3 mL/min; detector λ = 254 nm and 280 nm; mobile phase A (0.1 % trifluoroacetic acid (TFA) [v/v] in water), mobile phase B methanol (MeOH). Gradient: 0–8 min, 10–90 % B; 8–10 min, 90 % B; 10–11 min, 90-10 % B. Purities of the tested compounds were established to be ≥ 95 %, as determined by UPLC. The structures were drawn with ChemDraw 20.0 (PerkinElmer), the NMR spectra were analysed with MestReNova v12.0.0–20080 (© 2017 Mestrelab Research S.L.) and the HPLC-MS spectra were analysed with Advion Data Express v6.4.10.3.

4.2. Synthetic procedures and analytical data

2-(3-Nitrophenyl)-1*H*-imidazo[1,2-*a*]pyrimidin-4-ium bromide (3). To a solution of compound **1** (2.60 g, 27.32 mmol) and compound **2** (8.00 g, 32.78 mmol) in acetonitrile (120 mL), 4-dimethylaminopyridine (3.00 mg, 0.26 mmol) was added and the mixture was stirred at 85 °C for 15 h. The reaction mixture was than filtered, washed with acetonitrile and diethyl ether and dried to give **3** as a pink solid. Yield: 72 % (6.32 g); ^{1}H NMR (400 MHz, DMSO-d_6): δ 9.14 (dd, J = 6.8, 1.9 Hz, 1H, Ar–H), 8.85 (t, J = 1.9 Hz, 1H, Ar–H), 8.79–8.74 (m, 2H, Ar–H), 8.47–8.44 (m, 1H, Ar–H), 8.29–8.26 (m, 1H, Ar–H), 7.84 (t, J = 8.0 Hz, 1H, Ar–H), 7.32 (dd, J = 6.7, 4.2 Hz, 1H, Ar–H); MS (ESI) m/z (%) = 241.7 ([MH - Br]$^+$); 282.9 ([MH – Br + CH_3CN]$^+$).

5-(3-Nitrophenyl)-1*H*-imidazole-2-amine (4). To a suspension of compound **3** (600 mg, 1.86 mmol) in abs. ethanol (16 mL) in a 30 mL glass vessel, hydrazine hydrate (420 μL, 13.08 mmol, 35 % hydrazine in solution) was added. The vessel was placed in a microwave reactor and heated at 120 °C for 40 min. The mixture was cooled to rt and the solvent evaporated under reduced pressure. The resulting residue was purified by flash column chromatography using DCM/MeOH/NH_4OH = 10:1:0.1 as mobile phase, to afford **4** as an orange solid. Yield 82 % (312 mg); ^{1}H NMR (400 MHz, DMSO-d_6): δ 10.66 (s, 1H, NH), 8.41 (t, J = 2.0 Hz 1H, Ar–H), 8.06–7.99 (m, 1H, Ar–H), 7.91 (ddd, J = 8.1, 2.4, 0.9 Hz, 1H, Ar–H), 7.55 (t, J = 8.0 Hz, 1H, Ar–H), 7.26 (s, 1H, imidaz-H), 5.45 (s, 2H, NH_2); MS (ESI) m/z (%) = 204.8 ([M + H]$^+$); 245.7 ([MH + CH_3CN]$^+$).

***tert*-Butyl 2-amino-5-(3-nitrophenyl)-1*H*-imidazole-1-carboxylate (5).** To a suspension of compound **4** (590 mg, 2.87 mmol) in a mixture of methanol (70 mL) and water (35 mL), Boc-anhydride (1.57 g, 7.18 mmol) was added and the mixture was stirred at rt for 15 h. The precipitate was filtered off, washed with methanol and dried to give **5** as a yellow solid. Yield 93 % (817 mg); ^{1}H NMR (400 MHz, DMSO-d_6): δ 8.55 (t, J = 2.0 Hz,1H, Ar–H), 8.23–8.17 (m, 1H, Ar–H), 8.07 (ddd, J = 8.2, 2.3, 1.0 Hz, 1H, Ar–H), 7.67–7.62 (m, 2H, imidaz-H, Ar–H), 6.72 (s, 2H, NH_2), 1.60 (s, 9H, COOC(CH_3)$_3$); MS (ESI) m/z (%) = 204.1 ([MH - Boc]$^+$).

***tert*-Butyl 2-amino-5-(3-aminophenyl)-1*H*-imidazole-1-carboxylate (6).** Compound **5** (1.060 g, 3.49 mmol) was dissolved in anhydrous THF (110 mL) and anhydrous methanol (25 mL) and Pd/C (0.210 g, 20 %) was added. The reaction mixture was stirred under hydrogen atmosphere for 4h. The catalyst was filtered off and the solvent evaporated under reduced pressure to give **6** as a light brown solid. Yield 100 % (955 mg); ^{1}H NMR (400 MHz, DMSO-d_6): δ 7.11 (s, 1H, imidaz-H), 7.00–6.91 (m, 2H, Ar–H), 6.88–6.85 (m, 1H, Ar–H), 6.54 (s, 2H, imidaz-NH_2), 6.43 (ddd, J = 7.8, 2.3, 1.1 Hz, 1H, Ar–H), 5.02 (s, 2H, Ar-NH_2), 1.60 (s, 9H, COOC(CH_3)$_3$); MS (ESI) m/z (%) = 174.8 ([MH - Boc]$^+$); 215.8 ([MH - Boc + CH_3CN]$^+$).

General procedure A. Syntheses of compounds 7a-d and 7k (with 7a as an example). To a suspension of 3,4-dichloro-5-methyl-1*H*-pyrrole-2-carboxylic acid (530 mg, 2.73 mmol) and TBTU (940 mg, 2.92 mmol) in anhydrous DCM (42 mL), *N*-methylmorpholine (1.10 mL, 10.03 mmol) was added and the mixture was stirred at rt for 0.5 h under argon atmosphere. Compound **6** (500 mg, 1.82 mmol) was added and the mixture was stirred at 40 °C for 15 h. The solvent was evaporated under reduced pressure, the residue dissolved in ethyl acetate (300 mL) and washed successively with water (2 × 100 mL), saturated aqueous $NaHCO_3$ solution (2 × 100 mL), and brine (2 × 100 mL). The organic phase was dried over Na_2SO_4, filtered and the solvent evaporated under reduced pressure. The crude product was purified by flash column chromatography using EtOAc/Hex/NH_4OH = 2:1:0.05 as mobile phase. The obtained product was then suspended in DCM, filtered off and dried to afford **7a** as an orange solid.

***tert*-Butyl 2-amino-5-(3-(3,4-dichloro-5-methyl-1*H*-pyrrole-2-carboxamido)phenyl)-1*H*-imidazole-1-carboxylate (7a).** Synthesized according to General procedure A. Orange solid; yield 27 % (222 mg); ^{1}H NMR (400 MHz, DMSO-d_6): δ 12.15 (s, 1H, pyrr-NH), 9.40 (s, 1H, NH), 7.98 (t, J = 1.8 Hz, 1H, Ar–H), 7.61–7.55 (m, 1H, Ar–H), 7.49–7.43 (m, 1H, Ar–H), 7.34–7.27 (m, 2H, Ar–H, imidaz-H), 6.63 (s, 2H, NH_2), 2.23 (s, 3H, CH_3), 1.59 (s, 9H, COOC(CH_3)$_3$); MS (ESI): m/z (%) = 350.0 ([MH - Boc]$^+$); 391.0 ([MH – Boc + CH_3CN]$^+$).

***tert*-Butyl 2-amino-5-(3-(4,5-dibromo-1*H*-pyrrole-2-carboxamido)phenyl)-1*H*-imidazole-1-carboxylate (7b).** Synthesized according to General procedure A. Light-yellow solid; yield: 23 % (154 mg); ^{1}H NMR (400 MHz, DMSO-d_6): δ 12.87 (s, 1H, pyrr-NH), 9.87 (s, 1H, NH), 8.03 (t, J = 1.9 Hz, 1H, Ar–H), 7.67–7.61 (m, 1H, Ar–H), 7.48–7.41 (m, 1H, Ar–H), 7.35–7.21 (m, 3H, Ar–H, imidaz-H, pyrr-H), 6.62 (s, 2H, NH_2), 1.59 (s, 9H, COOC(CH_3)$_3$); MS (ESI): m/z (%) = 423.8 ([MH - Boc]$^+$); 464.9 ([MH – Boc + CH_3CN]$^+$).

***tert*-Butyl 2-amino-5-(3-(3-fluoro-1H-pyrrole-2-carboxamido)phenyl)-1*H*-imidazole-1-carboxylate (7c).** Synthesized according to General procedure A. Light-yellow solid; yield: 28 % (197 mg); ^{1}H NMR (400 MHz, DMSO-d_6): δ 11.53 (s, 1H, pyrr-NH), 9.19 (s, 1H, NH), 8.00 (t, J = 1.9 Hz, 1H, Ar–H), 7.60–7.57 (m, 1H, Ar–H), 7.45–7.43 (m, 1H, Ar–H), 7.35–7.20 (m, 2H, Ar–H, imidaz-H), 6.93–6.80 (m, 1H, pyrr-H), 6.69 (s, 2H, NH_2), 6.07 (t, J = 2.8 Hz, 1H, pyrr-H), 1.59 (s, 9H, COOC(CH_3)$_3$); MS (ESI): m/z (%) = 286.2 ([MH - Boc]$^+$); 327 ([MH – Boc + CH_3CN]$^+$); 386.2 ([M + H]$^+$).

***tert*-Butyl 2-amino-5-(3-(3-methyl-1*H*-pyrrole-2-carboxamido)phenyl)-1*H*-imidazole-1-carboxylate (7d).** Synthesized according to General procedure A. Grey solid; yield: 23 % (160 mg); ^{1}H NMR (400 MHz, DMSO-d_6): δ 11.27 (s, 1H, pyrr-NH), 9.33 (s, 1H, NH), 8.03–8.02 (m, 1H, Ar–H), 7.62–7.54 (m, 1H, Ar–H), 7.42–7.40 (m, 1H, Ar–H), 7.32–7.23 (m, 2H, Ar–H, imidaz-H), 6.90 (t, J = 2.7 Hz, 1H, pyrr-H), 6.61 (s, 2H, NH_2), 6.02–6.01 (m, 1H, pyrr-H), 2.33 (s, 3H, CH_3), 1.59 (s, 9H, N–COOC(CH_3)$_3$); MS (ESI): m/z (%) = 282.0 ([MH - Boc])$^+$; 323.0 ([MH – Boc + CH_3CN]$^+$).

***N*-(3-(2-Amino-1-(oxazole-5-carbonyl)-1*H*-imidazole-5-yl)phenyl)oxazole-5-carboxamide (7k).** Synthesized according to General procedure A. Off-white solid; yield: 12 % (112 mg); ^{1}H NMR (400 MHz, DMSO-d_6): δ 12.03 (s, 2H, NH_2), 10.42 (s, 1H, NH), 8.87–8.44 (m, 2H, Ar–H), 8.24–7.94 (m, 3H, Ar–H), 7.58–7.44 (m, 2H, Ar–H), 7.39–7.27 (m, 2H, Ar–H, imidaz-H); ^{13}C NMR (100 MHz, DMSO-d_6): δ 155.39, 154.73, 154.33, 145.69, 138.79, 130.91, 130.84, 130.49, 129.44, 120.64, 119.19, 116.94 ppm; MS (ESI): m/z (%) = 365.2 ([M + H]$^+$); 406.2 ([MH + CH_3CN]$^+$). HRMS for $C_{17}H_{12}N_6O_4$: [M+H]$^+$ calculated: 364.09200, found: 365.09864; HPLC (10–90 % MeOH in 0.1 % TFA in 11 min, UPLC): t_r 4.657 min (100 % at 254 nm, 100 % at 280 nm).

General procedure B. Syntheses of compounds 7e-j, 7l-m and 8 (with 7e as an example). To a suspension of 4-acetyl-3,5-dimethyl-1*H*-pyrrole-2-carboxylic acid (363 mg, 2.00 mmol) and HATU (832 mg, 2.19 mmol) in anhydrous DMF (20 mL), *N*,*N*-diisopropylethylamine (953 μL, 5.47 mmol) was added and the mixture was stirred at rt for 0.5 h under argon atmosphere. Compound **6** (500 mg, 1.82 mmol) and 4-dimethylaminopyridine (12 mg, 0.09 mmol) were added and the mixture was stirred at 50 °C for 15 h. The solvent was evaporated under reduced pressure, the residue dissolved in ethyl acetate (200 mL) and washed successively with saturated aqueous $NaHCO_3$ solution (2 × 100 mL), water (2 × 100 mL) and brine (2 × 100 mL). The organic phase was dried over Na_2SO_4, filtered and the solvent evaporated under reduced pressure. The crude product was purified by flash column chromatography using DCM/MeOH/NH_4OH = 20:1:0.1 as mobile phase to afford **7e** as a yellow solid.

***tert*-Butyl 5-(3-(4-acetyl-3,5-dimethyl-1*H*-pyrrole-2-carboxamido)phenyl)-2-amino-1*H*-imidazole-1-carboxylate (7e).** Synthesized according to General procedure B. Light-yellow solid; yield 32 % (258 mg); ^{1}H NMR (400 MHz, DMSO-d_6): δ 11.40 (s, 1H, pyrr-NH), 11.00 (s, 1H, NH), 7.70–7.65 (m, 1H, Ar–H), 7.62. 7.55 (m, 1H, Ar–H), 7.44–7.34 (m, 2H, Ar–H, imidaz-H), 7.22–7.14 (m, 1H, Ar–H), 6.61 (s, 2H, NH_2), 2.44 (s, 2H, CH_3), 2.42 (s, 2H, CH_3), 2.33 (s, 2H, CH_3), 1.59 (s, 9H, $COOC(CH_3)_3$); MS (ESI): *m/z* (%) = 337.9 ([MH - Boc])$^+$.

***tert*-Butyl 5-(3-(2-(1*H*-imidazole-5-yl)acetamido)phenyl)-2-amino-1*H*-imidazole-1-carboxylate (7f).** Synthesized according to General procedure B. Orange solid; yield 30 % (247 mg); ^{1}H NMR (400 MHz, DMSO-d_6): δ 12.24 (s, 1H, imidaz-NH), 10.11 (s, 1H, NH), 7.96 (t, J = 1.7 Hz, 1H, Ar–H), 7.71 (s, 1H, imidaz-H), 7.48–7.44 (m, 1H, Ar–H), 7.42–7.38 (m, 1H, Ar–H), 7.28–7.21 (m, 2H, Ar–H, imidaz-H), 6.99 (s, 1H, imidaz-H), 6.61 (s, 2H, NH_2), 3.60 (s, 2H, $COCH_2$), 1.58 (s, 9H, $COOC(CH_3)_3$); MS (ESI): *m/z* (%) = 282.8 ([MH - Boc])$^+$; HRMS for $C_{19}H_{22}N_6O_3$ $[M+H]^+$ calculated: 383.18262, found: 383.18231.

***tert*-Butyl 5-(3-(1*H*-imidazole-2-carboxamido)phenyl)-2-amino-1*H*-imidazole-1-carboxylate (7g).** Synthesized according to General procedure B. Yellow solid; yield 29 % (218 mg); ^{1}H NMR (400 MHz, DMSO-d_6): δ 13.20 (s, 1H, imidaz-NH), 10.30 (s, 1H, NH), 8.24 (t, J = 1.7 Hz, 1H, Ar–H), 7.74–7.65 (m, 1H, Ar–H), 7.48–7.43 (m, 1H, Ar–H), 7.38 (s, 1H, imidaz-H), 7.30 (t, J = 7.9 Hz, 1H, Ar–H), 7.26 (s, 1H, imidaz-H), 7.15 (s, 1H, imidaz-H), 6.66 (s, 2H, NH_2), 1.59 (s, 9H, $COOC(CH_3)_3$); MS (ESI): *m/z* (%) = 268.7 ([MH - Boc])$^+$; 368.7 ([M + H]$^+$).

***tert*-Butyl 2-amino-5-(3-(picolinamido)phenyl)-1*H*-imidazole-1-carboxylate (7h).** Synthesized according to General procedure B. White solid; yield: 35 % (289 mg); ^{1}H NMR (400 MHz, DMSO-d_6): δ 10.60 (s, 1H, NH), 8.78–8.73 (m, 1H, Ar–H), 8.34–8.27 (m, 1H, Ar–H), 8.20–8.16 (m, 1H, Ar–H), 8.09 (td, J = 7.7, 1.6 Hz, 1H, Ar–H), 7.79–7.73 (m, 1H, Ar–H), 7.72–7.67 (m, 1H, Ar–H), 7.53–7.48 (m, 1H, Ar–H), 7.38–7.27 (m, 2H, Ar–H, imidaz-H), 6.64 (s, 2H, NH_2), 1.60 (s, 9H, $COOC(CH_3)_3$); MS (ESI): *m/z* (%) = 279.8 ([MH - Boc])$^+$; 320.9 ([MH - Boc + CH_3CN]$^+$).

***tert*-Butyl 2-amino-5-(3-(nicotinamido)phenyl)-1*H*-imidazole-1-carboxylate (7i).** Synthesized according to General procedure B. Off-white solid; yield: 50 % (471 mg); ^{1}H NMR (400 MHz, DMSO-d_6): δ 10.46 (s, 1H, NH), 9.19–9.06 (m, 1H, Ar–H), 8.83–9.73 (m, 1H, Ar–H), 8.38–8.27 (m, 1H, Ar–H), 8.20–8.10 (m, 1H, Ar–H), 7.69–7.46 (m, 3H, Ar–H), 7.34 (t, J = 7.9 Hz, 1H, Ar–H), 7.29 (s, 1H, imidaz-H), 6.65 (s, 2H, NH_2), 1.60 (s, 9H, $COOC(CH_3)_3$); MS (ESI): *m/z* (%) = 279.7 ([MH - Boc])$^+$; 320.7 ([MH - Boc + CH_3CN]$^+$).

***tert*-Butyl 2-amino-5-(3-(isonicotinamido)phenyl)-1*H*-imidazole-1-carboxylate (7j).** Synthesized according to General procedure B. Off-white solid; yield: 40 % (330 mg); ^{1}H NMR (400 MHz, DMSO-d_6): δ 10.52 (s, 1H, NH), 8.80 (d, J = 5.9 Hz, 2H, pyrid-H), 8.19–8.12 (m, 1H, Ar–H), 7.89 (d, J = 5.9 Hz, 2H, pyrid-H), 7.60–7.62 (m, 1H, Ar–H), 7.56–7.49 (m,1H, Ar–H), 7.39–7.27 7.33 (m, 2H, Ar–H, imidaz-H), 6.65 (s, 2H, NH_2), 1.59 (s, 9H, $COOC(CH_3)_3$); MS (ESI): *m/z* (%) = 279.8 ([MH - Boc])$^+$; 320.7 ([MH - Boc + CH_3CN]$^+$).

***N*-(3-(2-amino-1-nicotinoyl-1*H*-imidazole-5-yl)phenyl) nicotinamide (7l).** Synthesized according to General procedure B. Yellow solid; 160 mg; ^{1}H NMR (400 MHz, DMSO-d_6): δ 12.03 (s, 2H, NH_2), 10.46 (s, 1H, NH), 9.21 (d, J = 1.8 Hz, 1H, pyrid-H), 9.14 (d, J = 1.7 Hz, 1H, pyrid-H), 8.78 (dd, J = 4.8, 1.6 Hz, 2H, pyrid-H), 8.44–8.37 (m, 1H, Ar–H), 8.35–8.26 (m, 2H, Ar–H), 7.62–7.51 (m, 4H, Ar–H), 7.40–7.32 (m, 2H, Ar–H, imidaz-H); ^{13}C NMR (100 MHz, DMSO-d_6): δ 164.85, 164.45, 152.95, 152.56, 149.50, 149.17, 139.55, 136.12, 135.93, 131.08, 129.58, 129.31, 123.99, 120.46, 118.90, 116.82 ppm; MS (ESI): *m/z* (%) = 384.7 ([M + H]$^+$); 425.8 ([MH + CH_3CN]$^+$); HRMS for $C_{21}H_{16}N_6O_2$ $[M+H]^+$ calculated: 385.14075, found: 385.13985; HPLC (10–90 % MeOH in 0.1 % TFA in 11 min, UPLC): t_r 3.720 min (100 % at 254 nm, 100 % at 280 nm).

***N*-(3-(2-amino-1-isonicotinoyl-1*H*-imidazole-5-yl)phenyl)isonicotinamide (7m).** Synthesized according to General procedure B. Yellow solid; 350 mg; ^{1}H NMR (400 MHz, DMSO-d_6): δ 12.14 (s, 2H, NH_2), 10.53 (s, 1H, NH), 8.79 (d, J = 5.9 Hz, 4H, pyrid-H), 8.35–8.18 (m, 1H, Ar–H), 7.95 (d, J = 5.9 Hz, 4H), 7.62–7.47 (m, 2H, Ar–H), 7.43–7.24 (m, 2H, Ar–H); ^{13}C NMR (100 MHz, DMSO-d_6): δ 165.24, 164.38, 150.75, 150.61, 142.44, 139.32, 134.88, 129.33, 122.26, 122.07, 120.57, 118.86, 116.80, 111.28 ppm. MS (ESI): *m/z* (%) = 425.7 ([MH + CH_3CN]$^+$); HRMS for $C_{21}H_{16}N_6O_2$ $[M+H]^+$ calculated: 385.14075, found: 385.13991; HPLC (10–90 % MeOH in 0.1 % TFA in 11 min, UPLC): t_r 3.523 min (97 % at 254 nm, 98 % at 280 nm).

General procedure C. Syntheses of compounds 8a-e (with 8a as an example). To a solution of compound **7a** (120 mg, 0.27 mmol) in anhydrous THF (15 mL), absolute ethanol (8 mL) and anhydrous DMF (2 mL), HCl (ca. 4 mol/L in 1,4-dioxane, 3.40 mL, 13.66 mmol) was added and the reaction mixture was stirred at rt under argon atmosphere. After 15 h, HCl (ca. 4 mol/L in 1,4-dioxane, 3.40 mL, 13.66 mmol) was added and the reaction mixture was stirred at rt under argon atmosphere. After additional 15 h, HCl (ca. 4 mol/L in 1,4-dioxane, 3.40 mL, 13.66 mmol) was added and the reaction mixture was stirred for 1 additional day. The solvent was evaporated under reduced pressure and the crude product was suspended in a mixture of diethyl ether and acetonitrile, filtered off and washed with acetonitrile (x 3) and with diethyl ether (x 3). The obtained solid was subsequently suspended in DCM and in THF, filtered off, washed with DCM (x 2) and THF and dried to afford **8a** as a white solid.

2-Amino-5-(3-(3,4-dichloro-5-methyl-1*H*-pyrrole-2-carboxamido)phenyl)-1*H*-imidazole-3-ium chloride (8a). Synthesized according to General procedure C. White solid; yield: 94 % (98 mg); ^{1}H NMR (400 MHz, DMSO-d_6): δ 12.82–12.79 (s, 2H, pyrr-NH, imidaz-NH), 12.17 (s, 1H, NH^+), 9.96 (s, 1H, NH), 8.70 (s, 2H, NH_2), 8.14–7.88 (m, 1H, Ar–H), 7.47–7.30 (m, 4H, Ar–H), 2.24 (s, 3H, CH_3); ^{13}C NMR (100 MHz, DMSO-d_6): δ 157.55, 148.28, 139.81, 129.81, 128.65, 128.36, 126.82, 120.17, 120.14, 119.23, 116.30, 113.20, 110.03, 109.25, 11.24 ppm; MS (ESI): *m/z* (%) = 350.1 ([MH - Cl]$^+$); 391.0 ([MH - Cl + CH_3CN]$^+$); HRMS for $C_{15}H_{14}Cl_2N_5O$: $[M+H]^+$ calculated: 350.05699, found: 350.05668; HPLC (10–90 % MeOH in 0.1 % TFA in 11 min, UPLC): t_r 6.620 min (94 % at 254 nm, 95 % at 280 nm).

2-Amino-5-(3-(4,5-dibromo-1*H*-pyrrole-2-carboxamido) phenyl)-1*H*-imidazole-3-ium chloride (8b). Synthesized according to General procedure C. Pale-yellow solid; yield: 85 % (89 mg); ^{1}H NMR (400 MHz, DMSO-d_6): δ 13.27–12.78 (m, 2H, imidaz-NH, pyrr-NH), 12.16 (s, 1H, NH^+), 10.16 (s, 1H, NH), 8.09–7.90 (m, 1H, Ar–H), 7.70–7.60 (m, 1H, Ar–H), 7.48–7.28 (m, 6H, NH_2, Ar–H, imidaz-H, pyrr-H); ^{13}C NMR (100 MHz, DMSO-d_6): δ 157.81, 148.29, 139.79, 129.80, 128.61, 128.24, 126.88, 120.60, 120.22, 116.74, 114.88, 109.93, 106.42, 98.78 ppm; MS (ESI): *m/z* (%) = 423.8 ([MH - Cl]$^+$); 464.8 ([MH - Cl + CH_3CN]$^+$); HRMS for $C_{14}H_{12}Br_2N_5O$: $[M+H]^+$ calculated: 423.94031, found: 423.93988; HPLC (10–90 % MeOH in 0.1 % TFA in 11 min, UPLC): t_r 5.950 min (95 % at 254 nm, 95 % at 280 nm).

2-Amino-5-(3-(3-fluoro-1*H*-pyrrole-2-carboxamido)phenyl)-1*H*-imidazole-3-ium chloride (8c). Synthesized according to General procedure C. White solid; yield: 96 % (96 mg); ^{1}H NMR (400 MHz, DMSO-d_6): δ 12.86 (s, 1H, imidaz-NH), 12.18 (s, 1H, pyrr-NH), 11.93 (s,

1H, NH^+), 9.64 (s, 1H, NH), 8.07–7.90 (m, 1H, Ar–H), 7.69–7.26 (m, 6H, NH_2, Ar–H, pyrr-H), 7.04–6.76 (m, 1H, pyrr-H), 6.21–5.90 (m, 1H, pyrr-H); ^{13}C NMR (100 MHz, DMSO-d_6): δ 157.94, 154.03, 151.55, 148.25, 139.90, 129.74, 128.55, 126.86, 120.25, 120.17, 116.58, 110.21, 109.94, 97.49 ppm; MS (ESI): *m/z* (%) = 423.8 ([MH - Cl]$^+$); 464.8 ([MH - Cl + CH_3CN]$^+$); HRMS for $C_{14}H_{13}FN_5O$: [M+H]+ calculated: 286.10986, found: 286.10915; HPLC (10–90 % MeOH in 0.1 % TFA in 11 min, UPLC): t_r 4.980 min (99 % at 254 nm, 99 % at 280 nm).

2-Amino-5-(3-(3-methyl-1*H*-pyrrole-2-carboxamido)phenyl)-1*H*-imidazole-3-ium chloride (8d). Synthesized according to General procedure C. Pink solid; yield: 87 % (87 mg); ^{1}H NMR (400 MHz, DMSO-d_6): δ 12.76 (s, 1H, imidaz-H), 12.14 (s, 1H, pyrr-H), 11.91 (s, 1H, NH^+), 9.97 (s, 1H, NH), 8.17–8.09 (m, 1H, Ar–H), 7.66–7.58 (m, 1H, Ar–H), 7.49–7.24 (m, 5H, NH_2, Ar–H, imidaz-H), 6.89 (t, J = 2.6 Hz, 1H, pyrr-H), 6.09–5.90 (m, 1H, pyrr-H), 2.35 (s, 3H, CH_3); ^{13}C NMR (100 MHz, DMSO-d_6): δ 160.26, 148.23, 140.66, 129.65, 128.48, 127.07, 126.08, 121.97, 121.01, 120.02, 119.53, 116.08, 112.19, 109.86, 13.54 ppm; MS (ESI): *m/z* (%) = 282.2 ([MH - Cl]$^+$); 323.3 ([MH – Cl + CH_3CN]$^+$); HRMS for $C_{15}H_{16}N_5O$: [M+H]$^+$ calculated: 282.13494, found: 282.13470; HPLC (10–90 % MeOH in 0.1 % TFA in 11 min, UPLC): t_r 4.897 min (100 % at 254 nm, 100 % at 280 nm).

5-(3-(4-Acetyl-3,5-dimethyl-1*H*-pyrrole-2-carboxamido) phenyl)-2-amino-1*H*-imidazole-3-ium chloride (8e). Synthesized according to General procedure C. Pink solid; yield: 91 % (93 mg); ^{1}H NMR (400 MHz, DMSO-d_6): δ 12.70 (s, 1H, imidaz-H), 12.32 (s, 1H, pyrr-H), 12.09 (s, 1H, NH^+), 10.06 (s, 1H, NH), 8.14–8.07 (m, 1H, Ar–H), 7.61–7.56 (m, 1H, Ar–H), 7.46–7.27 (m, 5H, NH_2, Ar–H, imidaz-H), 2.54 (s, 3H, CH_3), 2.38 (s, 3H, CH_3), the signal for one CH_3 overlapped with the signal for DMSO-d_6; ^{13}C NMR (100 MHz, DMSO-d_6): δ 194.84, 160.15, 148.23, 140.39, 137.41, 129.68, 128.51, 127.45, 127.03, 122.68, 121.22, 120.18, 119.83, 116.28, 109.93, 31.66, 15.06, 12.87 ppm; MS (ESI): *m/z* (%) = 337.8 ([MH - Cl]$^+$); HRMS for $C_{18}H_{19}N_5O_2$: [M+H]$^+$ calculated: 338.16115, found: 338.16066; HPLC (10–90 % MeOH in 0.1 % TFA in 11 min, UPLC): t_r 4.857 min (100 % at 254 nm, 100 % at 280 nm).

General procedure D. Syntheses of compounds 8f-j (with 8f as an example). To a solution of compound **7f** (66 mg, 0.17 mmol) in anhydrous DCM (8 mL) cooled on an ice bath, TFA (132 μL, 1.73 mmol) was added and the reaction mixture was stirred at rt under argon atmosphere for 2 days. The solvent was evaporated under reduced pressure and the crude product purified by flash column chromatography using DCM/MeOH/NH_4OH = 9:1:0.1 and then DCM/MeOH/NH_4OH = 7:1:0.1 (gradient elution) as mobile phases. To a solution of the obtained product in abs. EtOH (1 mL) and anhydrous THF (1 mL) cooled on an ice bath, HCl (ca. 4 mol/L in 1,4-dioxane, 50 μM) was added and the mixture was stirred at 0 °C under argon atmosphere for 2h. The solvent was evaporated under reduced pressure and the crude residue was suspended in diethyl ether, filtered off, washed with diethyl ether (x 2) and dried to afford **8f** as a yellow solid.

5-(3-(2-(1*H*-Imidazole-3-ium-5-yl)acetamido)phenyl)-2-amino-1*H*-imidazole-3-ium chloride (8f). Synthesized according to General procedure D. Yellow solid; yield: 90 % (55 mg); ^{1}H NMR (400 MHz, DMSO-d_6): δ 14.50 (s, 2H, imidaz-H), 12.93 (s, 1H, NH^+), 12.21 (s, 1H, NH^+), 10.78 (s, 1H, NH), 9.10–9.04 (m, 1H, Ar–H), 7.94 7.87 (m, 1H, Ar–H), 7.58–7.55 (m, 1H, Ar–H), 7.52–7.35 (m, 5H, NH_2, Ar–H), 7.25 (s, 1H, imidaz-H), 3.95 (s, 2H, CH_2); ^{13}C NMR (100 MHz, DMSO-d_6): δ 167.02, 148.36, 139.91, 134.24, 129.93, 128.74, 127.74, 126.71, 120.19, 119.63, 117.90, 115.58, 109.91, 32.44 ppm; MS (ESI): *m/z* (%) = 282.9 ([MH - 2Cl]$^+$); HRMS for $C_{14}H_{14}N_6O$: [M+H]$^+$ calculated: 283.13019, found: 283.12999; HPLC (10–90 % MeOH in 0.1 % TFA in 11 min, UPLC): t_r 2.273 min (96 % at 254 nm, 94 % at 280 nm).

5-(3-(1*H*-Imidazole-3-ium-2-carboxamido)phenyl)-2-amino-1*H*-imidazole-3-ium chloride (8g). Synthesized according to General procedure D. Pink solid; yield: 85 % (47 mg); ^{1}H NMR (400 MHz, DMSO-d_6): δ 12.90 (s, 1H, NH^+), 12.18 (s, 1H, NH^+), 11.16 (s, 1H, NH), 8.10–8.05 (m, 1H, Ar–H), 7.80–7.76 (m, 1H, Ar–H), 7.63 (s, 2H, NH_2), 7.53–7.42 (m, 4H, Ar–H), 7.29 (s, 1H, imidaz-H); ^{13}C NMR (100 MHz, DMSO-d_6): δ 153.30, 148.41, 138.77, 138.69, 130.11, 128.94, 126.53, 123.02, 121.35, 120.50, 116.59, 110.14, 107.45 ppm; MS (ESI): *m/z* (%) = 268.8 ([MH - 2Cl]$^+$); 309.8 ([MH – 2Cl + CH_3CN]$^+$); HRMS for $C_{13}H_{12}N_6O$: [M+H]$^+$ calculated: 269.11454, found: 269.11426; HPLC (10–90 % MeOH in 0.1 % TFA in 11 min, UPLC): t_r 3.153 min (97 % at 254 nm, 97 % at 280 nm).

2-Amino-5-(3-(picolinamido)phenyl)-1*H*-imidazole-3-ium chloride (8h). Synthesized according to General procedure D. Yellow solid; yield: 98 % (61 mg); ^{1}H NMR (400 MHz, DMSO-d_6): δ 13.01 (s, 1H, imidaz-NH), 12.27 (s, 1H, NH^+), 10.69 (s, 1H, NH), 8.79–8.74 (m, 1H, Ar–H), 8.22–8.08 (m, 3H, Ar–H), 7.90–7.84 (m, 1H, Ar–H), 7.82–7.39 (m, 5H, Ar–H, NH_2), 7.35 (s, 1H, imidaz-H); ^{13}C NMR (100 MHz, DMSO-d_6): δ 162.94, 149.95, 148.92, 148.33, 139.23, 138.85, 129.90, 128.72, 127.65, 126.68, 122.90, 120.47, 116.68, 110.05 ppm; MS (ESI): *m/z* (%) = 279.8 ([MH - Cl]$^+$); 320.9 ([MH – Cl + CH_3CN]$^+$); HRMS for $C_{15}H_{13}N_5O$: [M+H]$^+$ calculated: 280.11929, found: 280.11920; HPLC (10–90 % MeOH in 0.1 % TFA in 11 min, UPLC): t_r 4.793 min (99 % at 254 nm, 99 % at 280 nm).

2-Amino-5-(3-(nicotinamido)phenyl)-1*H*-imidazole-3-ium chloride (8i). Synthesized according to General procedure D. Pale-yellow solid; yield: 85 % (71 mg); ^{1}H NMR (400 MHz, DMSO-d_6): δ 13.01 (s, 1H, imidaz-NH), 12.26 (s, 1H, NH^+), 11.07 (s, 1H, NH), 9.43–9.34 (m, 1H, Ar–H), 9.00–8.92 (m, 1H, Ar–H), 8.83–8.75 (m, 1H, Ar–H), 8.18–8.03 (m, 1H, Ar–H), 7.98–7.89 (m, 1H, Ar–H), 7.74–7.67 (m, 1H, Ar–H), 7.65–7.33 (m, 4H, Ar–H, NH_2), 7.31 (s, 1H, imidaz-H); ^{13}C NMR (100 MHz, DMSO-d_6): δ 162.98, 148.39, 145.58, 140.87, 140.78, 139.56, 132.25, 129.89, 128.72, 126.66, 125.87, 121.01, 120.93, 117.05, 110.02 ppm; MS (ESI): *m/z* (%) = 279.7 ([MH - Cl]$^+$); 320.7 ([MH – Cl + CH_3CN]$^+$); HRMS for $C_{15}H_{13}N_5O$: [M+H]$^+$ calculated: 280.11929, found: 280.11913; HPLC (10–90 % MeOH in 0.1 % TFA in 11 min, UPLC): t_r 2.997 min (96 % at 254 nm, 95 % at 280 nm).

2-Amino-5-(3-(isonicotinamido)phenyl)-1*H*-imidazole-3-ium chloride (8j). Synthesized according to General procedure D. Orange solid; yield: 81 % (67 mg); ^{1}H NMR (400 MHz, DMSO-d_6): δ 13.00 (s, 1H, imidaz-H), 12.26 (s, 1H, NH^+), 11.11 (s, 1H, NH), 9.00 (dd, J = 4.9, 1.5 Hz, 2H, pyrid-H), 8.28 (d, J = 4.9 Hz, 2H, pyrid-H), 8.17–8.07 (m, 1H, Ar–H), 7.76–7.64 (m, 1H, Ar–H), 7.62–7.38 (m, 4H, Ar–H, NH_2), 7.33 (s, 1H, imidaz-H); ^{13}C NMR (100 MHz, DMSO-d_6): δ 163.29, 148.39, 146.88, 146.01, 139.32, 129.92, 128.75, 126.63, 124.12, 121.18, 117.24, 110.09 ppm; MS (ESI): *m/z* (%) = 279.7 ([MH - Cl]$^+$); 320.8 ([MH – Cl + CH_3CN]$^+$); HRMS for $C_{15}H_{13}N_5O$: [M+H]$^+$ calculated: 280.11929, found: 280.11899; HPLC (10–90 % MeOH in 0.1 % TFA in 11 min, UPLC): t_r 2.853 min (100 % at 254 nm, 100 % at 280 nm).

General procedure E. Syntheses of compounds 11a-t (with 11a as an example). To a solution of compound **10a** (796 mg, 5.85 mmol) in acetonitrile (25 mL), K_2CO_3 (1.62 g, 11.70 mmol) and compound **9a** (695 μL, 5.85 mmol) were added. The reaction mixture was stirred at 70 °C for 15h. Then the solvent was evaporated in vacuo, the residue dissolved in ethyl acetate (50 mL), and washed successively with saturated aqueous $NaHCO_3$ solution (2 × 30 mL), water (2 × 30 mL), and brine (2 × 30 mL). The organic phase was dried over Na_2SO_4, filtered and the solvent evaporated under reduced pressure to afford **11a** as white solid.

1-(4-(Benzyloxy)phenyl)ethan-1-one (11a). Synthesized according to General procedure E. White solid; yield: 89 % (1.18 g); ^{1}H NMR (400 MHz, DMSO-d_6): δ 7.95–7.91 (m, 2H, Ar–H), 7.49–7.32 (m, 5H, Ar–H), 7.12 (m, 2H, Ar–H), 5.21 (s, 2H, Ar–CH_2–O), 2.51 (s, 3H, CO–CH_3); MS (ESI) *m/z* (%) = 227.2 ([M + H]$^+$).

1-(4-((4-(Trifluoromethyl)benzyl)oxy)phenyl)ethan-1-one (11b). Synthesized according to General procedure E. White solid; yield: 98 % (1.69 g); ^{1}H NMR (400 MHz, DMSO-d_6): δ 7.97–7.91 (m, 2H, Ar–H), 7.80–7.75 (m, 2H, Ar–H), 7.71–7.67 (m, 2H, Ar–H), 7.16–7.11 (m, 2H, Ar–H), 5.34 (s, 2H, Ar–CH_2–O), 2.52 (s, 3H, CO–CH_3); MS (ESI) *m/z* (%) = 295.2 ([M + H]$^+$); 336.2 ([MH + CH_3CN]$^+$).

1-(4-((3-(Trifluoromethyl)benzyl)oxy)phenyl)ethan-1-one (11c). Synthesized according to General procedure E. White solid; yield:

86 % (1.11 g); ^{1}H NMR (400 MHz, DMSO-d_6): δ 7.98–7.92 (m, 2H, Ar–H), 7.88–7.82 (m, 1H, Ar–H), 7.81–7.76 (m, 1H, Ar–H), 7.75–7.70 (m, 1H, Ar–H), 7.68–7.62 (m, 1H, Ar–H), 7.18–7.11 (m, 1H, Ar–H), 5.33 (s, 2H, Ar–CH_2–O), 2.52 (s, 3H, CO–CH_3); MS (ESI) *m/z* (%) = 294.5 ([M + H]$^+$); 335.5 ([MH + CH_3CN]$^+$).

1-(4-((4-(Trifluoromethoxy)benzyl)oxy)phenyl)ethan-1-one (11d). Synthesized according to General procedure E. White solid; yield: 80 % (972 mg); ^{1}H NMR (400 MHz, DMSO-d_6): δ 7.96–7.92 (m, 2H, Ar–H), 7.62–7.57 (m, 2H, Ar–H), 7.43–7.38 (m, 2H, Ar–H), 7.15–7.10 (m, 2H, Ar–H), 5.25 (s, 2H, Ar–CH_2–O), 2.52 (s, 3H, CO–CH_3); MS (ESI) *m/z* (%) = 333.0 ([M + Na]$^+$).

1-(4-((4-Chlorobenzyl)oxy)phenyl)ethan-1-one (11e). Synthesized according to General procedure E. White solid; yield: 85 % (825 mg); ^{1}H NMR (400 MHz, DMSO-d_6): δ 0.97–7.90 (m, 2H, Ar–H), 7.54–7.43 (m, 4H, Ar–H), 7.15–7.07 (m, 2H, Ar–H), 5.22 (s, 2H, Ar–CH_2–O), 2.50 (s, 3H, CO–CH_3); MS (ESI) *m/z* (%) = 261.0 ([M + H]$^+$); 302.0 ([MH + CH_3CN]$^+$).

1-(4-((3-Chlorobenzyl)oxy)phenyl)ethan-1-one (11f). Synthesized according to General procedure E. White solid; yield: 97 % (1.87 g); ^{1}H NMR (400 MHz, DMSO-d_6): δ 7.97–7.91 (m, 2H, Ar–H), 7.57–7.91 (m, 1H, Ar–H), 7.45–7.39 (m, 3H, Ar–H), 7.15–7.09 (m, 2H, Ar–H), 5.23 (s, 2H, Ar–CH_2–O), 2.52 (s, 3H, CO–CH_3); MS (ESI) *m/z* (%) = 261.0 ([M + H]$^+$); 302.1 ([MH + CH_3CN]$^+$).

1-(4-((2,6-Difluorobenzyl)oxy)phenyl)ethan-1-one (11g). Synthesized according to General procedure E. White solid; yield: 95 % (1.47 g); ^{1}H NMR (400 MHz, DMSO-d_6): δ 7.98–7.93 (m, 2H, Ar–H), 7.60–7.50 (m, 1H, Ar–H), 7.24–7.13 (m, 4H, Ar–H), 5.22 (s, 2H, Ar–CH_2–O), 2.53 (s, 3H, CO–CH_3); MS (ESI) *m/z* (%) = 263.1 ([M + H]$^+$); 304.2 ([MH + CH_3CN]$^+$).

1-(4-((2,4,5-Trifluorobenzyl)oxy)phenyl)ethan-1-one (11h). Synthesized according to General procedure E. White solid; yield: 93 % (1.53 g); ^{1}H NMR (400 MHz, DMSO-d_6): δ 8.01–7.91 (m, 2H, Ar–H), 7.81–7.58 (m, 2H, Ar–H), 7.20–7.11 (m, 2H, Ar–H), 5.20 (s, 2H, Ar–CH_2–O), 2.53 (s, 3H, CO–CH_3); MS (ESI) *m/z* (%) = 263.1 ([M + H]$^+$); 304.2 ([MH + CH_3CN]$^+$).

1-(3-((4-Fluorobenzyl)oxy)phenyl)ethan-1-one (11i). Synthesized according to General procedure E. Pale-yellow oil; yield: 70 % (751 mg); ^{1}H NMR (400 MHz, DMSO-d_6): δ 7.59–7.51 (m, 4H, Ar–H), 7.47 (t, J = 8.0 Hz, 1H, Ar–H), 7.30 (ddd, J = 8.2, 2.7, 1.0 Hz, 1H, Ar–H), 7.27–7.20 (m, 2H, Ar–H), 5.17 (s, 2H, Ar–CH_2–O), 2.58 (s, 3H, CO–CH_3); MS (ESI) *m/z* (%) = 245.0 ([M + H]$^+$); 302.1 ([MH + CH_3CN]$^+$).

1-(3-((4-(Trifluoromethyl)benzyl)oxy)phenyl)ethan-1-one (11j). Synthesized according to General procedure E. Yellow oil; yield: 88 % (1.90 g); ^{1}H NMR (400 MHz, DMSO-d_6): δ 7.85–7.65 (m, 4H, Ar–H), 7.65–7.52 (m, 2H, Ar–H), 7.47 (t, J = 7.9 Hz, 1H, Ar–H), 7.34–7.29 (m, 1H, Ar–H), 5.31 (s, 2H, Ar–CH_2–O), 2.58 (s, 3H, CO–CH_3); MS (ESI) *m/z* (%) = 295.2 ([M + H]$^+$).

1-(3-((3-(Trifluoromethyl)benzyl)oxy)phenyl)ethan-1-one (11k). Synthesized according to General procedure E. Yellow oil; yield: 88 % (1.14 g); ^{1}H NMR (400 MHz, DMSO-d_6): δ 7.87–7.83 (m, 1H, Ar–H), 7.80–7.77 (m, 1H, Ar–H), 7.75–7.63 (m, 2H, Ar–H), 7.61–7.55 (m, 2H, Ar–H), 7.47 (t, J = 7.9 Hz, 1H, Ar–H), 7.32 (ddd, J = 8.2, 2.7, 1.0 Hz, 1H, Ar–H), 5.30 (s, 2H, Ar–CH_2–O), 2.58 (s, 3H, CO–CH_3); MS (ESI) *m/z* (%) = 295.0 ([M + H]$^+$).

1-(3-((4-(Trifluoromethoxy)benzyl)oxy)phenyl)ethan-1-one (11l). Synthesized according to General procedure E. Pale-yellow oil; yield: 78 % (1.42 g); ^{1}H NMR (400 MHz, DMSO-d_6): δ 7.64–7.53 (m, 4H, Ar–H), 7.46 (t, J = 7.9 Hz, 1H, Ar–H), 7.40 (d, J = 7.9 Hz, 2H, Ar–H), 7.30 (ddd, J = 8.2, 2.6, 0.9 Hz, 1H, Ar–H), 5.22 (s, 2H, Ar–CH_2–O), 2.58 (s, 3H, CO–CH_3); MS (ESI) *m/z* (%) = 311.2 ([M + H]$^+$); 352.1 ([MH + CH_3CN]$^+$).

1-(4-((3-Chlorobenzyl)oxy)phenyl)ethan-1-one (11m). Synthesized according to General procedure E. Pale-yellow oil; yield: 96 % (919 mg); ^{1}H NMR (400 MHz, DMSO-d_6): δ 7.60–7.53 (m, 3H, Ar–H), 7.49–7.39 (m, 4H, Ar–H), 7.30 (ddd, J = 8.2, 2.7, 0.9 Hz, 1H, Ar–H), 5.20 (s, 2H, Ar–CH_2–O), 2.58 (s, 3H, CO–CH_3); MS (ESI) *m/z* (%) = 260.6 ([M + H]$^+$).

1-(3-((3-Methylbenzyl)oxy)phenyl)ethan-1-one (11n). Synthesized according to General procedure E. Orange oil; yield: 82 % (1.05 g); ^{1}H NMR (400 MHz, DMSO-d_6): δ 7.58–7.51 (m, 2H, Ar–H), 7.45 (t, J = 7.9 Hz, 1H, Ar–H), 7.31–7.22 (m, 4H, Ar–H), 7.17–7.13 (m, 1H, Ar–H), 5.13 (s, 2H, Ar–CH_2–O), 2.57 (s, 3H, CO–CH_3), 2.32 (s, 3H, Ar-CH_3); MS (ESI) *m/z* (%) = 282.1 ([MH + CH_3CN]$^+$).

1-(3-((2,6-Difluorobenzyl)oxy)phenyl)ethan-1-one (11o). Synthesized according to General procedure E. Pale-yellow oil; yield: 91 % (1.40 g); ^{1}H NMR (400 MHz, DMSO-d_6): δ 7.61–7.45 (m, 4H, Ar–H), 7.34–7.29 (m, 1H, Ar–H), 7.24–7.16 (m, 2H, Ar–H), 5.20 (s, 2H, Ar–CH_2–O), 2.58 (s, 3H, CO–CH_3); MS (ESI) *m/z* (%) = 263.2 ([M + H]$^+$).

1-(3-((2,4,5-Trifluorobenzyl)oxy)phenyl)ethan-1-one (11p). Synthesized according to General procedure E. White solid; yield: 98 % (1.61 g); ^{1}H NMR (400 MHz, DMSO-d_6): δ 7.79–7.69 (m, 1H, Ar–H), 7.69–7.54 (m, 3H, Ar–H), 7.48 (t, J = 7.9 Hz, 1H, Ar–H), 7.32 (ddd, J = 8.2, 2.6, 0.8 Hz, 1H, Ar–H), 5.18 (s, 2H, Ar–CH_2–O), 2.58 (s, 3H, CO–CH_3); MS (ESI) *m/z* (%) = 281.3 ([M + H]$^+$).

1-(3-((4-Chloro-3-(trifluoromethyl)benzyl)oxy)phenyl)ethan-1-one (11q). Synthesized according to General procedure E. Orange oil; yield: 81 % (1.57 g); ^{1}H NMR (400 MHz, DMSO-d_6): δ 7.99–7.97 (m, 1H, Ar–H), 7.82–7.76 (m, 2H, Ar–H), 7.61–7.54 (m, 2H, Ar–H), 7.48 (t, J = 7.9 Hz, 1H, Ar–H), 7.32 (ddd, J = 8.2, 2.6, 0.9 Hz, 1H, Ar–H), 5.29 (s, 2H, Ar–CH_2–O), 2.58 (s, 3H, CO–CH_3); MS (ESI) *m/z* (%) = 370.0 ([MH + CH_3CN]$^+$).

1-(4-Phenethoxyphenyl)ethan-1-one (11r). Synthesized according to General procedure E. Orange oil; yield: 68 % (1.21 g); ^{1}H NMR (400 MHz, DMSO-d_6): δ 8.00–7.85 (m, 2H, Ar–H), 7.40–7.29 (m, 4H, Ar–H), 7.29–7.18 (m, 1H, Ar–H), 7.09–6.99 (m, 2H, Ar–H), 4.29 (t, J = 6.9 Hz, 2H, CH_2–O), 3.06 (t, J = 6.9 Hz, 2H, Ar-CH_2), the signal for CO–CH_3 overlapped with the signal for DMSO-d_6; MS (ESI) *m/z* (%) = 241.2 ([M + H]$^+$).

1-(3-Phenethoxyphenyl)ethan-1-one (11s). Synthesized according to General procedure E. Yellow oil; yield: 40 % (557 mg); ^{1}H NMR (400 MHz, DMSO-d_6): δ 7.56–7.52 (m, 1H, Ar–H), 7.45–7.40 (m, 2H, Ar–H), 7.37–7.30 (m, 4H, Ar–H), 7.26–7.20 (m, 2H, Ar–H), 4.27 (t, J = 6.8 Hz, 2H, CH_2–O), 3.06 (t, J = 6.8 Hz, 2H, Ar-CH_2), 2.57 (s, 3H, CO–CH_3); MS (ESI) *m/z* (%) = 240.8 ([M + H]$^+$).

1-(3-(4-Fluorophenethoxy)phenyl)ethan-1-one (11t). Synthesized according to General procedure E. Brown solid; yield: 45 % (1.72 g); ^{1}H NMR (400 MHz, DMSO-d_6): δ 7.56–7.52 (m, 1H, Ar–H), 7.45–7.35 (m, 4H, Ar–H), 7.23–7.11 (m, 3H, Ar–H), 4.24 (t, J = 6.8 Hz, 2H, CH_2–O), 3.05 (t, J = 6.7 Hz, 2H, Ar-CH_2), 2.56 (s, 3H, CO–CH_3); MS (ESI) *m/z* (%) = 299.8 ([MH + CH_3CN]$^+$).

General procedure F. Syntheses of compounds 12a-t (with 12a as an example). To a suspension of compound **11a** (1.15 g, 5.07 mmol) in anhydrous DCM (15 mL), a solution of Br_2 (261 μL, 5.07 mmol) in anhydrous DCM (5 mL) and anhydrous MeOH (2 mL) was added dropwise at 0 °C. The reaction mixture was stirred at rt for 3 h under argon atmosphere. Then the reaction was quenched with cold water (20 mL) and saturated aqueous $Na_2S_2O_3$ solution (20 mL) was added. The product was extracted with DCM (100 mL) and the organic layer was washed with saturated aqueous $Na_2S_2O_3$ solution (4 × 50 mL) and with brine (2 × 100 mL), dried over Na_2SO_4 and filtered. The solvent was evaporated under reduced pressure and the crude product was purified by flash column chromatography using DCM/PE 1:2 and then DCM/PE 2:1 (gradient elution) as mobile phases to afford **12a** as a white solid, which was used in the next step without further purification.

1-(4-(Benzyloxy)phenyl)-2-bromoethan-1-one (12a). Synthesized according to General procedure F. White solid; yield: 47 % (723 mg); used in the next step without further purification.

2-Bromo-1-(4-((4-(trifluoromethyl)benzyl)oxy)phenyl)ethan-1-one (12b). Synthesized according to General procedure F. White solid; yield: 60 % (1.22 g); ^{1}H NMR (400 MHz, DMSO-d_6): δ 8.03–7.98 (m, 2H, Ar–H), 7.82–7.75 (m, 2H, Ar–H), 7.72–7.67 (m, 2H, Ar–H), 7.20–7.14

(m, 2H, Ar–H), 5.37 (s, 1H, Ar–CH_2–O), 4.85 (s, 1H, CH_2–Br); MS (ESI) *m/z* (%) = 371.0 ([M − H]$^-$).

2-Bromo-1-(4-((3-(trifluoromethyl)benzyl)oxy)phenyl)ethan-1-one (12c). Synthesized according to General procedure F. Yellow solid; yield: 57 % (775 mg); ^{1}H NMR (400 MHz, DMSO-d_6): δ 8.03–7.98 (m, 2H, Ar–H), 7.86–7.64 (m, 4H, Ar–H), 7.21–7.16 (m, 2H, Ar–H), 5.36 (s, 2H, Ar–CH_2–O), 4.86 (s, 1H, CH_2–Br); MS (ESI) *m/z* (%) = 413.2 ([MH + CH_3CN]$^+$).

2-Bromo-1-(4-((4-(trifluoromethoxy)benzyl)oxy)phenyl)ethan-1-one (12d). Synthesized according to General procedure F. Light-brown solid; yield: 60 % (564 mg); ^{1}H NMR (400 MHz, DMSO-d_6): δ 8.05–7.88 (m, 2H, Ar–H), 7.66–7.56 (m, 2H, Ar–H), 7.46–7.35 (m, 2H, Ar–H), 7.27–7.09 (m, 2H, Ar–H), 5.28 (s, 2H, Ar–CH_2–O), 4.85 (s, 2H, CH_2–Br); MS (ESI) *m/z* (%) = 371.9 ([M + H]$^+$).

2-Bromo-1-(4-((4-chlorobenzyl)oxy)phenyl)ethan-1-one (12e). Synthesized according to General procedure F. White solid; yield: 63 % (521 mg); ^{1}H NMR (400 MHz, DMSO-d_6): δ 8.02–8.07 (m, 2H, Ar–H), 7.52–7.45 (m, 4H, Ar–H), 7.18–7.11 (m, 2H, Ar–H), 5.23 (s, 2H, Ar–CH_2–O), 4.85 (s, 2H, CH_2–Br); MS (ESI) *m/z* (%) = 339.0 ([M + H]$^+$).

2-Bromo-1-(4-((3-chlorobenzyl)oxy)phenyl)ethan-1-one (12f). Synthesized according to General procedure F. White solid; yield: 55 % (1.30 g); ^{1}H NMR (400 MHz, DMSO-d_6): δ 8.02–8.07 (m, 2H, Ar–H), 7.52–7.45 (m, 4H, Ar–H), 7.18–7.11 (m, 2H, Ar–H), 5.23 (s, 2H, Ar–CH_2–O), 4.85 (s, 2H, CH_2–Br); MS (ESI) *m/z* (%) = 339.0 ([M + H]$^+$).

2-Bromo-1-(4-((2,6-difluorobenzyl)oxy)phenyl)ethan-1-one (12g). Synthesized according to General procedure F. White solid; yield: 53 % (987 mg); ^{1}H NMR (400 MHz, DMSO-d_6): δ 8.04–7.99 (m, 2H), 7.58–7.52 (m, 1H), 7.24–7.18 (m, 4H), 5.25 (s, 2H, Ar–CH_2–O), 4.87 (s, 2H, CH_2–Br); MS (ESI) *m/z* (%) = 340.9 ([M + H]$^+$).

2-Bromo-1-(4-((2,4,5-trifluorobenzyl)oxy)phenyl)ethan-1-one (12h). Synthesized according to General procedure F. White solid; yield: 62 % (1.21 g); ^{1}H NMR (400 MHz, DMSO-d_6): δ 8.04–7.97 (m, 2H, Ar–H), 7.80–7.72 (m, 1H, Ar–H), 7.70–7.61 (m, 1H, Ar–H), 7.22–7.16 (m, 2H, Ar–H), 5.22 (s, 2H, Ar–CH_2–O), 4.86 (s, 2H, CH_2–Br); MS (ESI) *m/z* (%) = 399.1 ([MH + CH_3CN]$^+$).

2-Bromo-1-(3-((4-fluorobenzyl)oxy)phenyl)ethan-1-one (12i). Synthesized according to General procedure F. White solid; yield: 47 % (480 mg); ^{1}H NMR (400 MHz, DMSO-d_6): δ 8.63–7.57 (m, 2H, Ar–H), 7.56–7.46 (m, 3H, Ar–H), 7.33 (ddd, *J* = 8.2, 2.5, 1.0 Hz, 1H, Ar–H), 7.27–7.21 (m, 2H, Ar–H), 5.17 (s, 2H, Ar–CH_2–O), 4.94 (s, 2H, CH_2–Br); MS (ESI) *m/z* (%) = 323.4 ([M + H]$^+$).

2-Bromo-1-(3-((4-(trifluoromethyl)benzyl)oxy)phenyl)ethan-1-one (12j). Synthesized according to General procedure F. White solid; yield: 45 % (1.07 g); ^{1}H NMR (400 MHz, DMSO-d_6): δ 7.81–7.59 (m, 6H, Ar–H), 7.50 (t, *J* = 7.9 Hz, 1H, Ar–H), 7.38–7.33 (m, 1H, Ar–H), 5.32 (s, 2H, Ar–CH_2–O), 4.94 (s, 2H, CH_2–Br); MS (ESI) *m/z* (%) = 371.3 ([M − H]$^-$).

2-Bromo-1-(3-((3-(trifluoromethyl)benzyl)oxy)phenyl)ethan-1-one (12k). Synthesized according to General procedure F. White solid; yield: 49 % (916 mg); ^{1}H NMR (400 MHz, DMSO-d_6): δ 7.87–7.83 (m, 1H, Ar–H), 7.82–7.77 (m, 1H, Ar–H), 7.76–7.69 (m, 1H, Ar–H), 7.79–7.59 (m, 3H, Ar–H), 7.53–7.48 (m, 1H, Ar–H), 7.37 (ddd, *J* = 8.3, 2.5, 1.1 Hz, 1H, Ar–H), 5.31 (s, 2H, Ar–CH_2–O), 4.94 (s, 2H, CH_2–Br); MS (ESI) *m/z* (%) = 370.8 ([M − H]$^-$).

2-Bromo-1-(3-((4-(trifluoromethoxy)benzyl)oxy)phenyl)ethan-1-one (12l). Synthesized according to General procedure F. White solid; yield: 45 % (801 mg); ^{1}H NMR (400 MHz, DMSO-d_6): δ 7.65–7.57 (m, 4H, Ar–H), 7.49 (t, *J* = 7.9 Hz, 1H, Ar–H), 7.43–7.38 (m, 2H, Ar–H), 7.34 (ddd, *J* = 8.2, 2.6, 0.9 Hz, 1H, Ar–H), 5.23 (s, 2H, Ar–CH_2–O), 4.94 (s, 2H, CH_2–Br); MS (ESI) *m/z* (%) = 389.0 ([M + H]$^+$).

2-Bromo-1-(4-((3-chlorobenzyl)oxy)phenyl)ethan-1-one (12m). Synthesized according to General procedure F. Pale-yellow solid; yield: 45 % (495 mg); ^{1}H NMR (400 MHz, DMSO-d_6): δ 7.64–7.58 (m, 2H, Ar–H), 7.57–7.54 (m, 1H, Ar–H), 7.49 (t, *J* = 7.9 Hz, 1H, Ar–H), 7.46–7.40 (m, 3H, Ar–H), 7.34 (ddd, *J* = 8.2, 2.6, 0.9 Hz, 1H, Ar–H), 5.21 (s, 2H, Ar–CH_2–O), 4.95 (s, 2H, CH_2–Br); MS (ESI) *m/z* (%) = 338.8 ([M + H]$^+$).

2-Bromo-1-(3-((3-methylbenzyl)oxy)phenyl)ethan-1-one (12n). Synthesized according to General procedure F. Pale-yellow oil; yield: 45 % (605 mg); ^{1}H NMR (400 MHz, DMSO-d_6): δ 7.65–7.10 (m, 8H, Ar–H), 5.20–5.11 (s, 2H, Ar–CH_2–O), 4.94 (s, 2H, CH_2–Br), 2.32 (s, 3H, Ar-CH_3); MS (ESI) *m/z* (%) = 317.2 ([M − H]$^-$).

2-Bromo-1-(3-((2,6-difluorobenzyl)oxy)phenyl)ethan-1-one (12o). Synthesized according to General procedure F. White solid; yield: 49 % (856 mg); ^{1}H NMR (400 MHz, DMSO-d_6): δ 7.66–7.48 (m, 4H, Ar–H), 7.39–7.33 (m, 1H, Ar–H), 7.24–7.16 (m, 2H, Ar–H), 5.21 (s, 2H, Ar–CH_2–O), 4.96 (s, 2H, CH_2–Br); MS (ESI) *m/z* (%) = 381.2 ([MH + CH_3CN]$^+$).

2-Bromo-1-(3-((2,4,5-trifluorobenzyl)oxy)phenyl)ethan-1-one (12p). Synthesized according to General procedure F. White solid; yield: 64 % (1.28 g); ^{1}H NMR (400 MHz, DMSO-d_6): δ 7.79–7.72 (m, 1H, Ar–H), 7.68–7.60 (m, 3H, Ar–H), 7.51 (t, *J* = 8.0 Hz, 1H, Ar–H), 7.39–7.34 (m, 1H, Ar–H), 5.19 (s, 2H, Ar–CH_2–O), 4.95 (s, 2H, CH_2–Br); MS (ESI) *m/z* (%) = 359.0 ([M + H]$^+$).

2-Bromo-1-(3-((4-chloro-3-(trifluoromethyl)benzyl)oxy) phenyl)ethan-1-one (12q). Synthesized according to General procedure F. White solid; yield: 58 % (1.13 g); ^{1}H NMR (400 MHz, DMSO-d_6): δ 8.00–7.96 (m, 1H, Ar–H), 7.83–7.76 (m, 2H, Ar–H), 7.65–7.59 (m, 2H, Ar–H), 7.50 (t, *J* = 7.9 Hz, 1H, Ar–H), 7.37 (ddd, *J* = 8.3, 2.7, 0.9 Hz, 1H, Ar–H), 5.30 (s, 2H, Ar–CH_2–O), 4.94 (s, 2H, CH_2–Br); MS (ESI) *m/z* (%) = 407.2 ([M + H]$^+$).

2-Bromo-1-(4-phenethoxyphenyl)ethan-1-one (12r). Synthesized according to General procedure F. Orange oil; yield: 50 % (769 mg); ^{1}H NMR (400 MHz, DMSO-d_6): δ 8.20–7.88 (m, 2H, Ar–H), 7.48–7.18 (m, 5H, Ar–H), 7.22–6.96 (m, 2H, Ar–H), 4.84 (s, 2H, CH_2–Br), 4.32 (t, *J* = 6.9 Hz, 2H, CH_2–O), 3.08 (t, *J* = 6.9 Hz, 2H, Ar-CH_2); MS (ESI) *m/z* (%) = 319.1 ([M − H]$^-$).

2-Bromo-1-(3-phenethoxyphenyl)ethan-1-one (12s). Synthesized according to General procedure F. Pale-yellow oil; yield: 55 % (269 mg); ^{1}H NMR (400 MHz, DMSO-d_6): δ 7.60–7.55 (m, 1H, Ar–H), 7.51–7.48 (m, 1H, Ar–H), 7.45 (t, *J* = 7.9 Hz, 1H, Ar–H), 7.36–7.29 (m, 4H, Ar–H), 7.28–7.20 (m, 2H, Ar–H), 4.95 (s, 2H, CH_2–Br), 4.27 (t, *J* = 6.9 Hz, 2H, CH_2–O), 3.06 (t, *J* = 6.9 Hz, 2H, Ar-CH_2); MS (ESI) *m/z* (%) = 319.1 ([M + H]$^+$).

2-Bromo-1-(3-(4-fluorophenethoxy)phenyl)ethan-1-one (12t). Synthesized according to General procedure F. White solid; yield: 52 % (655 mg); ^{1}H NMR (400 MHz, DMSO-d_6): δ 7.60–7.56 (m, 1H, Ar–H), 7.50–7.48 (m, 1H, Ar–H), 7.45 (t, *J* = 7.9 Hz, 1H, Ar–H), 7.40–7.34 (m, 2H, Ar–H), 7.28–7.23 (m, 1H, Ar–H), 7.18–7.10 (m, 2H, Ar–H), 4.95 (s, 2H, CH_2–Br), 4.25 (t, *J* = 6.8 Hz, 2H, CH_2–O), 3.06 (t, *J* = 6.8 Hz, 2H, Ar-CH_2); MS (ESI) *m/z* (%) = 377.7 ([MH + CH_3CN]$^+$).

General procedure G. Syntheses of compounds 13a-t (with 13a as an example). To a solution of compound **12a** (720 mg, 2.36 mmol) in acetonitrile (10 mL) 2-aminopyrimidine (187 mg, 1.97 mmol) and 4-dimethylaminopyridine (2.40 mg, 0.02 mmol) were added. The reaction mixture was stirred at 85 °C for 15 h. The resulting suspension was cooled on an ice bath and the solid was filtered off, washed with acetonitrile and diethyl ether (x 3) and dried to give **13a** as a pink solid.

2-(4-(Benzyloxy)phenyl)-1*H*-imidazo[1,2-*a*]pyrimidin-4-ium bromide (13a). Synthesized according to General procedure G. Purple solid; yield: 50 % (372 mg); ^{1}H NMR (400 MHz, DMSO-d_6): δ 9.25–9.19 (m, 1H, pyrimidin-H), 8.93–8.86 (m, 1H, pyrimidin-H), 8.58 (s, 1H, imidaz-H), 8.00–7.91 (m, 2H, Ar–H), 7.57–7.32 (m, 6H, Ar–H), 7.28–7.19 (m, 2H, Ar–H), 5.22 (s, 2H, Ar–CH_2–O); HRMS for $C_{19}H_{16}N_3O$: [M+H]$^+$ calculated: 302.12872, found: 302.12802.

2-(4-((4-(Trifluoromethyl)benzyl)oxy)phenyl)-1*H*-imidazo[1,2-*a*]pyrimidin-4-ium bromide (13b). Synthesized according to General procedure G. Pale-pink solid; yield: 52 % (752 mg); ^{1}H NMR (400 MHz, DMSO-d_6): δ 9.24 (dd, *J* = 6.7, 1.7 Hz, 1H, pyrimidin-H), 8.92 (dd, *J* = 4.3, 1.7 Hz, 1H, pyrimidin-H), 8.61 (s, 1H, imidaz-H), 8.01–7.94 (m, 2H, Ar–H), 7.83–7.78 (m, 2H, Ar–H), 7.75–7.68 (m, 2H, Ar–H), 7.58–7.53 (m, 2H, pyrimidin-H), 7.29–7.23 (m, 2H, Ar–H), 5.35 (s, 2H,

Ar–CH_2–O); MS (ESI) *m/z* (%) = 371.0 ([MH - Br]$^+$).

2-(4-((3-(Trifluoromethyl)benzyl)oxy)phenyl)-1*H*-imidazo[1,2-*a*]pyrimidin-4-ium bromide (13c). Synthesized according to General procedure G. Purple solid; yield: 56 % (521 mg); ^{1}H NMR (400 MHz, DMSO-d_6): δ 9.22 (dd, J = 6.7, 1.6 Hz, 1H, pyrimidin-H), 8.93–8.87 (m, 1H, pyrimidin-H), 8.58 (s, 1H, imidaz-H), 8.01–7.95 (m, 2H, Ar–H), 7.88–7.65 (m, 4H, Ar–H), 7.56–7.49 (m, 1H, pyrimidin-H), 7.30–7.23 (m, 2H, Ar–H), 5.33 (s, 2H, Ar–CH_2–O); MS (ESI) *m/z* (%) = 370.6 ([MH - Br]$^+$).

2-(4-((4-(Trifluoromethoxy)benzyl)oxy)phenyl)-1*H*-imidazo[1,2-*a*]pyrimidin-4-ium bromide (13d). Synthesized according to General procedure G. Pink solid; yield: 47 % (252 mg); ^{1}H NMR (400 MHz, DMSO-d_6): δ 9.16–9.13 (m, 1H, pyrimidin-H), 8.82–8.78 (m, 1H, pyrimidin-H), 8.50 (s, 1H, imidaz-H), 7.99–7.92 (m, 2H, Ar–H), 7.65–7.60 (m, 2H, Ar–H), 7.44–7.39 (m, 3H, Ar–H), 7.23–7.19 (m, 2H, Ar–H), 5.24 (s, 2H, Ar–CH_2–O); HRMS for $C_{20}H_{15}F_3N_3O_2$: [M+H]$^+$ calculated: 386.11109, found: 386.11007.

2-(4-((4-Chlorobenzyl)oxy)phenyl)-1*H*-imidazo[1,2-*a*]pyrimidin-4-ium bromide (13e). Synthesized according to General procedure G. Pale-pink solid; yield: 59 % (245 mg); ^{1}H NMR (400 MHz, DMSO-d_6): δ 9.25 (dd, J = 6.8, 1.8 Hz, 1H, pyrimidin-H), 8.94 (dd, J = 4.4, 1.8 Hz, 1H, pyrimidin-H), 8.62 (s, 1H, imidaz-H), 8.03–7.92 (m, 2H, Ar–H), 7.60–7.55 (m, 1H, pyrimidin-H), 7.56–7.45 (m, 4H, Ar–H), 7.31–7.17 (m, 2H, Ar–H), 5.22 (s, 2H, Ar–CH_2–O); MS (ESI) *m/z* (%) = 336.0 ([MH - Br]$^+$); 377.0 ([M − Br + CH_3CN]$^+$).

2-(4-((3-Chlorobenzyl)oxy)phenyl)-1*H*-imidazo[1,2-*a*]pyrimidin-4-ium bromide (13f). Synthesized according to General procedure G. White solid; yield: 85 % (460 Mg); ^{1}H NMR (400 MHz, DMSO-d_6): δ 9.27–9.21 (m, 1H, pyrimidin-H), 8.99–8.88 (m, 1H, pyrimidin-H), 8.61 (s, 1H, imidaz-H), 8.05–7.89 (m, 2H, Ar–H), 7.60–7.39 (m, 5H, Ar–H, pyrimidin-H), 7.29–7.21 (m, 2H, Ar–H), 5.25 (s, 2H, Ar–CH_2–O); MS (ESI) *m/z* (%) = 337.6 ([MH - Br]$^+$).

2-(4-((2,6-Difluorobenzyl)oxy)phenyl)-1*H*-imidazo[1,2-*a*]pyrimidin-4-ium bromide (13g). Synthesized according to General procedure G. Pale-pink solid; yield: 63 % (556 mg); ^{1}H NMR (400 MHz, DMSO-d_6): δ 9.23 (dd, J = 6.7, 1.7 Hz, 1H, pyrimidin-H), 8.91 (dd, J = 4.3, 1.7 Hz, 1H, pyrimidin-H), 8.61 (s, 1H, imidaz-H), 8.01–7.95 (m, 2H, Ar–H), 7.60–7.52 (m, 2H, Ar–H, pyrimidin-H), 7.30–7.17 (m, 4H, Ar–H), 5.23 (s, 2H, Ar–CH_2–O); MS (ESI) *m/z* (%) = 339.0 ([MH - Br]$^+$).

2-(4-((2,4,5-Trifluorobenzyl)oxy)phenyl)-1*H*-imidazo[1,2-*a*]pyrimidin-4-ium bromide (13h). Synthesized according to General procedure G. Pink solid; yield: 65 % (589 mg); ^{1}H NMR (400 MHz, DMSO-d_6): δ 9.22 (dd, J = 6.7, 1.7 Hz, 1H, pyrimidin-H), 8.90 (dd, J = 4.2, 1.7 Hz, 1H, pyrimidin-H), 8.59 (s, 1H, imidaz-H), 8.01–7.94 (m, 2H, Ar–H), 7.81–7.62 (m, 2H, Ar–H), 7.52 (dd, J = 6.7, 4.2 Hz, 1H, pyrimidin-H), 7.30–7.23 (m, 2H, Ar–H), 5.20 (s, 2H, Ar–CH_2–O); MS (ESI) *m/z* (%) = 357.0 ([MH - Br]$^+$).

2-(3-((4-Fluorobenzyl)oxy)phenyl)-1*H*-imidazo[1,2-*a*]pyrimidin-4-ium bromide (13i). Synthesized according to General procedure G. Pink solid; yield: 95 % (218 g); ^{1}H NMR (400 MHz, DMSO-d_6): δ 9.30–9.20 (m, 1H, pyrimidin-H), 9.00–8.87 (m, 1H, pyrimidin-H), 8.72 (s, 1H, imidaz-H), 7.75–7.45 (m, 6H, Ar–H, pyrimidin-H), 7.31–7.15 (m, 3H, Ar–H), 5.21 (s, 2H, Ar–CH_2–O); MS (ESI) *m/z* (%) = 321.3 ([MH - Br]$^+$).

2-(3-((4-(Trifluoromethyl)benzyl)oxy)phenyl)-1*H*-imidazo[1,2-*a*]pyrimidin-4-ium bromide (13j). Synthesized according to General procedure G. Off-white solid; yield: 27 % (276 mg); ^{1}H NMR (400 MHz, DMSO-d_6): δ 9.21 (dd, J = 6.7, 1.8 Hz, 1H, pyrimidin-H), 8.89–8.87 (m, 1H, pyrimidin-H), 8.68 (s, 1H, imidaz-H), 7.82–7.60 (m, 5H, Ar–H), 7.64–7.60 (m, 1H, Ar–H), 7.54–7.45 (m, 2H, Ar–H, pyrimidin-H), 7.18–7.15 (m, 1H, Ar–H), 5.35 (s, 2H, Ar–CH_2–O); HRMS for $C_{20}H_{15}F_3N_3O$: [M+H]$^+$ calculated: 370.11617, found: 370.11531.

2-(3-((3-(Trifluoromethyl)benzyl)oxy)phenyl)-1*H*-imidazo[1,2-*a*]pyrimidin-4-ium bromide (13k). Synthesized according to General procedure G. Pale-pink solid; yield: 85 % (545 mg); ^{1}H NMR (400 MHz, DMSO-d_6): δ 9.16–9.10 (m, 1H, pyrimidin-H), 8.83–8.72 (m, 1H, pyrimidin-H), 8.62 (s, 1H, imidaz-H), 7.90–7.79 (m, 2H, Ar–H), 7.75–7.59 (m, 4H, Ar–H), 7.51–7.44 (m, 1H, pyrimidin-H), 7.41–7.32 (m, 1H, Ar–H), 7.18–7.10 (m, 1H, Ar–H), 5.34 (s, 2H, Ar–CH_2–O); MS (ESI) *m/z* (%) = 371.3 ([MH - Br]$^+$).

2-(3-((4-(Trifluoromethoxy)benzyl)oxy)phenyl)-1*H*-imidazo[1,2-*a*]pyrimidin-4-ium bromide (13l). Synthesized according to General procedure G. Pale-pink solid; yield: 21 % (129 mg); ^{1}H NMR (400 MHz, DMSO-d_6): δ 9.22 (dd, J = 6.7, 1.7 Hz, 1H, pyrimidin-H), 8.89 (dd, J = 4.4, 1.7 Hz, 1H, pyrimidin-H), 8.69 (s, 1H, imidaz-H), 8.53–8.49 (m, 1H, Ar–H), 7.72–7.69 (m, 1H, Ar–H), 7.65–7.59 (m, 3H, Ar–H), 7.53–7.48 (m, 1H, pyrimidin-H), 7.45–7.41 (m, 2H, Ar–H), 7.19–7.14 (m, 1H, Ar–H), 5.26 (s, 2H, Ar–CH_2–O); MS (ESI) *m/z* (%) = 387.1 ([MH - Br]$^+$).

2-(3-((3-Chlorobenzyl)oxy)phenyl)-1*H*-imidazo[1,2-*a*]pyrimidin-4-ium bromide (13m). Synthesized according to General procedure G. Pink solid; yield: 85 % (445 mg); ^{1}H NMR (400 MHz, DMSO-d_6): δ 9.21 (dd, J = 6.7, 1.7 Hz, 1H, pyrimidin-H), 8.89 (dd, J = 4.3, 1.7 Hz, 1H, pyrimidin-H), 8.69 (s, 1H, imidaz-H), 7.73–6.68 (m, 1H, Ar–H), 7.61–7.34 (m, 7H, pyrimidin-H), 7.17–7.13 (m, 1H, Ar–H), 5.25 (s, 2H, Ar–CH_2–O); MS (ESI) *m/z* (%) = 337.5 ([MH - Br]$^+$).

2-(3-((3-Methylbenzyl)oxy)phenyl)-1*H*-imidazo[1,2-*a*]pyrimidin-4-ium bromide (13n). Synthesized according to General procedure G. Dark-pink solid; yield: 52 % (307 mg); ^{1}H NMR (400 MHz, DMSO-d_6): δ 9.18 (dd, J = 6.6, 1.7 Hz, 1H, pyrimidin-H), 8.94–8.77 (m, 1H, pyrimidin-H), 8.66 (s, 1H, imidaz-H), 7.71–7.65 (m, 1H, Ar–H), 7.62–7.57 (m, 1H, Ar–H), 7.52–7.42 (m, 1H, pyrimidin-H), 7.35–7.25 (m, 3H, Ar–H), 7.21–7.10 (m, 3H, Ar–H), 5.18 (s, 2H, Ar–CH_2–O), 2.34 (s, 3H, Ar-CH_3); HRMS for $C_{20}H_{18}N_3O$: [M+H]$^+$ calculated: 316.14444, found: 316.14361.

2-(3-((2,6-Difluorobenzyl)oxy)phenyl)-1*H*-imidazo[1,2-*a*]pyrimidin-4-ium bromide (13o). Synthesized according to General procedure G. Dark-pink solid; yield: 57 % (436 mg); ^{1}H NMR (400 MHz, DMSO-d_6): δ 9.23–9.18 (m, 1H, pyrimidin-H), 8.90–8.88 (m, 1H, pyrimidin-H), 8.68 (s, 1H, imidaz-H), 7.74–7.43 (m, 5H, Ar–H, pyrimidin-H), 7.22–7.16 (m, 3H, Ar–H), 5.24 (s, 2H, Ar–CH_2–O); MS (ESI) *m/z* (%) = 339.1 ([MH - Br]$^+$).

2-(3-((2,4,5-Trifluorobenzyl)oxy)phenyl)-1*H*-imidazo[1,2-*a*]pyrimidin-4-ium bromide (13p). Synthesized according to General procedure G. Pink solid; yield: 45 % (689 mg); ^{1}H NMR (400 MHz, DMSO-d_6): δ 9.29 (dd, J = 6.7, 1.6 Hz, 1H, pyrimidin-H), 8.97 (dd, J = 4.3, 1.6 Hz, 1H, pyrimidin-H), 8.78 (s, 1H, imidaz-H), 7.83–7.52 (m, 6H, Ar–H, pyrimidin-H), 7.26–7.19 (m, 1H, Ar–H), 5.23 (s, 2H, Ar–CH_2–O); MS (ESI) *m/z* (%) = 357.1 ([MH - Br]$^+$).

2-(3-((4-Chloro-3-(trifluoromethyl)benzyl)oxy)phenyl)-1*H*-imidazo[1,2-*a*]pyrimidin-4-ium bromide (13q). Synthesized according to General procedure G. Pale-pink solid; yield: 53 % (588 mg); ^{1}H NMR (400 MHz, DMSO-d_6): δ 9.25 (dd, J = 6.8, 1.8 Hz, 1H, pyrimidin-H), 8.93 (dd, J = 4.4, 1.8 Hz, 1H, pyrimidin-H), 8.73 (s, 1H, imidaz-H), 8.58–8.53 (m, 1H, Ar–H), 8.02–7.98 (m, 1H, Ar–H), 7.85–7. 52 (m, 6H, Ar–H, pyrimidin-H), 7.24–7.16 (m, 1H, Ar–H), 5.33 (s, 2H, Ar–CH_2–O); MS (ESI) *m/z* (%) = 405.3 ([MH - Br]$^+$).

2-(4-Phenethoxyphenyl)-1*H*-imidazo[1,2-*a*]pyrimidin-4-ium bromide (13r). Synthesized according to General procedure G. Purple solid; yield: 41 % (285 mg); ^{1}H NMR (400 MHz, DMSO-d_6): δ 9.28 (dd, J = 6.7, 1.7 Hz, 1H, pyrimidin-H), 8.97 (dd, J = 4.4, 1.7 Hz, 1H, pyrimidin-H), 8.65 (s, 1H, imidaz-H), 7.96–7.93 (m, 2H, Ar–H), 7.63–7.59 (m, 1H, pyrimidin-H), 7.35–7.16 (m, 7H, Ar–H), 4.31 (t, J = 6.9 Hz, 2H, CH_2–O), 3.08 (t, J = 6.8 Hz, 2H, Ar-CH_2); HRMS for $C_{20}H_{18}N_3O$: [M+H]$^+$ calculated: 316.14444, found: 316.14382.

2-(3-Phenethoxyphenyl)-1*H*-imidazo[1,2-*a*]pyrimidin-4-ium bromide (13s). Synthesized according to General procedure G. Pale-pink solid; yield: 46 % (752 mg); ^{1}H NMR (400 MHz, DMSO-d_6): δ 9.22 (dd, J = 6.7, 1.8 Hz, 1H, pyrimidin-H), 8.93 (dd, J = 4.3, 1.7 Hz, 1H, pyrimidin-H), 8.73 (s, 1H, imidaz-H), 7.61–7.45 (m, 4H, Ar–H), 7.39–7.21 (m, 5H, Ar–H, pyrimidin-H), 7.11–7.08 (m, 1H, Ar–H), 4.30 (t, J = 6.9 Hz, 2H, CH_2–O), 3.10 (t, J = 6.9 Hz, 2H, Ar-CH_2); MS (ESI) *m/*

z (%) = 316.8 ([MH - Br]$^+$).

2-(3-(4-Fluorophenethoxy)phenyl)-1*H*-imidazo[1,2-*a*] pyrimidin-4-ium bromide (13t). Synthesized according to General procedure G. Pink solid; yield: 57 % (451 mg); ^{1}H NMR (400 MHz, DMSO-d_6): δ 9.26–9.21 (m, 1H, pyrimidin-H), 8.96–8.90 (m, 1H, pyrimidin-H), 8.74 (s, 1H, imidaz-H), 7.64–7.32 (m, 6H, Ar–H), 7.21–7.04 (m, 3H, Ar–H), 4.28 (t, J = 6.8 Hz, 2H, CH_2–O), 3.10 (t, J = 6.8 Hz, 2H, Ar-CH_2); MS (ESI) *m/z* (%) = 334.9 ([MH - Br]$^+$).

General procedure H. Syntheses of compounds 14a-t (with 14a as an example). To a suspension of **13a** (344 mg, 0.90 mmol) in abs. ethanol (12 mL) in a 30 mL glass vessel, hydrazine hydrate (240 μL, 7.65 mmol, 35 % hydrazine in solution) was added, the vessel was sealed, placed in a microwave reactor, and heated at 120 °C for 80 min. The mixture was cooled to rt, the solvent was evaporated under reduced pressure the crude residue was purified by flash column chromatography using DCM/MeOH/NH_4OH = 20:1:0.1 and then DCM/MeOH/NH_4OH = 9:1:0.1 (gradient elution) as mobile phases, to afford **14a** as a light-brown solid.

5-(4-(Benzyloxy)phenyl)-1*H*-imidazole-2-amine (14a). Synthesized according to General procedure H. Pale-brown solid; yield: 90 % (215 mg); ^{1}H NMR (400 MHz, DMSO-d_6): δ 11.71 (s, 1H, imidaz-NH), 7.57–7.52 (m, 2H, Ar–H), 7.47–7.30 (m, 5H, Ar–H), 7.10–6.99 (m, 3H, imidaz-H, Ar–H), 6.46 (s, 2H, NH_2), 5.12 (s, 2H, Ar–CH_2–O); ^{13}C NMR (100 MHz, DMSO-d_6): δ 157.80, 148.92, 137.49, 129.79, 128.90, 128.31, 128.17, 125.76, 123.84, 115.52, 108.84, 69.71 ppm; HRMS for $C_{16}H_{16}N_3O$: [M+H]$^+$ calculated: 266.12879, found: 266.12804; HPLC (10–90 % MeOH in 0.1 % TFA in 11 min, UPLC): t_r 6.073 min (99 % at 254 nm, 99 % at 280 nm).

5-(4-((4-(Trifluoromethyl)benzyl)oxy)phenyl)-1*H*-imidazole-2-amine (14b). Synthesized according to General procedure H. Off-white solid; yield: 89 % (282 mg); ^{1}H NMR (400 MHz, DMSO-d_6): δ 7.79–7.73 (m, 2H, Ar–H), 7.71–7.64 (m, 2H, Ar–H), 7.54–7.48 (m, 2H, Ar–H), 6.96–6.93 (m, 2H, Ar–H), 6.85 (s, 1H, imidaz-H), 5.31–5.14 (m, 4H, NH_2, Ar–CH_2–O); ^{13}C NMR (100 MHz, DMSO-d_6): δ 156.28, 150.55, 142.72, 128.83, 128.52, 128.40, 126.07, 125.74, 125.07, 123.37, 115.20, 68.72 ppm; MS (ESI): *m/z* (%) = 333.8 ([M + H]$^+$); 374.7 ([MH + CH_3CN]$^+$); HRMS for $C_{17}H_{14}F_3N_3O$: [M+H]$^+$ calculated: 334.11617, found: 334.11516; HPLC (10–90 % MeOH in 0.1 % TFA in 11 min, UPLC): t_r 6.957 min (100 % at 254 nm, 100 % at 280 nm).

5-(4-((3-(Trifluoromethyl)benzyl)oxy)phenyl)-1*H*-imidazole-2-amine (14c). Synthesized according to General procedure H. Pale-yellow solid; yield: 71 % (132 mg); ^{1}H NMR (400 MHz, DMSO-d_6): δ 7.83–7.75 (m, 2H, Ar–H), 7.63–7.71 (m, 2H, Ar–H), 7.57–7.49 (m, 2H, Ar–H), 7.00–6.93 (m, 2H, Ar–H), 6.87 (s, 1H, imidaz-H), 5.34 (s, 2H, NH_2), 5.20 (s, 2H, Ar–CH_2–O); ^{13}C NMR (100 MHz, DMSO-d_6): δ 156.44, 150.38, 139.31, 133.82, 132.08, 130.01, 129.76, 129.45, 128.11, 126.03, 125.13, 124.91, 124.44, 123.32, 115.24, 109.24, 68.74 ppm; MS (ESI): *m/z* (%) = 333.6 ([M + H]$^+$); 374.4 ([MH + CH_3CN]$^+$); HRMS for $C_{17}H_{14}F_3N_3O$: [M+H]$^+$ calculated: 334.11617, found: 334.11577; HPLC (10–90 % MeOH in 0.1 % TFA in 11 min, UPLC): t_r 6.657 min (99 % at 254 nm, 100 % at 280 nm).

5-(4-((4-(Trifluoromethoxy)benzyl)oxy)phenyl)-1*H*-imidazole-2-amine (14d). Synthesized according to General procedure H. Grey solid; yield: 76 % (133 mg); ^{1}H NMR (400 MHz, DMSO-d_6): δ 10.14 (s, 1H, NH), 7.61–7.48 (m, 4H, Ar–H), 7.41–7.36 (m, 2H, Ar–H), 6.98–6.85 (m, 2H, Ar–H), 6.82 (s, 1H, imidaz-H), 5.29–5.16 (m, 2H, NH_2), 5.13 (s, 2H, Ar–CH_2–O); ^{13}C NMR (100 MHz, DMSO-d_6): δ 156.39, 150.56, 148.25, 137.33, 129.96, 125.04, 121.83, 121.50, 119.28, 115.17, 68.69 ppm; HRMS for $C_{17}H_{15}F_3N_3O_2$: [M+H]$^+$ calculated: 350.11109, found: 350.10997; HPLC (10–90 % MeOH in 0.1 % TFA in 11 min, UPLC): t_r 7.047 min (98 % at 254 nm, 100 % at 280 nm).

5-(4-((4-Chlorobenzyl)oxy)phenyl)-1*H*-imidazole-2-amine (14e). Synthesized according to General procedure H. Orange solid; yield: 75 % (277 mg); ^{1}H NMR (400 MHz, DMSO-d_6): δ 7.52–7.45 (m, 6H, Ar–H), 6.95–6.91 (m, 2H, Ar–H), 6.86 (s, 1H, imidaz-H), 5.35 (s, 2H, NH_2), 5.09 (s, 2H, Ar–CH_2–O); ^{13}C NMR (100 MHz, DMSO-d_6): δ 156.40, 150.53, 136.83, 132.76, 129.92, 128.87, 128.37, 125.03, 115.19, 68.75 ppm; MS (ESI): *m/z* (%) = 300.2 ([M + H]$^+$); 341.3 ([MH + CH_3CN]$^+$); HRMS for $C_{16}H_{14}ClN_3O$: [M+H]$^+$ calculated: 300.08982, found: 300.08959; HPLC (10–90 % MeOH in 0.1 % TFA in 11 min, UPLC): t_r 6.627 min (98 % at 254 nm, 99 % at 280 nm).

5-(4-((3-Chlorobenzyl)oxy)phenyl)-1*H*-imidazole-2-amine (14f). Synthesized according to General procedure H. Yellow solid; yield: 73 % (234 mg); ^{1}H NMR (400 MHz, DMSO-d_6): δ 7.53–7.49 (m, 3H, Ar–H), 7.44–7.38 (m, 3H, Ar–H), 6.96–6.92 (m, 2H, Ar–H), 6.86 (s, 1H, imidaz-H), 5.32 (s, 2H, NH_2), 5.11 (s, 2H, Ar–CH_2–O); ^{13}C NMR (100 MHz, DMSO-d_6): δ 156.31, 150.56, 140.40, 133.54, 130.82, 128.12, 127.71, 126.60, 125.03, 115.18, 68.65 ppm; MS (ESI): *m/z* (%) = 300.1 ([M + H]$^+$); 341.2 ([MH + CH_3CN]$^+$); HRMS for $C_{16}H_{14}ClN_3O$: [M+H]$^+$ calculated: 300.08982, found: 300.08924; HPLC (10–90 % MeOH in 0.1 % TFA in 11 min, UPLC): t_r 6.603 min (99 % at 254 nm, 100 % at 280 nm).

5-(4-((2,6-Difluorobenzyl)oxy)phenyl)-1*H*-imidazole-2-amine (14g). Synthesized according to General procedure H. Off-white solid; yield: 83 % (323 mg); ^{1}H NMR (400 MHz, DMSO-d_6): δ 7.57–7.49 (m, 3H, Ar–H), 7.22–7.14 (m, 2H, Ar–H), 7.01–6.90 (m, 2H, Ar–H), 6.86 (s, 1H, imidaz-H), 5.27 (s, 2H, NH_2), 5.09 (s, 2H, Ar–CH_2–O); ^{13}C NMR (100 MHz, DMSO-d_6): δ 162.96, 160.48, 156.38, 150.55, 132.10, 128.70, 125.06, 115.14, 112.88, 112.36, 112.11, 58.11 ppm; MS (ESI): *m/z* (%) = 302.0 ([M + H]$^+$); 343.1 ([MH + CH_3CN]$^+$); HRMS for $C_{16}H_{13}F_2N_3O$: [M+H]$^+$ calculated: 302.10923, found: 302.10995; HPLC (10–90 % MeOH in 0.1 % TFA in 11 min, UPLC): t_r 6.070 min (100 % at 254 nm, 100 % at 280 nm).

5-(4-((2,4,5-Trifluorobenzyl)oxy)phenyl)-1*H*-imidazole-2-amine (14h). Synthesized according to General procedure H. Off-white solid; yield: 86 % (369 mg); ^{1}H NMR (400 MHz, DMSO-d_6): δ 7.74–7.58 (m, 2H, Ar–H), 7.56–7.48 (m, 2H, Ar–H), 6.99–6.92 (m, 2H, Ar–H), 6.86 (s, 1H, imidaz-H), 5.25 (s, 2H, NH_2), 5.08 (s, 2H, Ar–CH_2–O); ^{13}C NMR (100 MHz, DMSO-d_6): δ 157.26, 156.13, 154.90, 150.58, 148.29, 147.59, 145.19, 128.79, 125.05, 121.71, 118.98, 115.18, 106.69, 63.13 ppm; MS (ESI): *m/z* (%) = 319.9 ([M + H]$^+$); 360.9 ([MH + CH_3CN]$^+$); HRMS for $C_{16}H_{12}F_3N_3O$: [M+H]$^+$ calculated: 320.10052, found: 320.09967; HPLC (10–90 % MeOH in 0.1 % TFA in 11 min, UPLC): t_r 6.547 min (100 % at 254 nm, 100 % at 280 nm).

5-(3-((4-Fluorobenzyl)oxy)phenyl)-1*H*-imidazole-2-amine (14i). Synthesized according to General procedure H. Yellow solid; yield: 27 % (41 mg); ^{1}H NMR (400 MHz, DMSO-d_6): δ 10.67 (s, 1H, NH), 7.54–7.48 (m, 2H, Ar–H), 7.25–7.16 (m, 5H, Ar–H), 7.00 (s, 1H, imidaz-H), 6.76–6.70 (m, 1H, Ar–H), 5.38 (s, 2H, NH_2), 5.08 (s, 2H, Ar–CH_2–O); ^{13}C NMR (100 MHz, DMSO-d_6): δ 163.39, 160.97, 158.93, 150.63, 136.23, 133.98, 130.39, 129.80, 116.64, 115.78, 115.57, 112.10, 110.02, 68.75, ppm; MS (ESI): *m/z* (%) = 284.0 ([M + H]$^+$); 325.2 ([MH + CH_3CN]$^+$); HRMS for $C_{16}H_{15}FN_3O$: [M+H]$^+$ calculated: 284.11937, found: 284,11867; HPLC (10–90 % MeOH in 0.1 % TFA in 11 min, UPLC): t_r 6.153 min (98 % at 254 nm, 97 % at 280 nm).

5-(3-((4-(Trifluoromethyl)benzyl)oxy)phenyl)-1*H*-imidazole-2-amine (14j). Synthesized according to General procedure H. Yellow solid; yield: 46 % (88 mg); ^{1}H NMR (400 MHz, DMSO-d_6): δ 7.78–7.68 (m, 4 H, Ar–H), 7.33–7.10 (m, 3H, Ar–H), 7.00 (s, 1H, imidaz-H), 6.79–6.67 (m, 1H, Ar–H), 5.47–5.10 (m, 4H, NH_2, Ar–CH_2–O); ^{13}C NMR (100 MHz, DMSO-d_6): δ 158.74, 150.75, 142.74, 129.83, 128.84, 128.52, 128.39, 126.08, 125.75, 123.38, 116.81, 111.95, 110.02, 109.91, 68.55 ppm; HRMS for $C_{17}H_{15}F_3N_3O$: [M+H]$^+$ calculated: 334.11617, found: 334.11518; HPLC (10–90 % MeOH in 0.1 % TFA in 11 min, UPLC): t_r 6.930 min (94 % at 254 nm, 96 % at 280 nm).

5-(3-((3-(Trifluoromethyl)benzyl)oxy)phenyl)-1*H*-imidazole-2-amine (14k). Synthesized according to General procedure H. Dark-yellow solid; yield: 41 % (44 mg); ^{1}H NMR (400 MHz, DMSO-d_6): δ 7.85–7.77 (m, 2H, Ar–H), 7.74–7.65 (m, 2H, Ar–H), 7.30–7.27 (m, 1H, Ar–H), 7.25–7.16 (m, 2H, Ar–H), 7.04 (s, 1H, imdaz-H), 6.83–6.72 (m, 1H, Ar–H), 5.47 (s, 2H, NH_2), 5.22 (s, 2H, Ar–CH_2–O); ^{13}C NMR (100 MHz, DMSO-d_6): δ 158.77, 150.69, 139.33, 136.40, 132.08, 130.02,

129.86, 129.77, 129.45, 126.04, 124.91, 124.39, 123.33, 116.81, 112.00, 110.04, 68.57 ppm; MS (ESI): *m/z* (%) = 334.1 ($[M + H]^+$); HRMS for $C_{17}H_{14}F_3N_3O$: $[M+H]^+$ calculated: 334.11617, found: 334.11555; HPLC (10–90 % MeOH in 0.1 % TFA in 11 min, UPLC): t_r 6.813 min (95 % at 254 nm, 97 % at 280 nm).

5-(3-((4-(Trifluoromethoxy)benzyl)oxy)phenyl)-1*H*-imidazole-2-amine (14l). Synthesized according to General procedure H. Pale-brown solid; yield: 50 % (49 mg); ^{1}H NMR (400 MHz, DMSO-d_6): δ 7.63–7.58 (m, 2H, Ar–H), 7.43–7.36 (m, 2H, Ar–H), 7.27–7.16 (m, 3H, Ar–H), 7.00 (s, 1H, imidaz-H), 6.77–6.70 (m, 1H, Ar–H), 5.35 (s, 2H, NH_2), 5.14 (s, 2H, Ar–CH_2–O); ^{13}C NMR (100 MHz, DMSO-d_6): δ 158.85, 150.71, 148.27, 137.33, 136.48, 129.94, 129.81, 121.83, 121.51, 119.29, 116.73, 112.01, 109.98, 68.52 ppm; MS (ESI): *m/z* (%) = 350.0 ($[M + H]^+$); HRMS for $C_{17}H_{15}O_2N_3F_3$: $[M+H]^+$ calculated: 350.11109, found: 350.11091; HPLC (10–90 % MeOH in 0.1 % TFA in 11 min, UPLC): t_r 7.173 min (97 % at 254 nm, 99 % at 280 nm).

5-(3-((3-Chlorobenzyl)oxy)phenyl)-1*H*-imidazole-2-amine (14m). Synthesized according to General procedure H. Orange solid; yield: 69 % (172 mg); ^{1}H NMR (400 MHz, DMSO-d_6): δ 10.61 (s, 1H, NH), 7.55–7.50 (m, 1H, Ar–H), 7.44–7.37 (m, 3H, Ar–H), 7.27–7.22 (m, 1H, Ar–H), 7.21–7.16 (m, 2H, Ar–H), 7.01 (s, 1H, imidaz-H), 6.76–6.71 (m, 1H, Ar–H), 5.36 (s, 2H, NH_2), 5.12 (s, 2H, Ar–CH_2–O); ^{13}C NMR (100 MHz, DMSO-d_6): δ 158.78, 150.70, 140.41, 136.46, 133.55, 130.81, 129.82, 128.12, 127.68, 126.58, 116.75, 112.00, 110.01, 68.51 ppm; MS (ESI): *m/z* (%) = 299.7 ($[M + H]^+$); 340.5 ($[MH + CH_3CN]^+$); HRMS for $C_{16}H_{14}ClN_3O$: $[M+H]^+$ calculated: 300.08982, found: 300.08950; HPLC (10–90 % MeOH in 0.1 % TFA in 11 min, UPLC): t_r 6.597 min (99 % at 254 nm, 95 % at 280 nm).

5-(3-((3-Methylbenzyl)oxy)phenyl)-1*H*-imidazole-2-amine (14n). Synthesized according to General procedure H. Pale-brown solid; yield: 84 % (163 mg); ^{1}H NMR (400 MHz, DMSO-d_6): δ 10.42 (s, 1H, NH), 7.29–7,11 (m, 7H, Ar–H), 6.98 (s, 1H, imidaz-H), 6.77–6.68 (m, 1H, Ar–H), 5.27 (s, 2H, NH_2), 5.05 (s, 2H, Ar–CH_2–O), 2.32 (s, 3H, CH_3); ^{13}C NMR (100 MHz, DMSO-d_6): δ 159.07, 150.76, 138.01, 137.69, 129.75, 128.83, 128.77, 128.65, 125.19, 116.53, 111.94, 109.96, 69.48, 21.48 ppm; HRMS for $C_{17}H_{18}N_3O$: $[M+H]^+$ calculated: 280.14444, found: 280.14360; HPLC (10–90 % MeOH in 0.1 % TFA in 11 min, UPLC): t_r 6.620 min (95 % at 254 nm, 95 % at 280 nm).

5-(3-((2,6-Difluorobenzyl)oxy)phenyl)-1*H*-imidazole-2-amine (14o). Synthesized according to General procedure H. Pale-brown solid; yield: 66 % (125 mg); ^{1}H NMR (400 MHz, DMSO-d_6): δ 7.57–7.48 (m, 1H, Ar–H), 7.28–7.15 (m, 5H, Ar–H), 7.02 (s, 1H, imidaz-H), 6.80–6.71 (m, 1H, Ar–H), 5.33 (s, 2H, NH_2), 5.11 (s, 2H, Ar–CH_2–O); ^{13}C NMR (100 MHz, DMSO-d_6): δ 162.97, 160.42, 158.81, 150.76, 136.56, 132.09, 129.86, 116.98, 112.90, 112.37, 112.12, 111.87, 109.86, 57.91 ppm; MS (ESI): *m/z* (%) = 302.2 ($[M + H]^+$); 343.2 ($[MH + CH_3CN]^+$); HRMS for $C_{16}H_{13}F_2N_3O$: $[M+H]^+$ calculated: 302.10995, found: 302.10919; HPLC (10–90 % MeOH in 0.1 % TFA in 11 min, UPLC): t_r 6.173 min (98 % at 254 nm, 99 % at 280 nm).

5-(3-((2,4,5-Trifluorobenzyl)oxy)phenyl)-1*H*-imidazole-2-amine (14p). Synthesized according to General procedure H. White solid; yield: 83 % (210 mg); ^{1}H NMR (400 MHz, DMSO-d_6): δ 7.76–7.58 (m, 2H, Ar–H), 7.28–7.17 (m, 3H, Ar–H), 7.03 (s, 1H, imidaz-H), 6.80–6.72 (m, 1H, Ar–H), 5.36 (s, 2H, NH_2), 5.10 (s, 2H, Ar–CH_2–O); ^{13}C NMR (100 MHz, DMSO-d_6): δ 158.60, 157.36, 154.92, 150.73, 148.28, 147.64, 145.19, 136.50, 129.86, 121.68, 118.93, 116.97, 111.97, 109.88, 106.63, 62.95 ppm; MS (ESI): *m/z* (%) 320.2 ($[M + H]^+$); 361.2 ($[MH + CH_3CN]^+$); HRMS for $C_{16}H_{12}F_3N_3O$: $[M+H]^+$ calculated: 320.10052, found: 320.09968; HPLC (10–90 % MeOH in 0.1 % TFA in 11 min, UPLC): t_r 6.643 min (99 % at 254 nm, 99 % at 280 nm).

5-(3-((4-Chloro-3-(trifluoromethyl)benzyl)oxy)phenyl)-1*H*-imidazole-2-amine (14q). Synthesized according to General procedure H. Yellow solid; yield: 59 % (173 mg); ^{1}H NMR (400 MHz, DMSO-d_6): δ 10.59 (s, 1H, NH), 7.95 (s, 1H, Ar–H), 7.81–7.75 (m, 2H, Ar–H), 7.28–7.16 (m, 3H, Ar–H), 7.01 (s, 1H, imidaz-H), 6.76–6.70 (m, 1H, Ar–H), 5.36–5.15 (m, 4H, NH_2, Ar–CH_2–O); ^{13}C NMR (100 MHz, DMSO-d_6): δ 158.62, 150.73, 138.09, 136.62, 133.58, 132.24, 130.33, 129.86, 127.21, 127.15, 126.91, 124.67, 121.96, 116.90, 111.93, 110.04, 67.90 ppm; MS (ESI): *m/z* (%) = 368.1 ($[M + H]^+$); HRMS for $C_{17}H_{14}ON_3ClF_3$: $[M+H]^+$ calculated: 368.07720, found: 368.007711; HPLC (10–90 % MeOH in 0.1 % TFA in 11 min, UPLC): t_r 7.233 min (97 % at 254 nm, 98 % at 280 nm).

5-(4-Phenethoxyphenyl)-1*H*-imidazole-2-amine (14r). Synthesized according to General procedure H. Dark-yellow solid; yield: 44 % (80 mg); ^{1}H NMR (400 MHz, DMSO-d_6): δ 10.50 (s, 1H, NH), 7.50–7.46 (m, 2H, Ar–H), 7.34–7.29 (m, 4H, Ar–H), 7.25–7.19 (m, 1H, Ar–H), 6.88–6.80 (m, 3H, Ar–H, imidaz-H), 5.28 (s, 2H, NH_2), 4.16 (t, J = 6.9 Hz, 2H, CH_2–O), 3.02 (t, J = 6.9 Hz, 2H, Ar-CH_2); HRMS for $C_{17}H_{18}N_3O$: $[M+H]^+$ calculated: 280.14444, found: 280.14365; HPLC (10–90 % MeOH in 0.1 % TFA in 11 min, UPLC): t_r 6.493 min (95 % at 254 nm, 97 % at 280 nm).

5-(3-Phenethoxyphenyl)-1*H*-imidazole-2-amine (14s). Synthesized according to General procedure H. Yellow solid; yield: 82 % (260 mg); ^{1}H NMR (400 MHz, DMSO-d_6): δ 10.55 (s, 1H, NH), 7.36–7.11 (m, 8H, Ar–H), 6.98 (s, 1H, imidaz-H), 6.77–6.51 (m, 1H, Ar–H), 5.30 (s, 2H, NH_2), 4.17 (t, J = 6.9 Hz, 2H, CH_2–O), 3.04 (t, J = 6.9 Hz, 2H, Ar-CH_2); ^{13}C NMR (100 MHz, DMSO-d_6): δ 159.09, 150.71, 138.96, 136.40, 129.75, 129.45, 128.78, 126.73, 116.34, 111.70, 109.56, 68.43, 35.50. ppm MS (ESI): *m/z* (%) = 279.8 ($[M + H]^+$); HRMS for $C_{17}H_{17}N_3O$: $[M+H]^+$ calculated: 280.14444, found: 280.14412; HPLC (10–90 % MeOH in 0.1 % TFA in 11 min, UPLC): t_r 6.600 min (99 % at 254 nm, 99 % at 280 nm).

5-(3-(4-Fluorophenethoxy)phenyl)-1*H*-imidazole-2-amine (14t). Synthesized according to General procedure H. Off-white solid; yield: 72 % (185 mg); ^{1}H NMR (400 MHz, DMSO-d_6): δ 10.56 (s, 1H, NH), 7.40–7.34 (m, 2H, Ar–H), 7.18–7.09 (m, 5H, Ar–H), 6.99 (s, 1H, imidaz-H), 6.69–6.60 (m, 1H, Ar–H), 5.32 (s, 2H, NH_2), 4.16 (t, J = 6.7 Hz, 2H, CH_2–O), 3.03 (t, J = 6.7 Hz, 2H, Ar-CH_2); ^{13}C NMR (100 MHz, DMSO-d_6): δ 162.61, 160.21, 159.05, 150.73, 136.42, 135.15, 131.27, 129.75, 116.37, 115.54, 115.33, 111.67, 109.58, 68.36, 34.60. ppm; MS (ESI): *m/z* (%) = 297.8 ($[M + H]^+$); HRMS for $C_{17}H_{16}FN_3O$: $[M+H]^+$ calculated: 298.13502, found: 298.13471; HPLC (10–90 % MeOH in 0.1 % TFA in 11 min, UPLC): t_r 6.660 min (99 % at 254 nm, 100 % at 280 nm).

4.3. Molecular docking

Molecular docking calculations were performed with Schrödinger Release 2023–1 (Schrödinger, LLC, New York, NY, USA, 2023). A structural model of the open state of the human H_V1 channel [52,53] was used for the molecular docking calculations of the designed inhibitors. A library of compounds was docked to the binding site of guanidine derivatives, which bind to the voltage-sensing domain of the H_V1 channel from the intracellular side [38]. Prior to docking calculations, protein structure was prepared using Protein Preparation Wizard with the default settings: bond orders were assigned using CCD database, missing hydrogens were added, termini were capped, the missing side chains were modelled with Prime, and het protonation states (pH 7.0 ± 2.0) were modelled with Epik [54]. The receptor grids were calculated for the ligand-binding sites. Ligand structures were prepared using LigPrep module and ionized with Epik at pH = 7.4 using OPLS4 force field. The compounds were then docked using the Glide XP protocol as implemented in Schrödinger Release 2023–1 (Glide, Schrödinger, LLC, New York, NY, USA, 2023).

4.4. Evaluation of inhibitory activities on H_V1, $K_V1.3$ and $Na_V1.5$ channels

Cells for Patch Clamp Recordings. Chinese hamster ovary (CHO) cells were cultured in Dulbecco's modified Eagle's medium (DMEM, Gibco, Thermo Fisher Scientific, Waltham, MA, USA, Cat# 11965084) containing 10 % fetal bovine serum (FBS, Sigma-Aldrich), 2 mM L-

glutamine, 100 μg/mL streptomycin, and 100 U/mL penicillin-g (Sigma-Aldrich, St. Louis, MO, USA) at 37 °C in a 5 % CO_2 and 95 % air humidified atmosphere. Cells were passaged twice per week following a 2–3 min incubation in PBS containing 0.2 g EDTA/L (Invitrogen, Waltham, MA, USA). For the patch-clamp experiments, CHO cells were carefully washed twice with 2 mL of ECS (see below).

Human lymphocytes were obtained from heparinized human peripheral venous blood from healthy volunteers. Mononuclear cells were separated by Ficoll-Hypaque density gradient centrifugation. Collected cells were washed twice with Ca^{2+} and Mg^{2+} free Hank's solution containing 25 mM HEPES buffer (pH 7.4). Cells were cultured in a 5 % CO_2 incubator at 37 °C in 24 well culture plates in RPMI-1640 supplements with 10 % FCS (Hyclone, Logan, Utah, USA), 100 μg/ml penicillin, 100 μg/ml streptomycin and 2 mM L-glutamine at 0.5 × 10^6/ml density for 3–4 days. The culture medium also contained 6 or 8 μg/ml of phytohemagglutinin A (PHA-P, Sigma-Aldrich Kft, Hungary) to increase K^+ channel expression.

CHO cells were transiently transfected using a Lipofectamine 2000 kit (Invitrogen, Carlsbad, CA, USA) according to the manufacturer's protocol with a pQBI25 vector containing the GFP-tagged hH_V1 gene (*hHVCN1*, GenBank accession no. BC007277.1, a kind donation from Kenton Swartz, NIH, Bethesda, MD, USA) or the GFP-tagged $hNa_V1.5$ gene (SCN5A). Transfected cells were washed twice with 2 mL of ECS (see below) and replated onto 35 mm polystyrene cell culture dishes (Cellstar, Greiner Bio-One, Kremsmünster, Austria). GFP-positive transfectants were identified with a Nikon Eclipse TS100 fluorescence microscope (Nikon, Tokyo, Japan) using bandpass filters of 455–495 nm and 515–555 nm for excitation and emission, respectively, and were used for current recordings. In general, ion currents were recorded 24–36 h after transfection.

Electrophysiology. The standard whole-cell patch clamp method[42] was used to record the ion currents. Micropipettes were pulled in four stages using a Flaming Brown automatic pipette puller (Sutter Instruments, San Rafael, CA, USA) from GC 150F-15 borosilicate glass capillaries (Harvard Apparatus Co., Holliston, MA, USA) with a typical tip resistance between 2 and 10 MΩ depending on pipette size and the solutions used. All measurements were performed using Axopatch 200B amplifiers connected to personal computers with Digidata 1550A data acquisition hardware (Molecular Devices Inc., Sunnyvale, CA, USA). Recordings were discarded if a leak at the holding potential was more than 10 % of the peak current at the given test potential. The experiments were conducted at room temperature, which was between 20 and 24 °C.

Solutions. To record H_V1 currents, the extracellular (bath) solution (ECS) contained (in mM) 75 *N*-methyl D-glucamine (NMDG), 180 HEPES, 15 glucose, 3 $MgCl_2$, and 1 EGTA (pH = 7.4 with CsOH), and the intracellular (pipette) solution (ICS) contained (in mM) 75 NMDG, 180 MES, 3 $MgCl_2$, 15 glucose, and 1 EGTA (pH = 6.4 with CsOH). The osmolarities of ECS and ICS were between 302 and 308 mOsm/L and ~295 mOsm/L, respectively. Bath perfusion around the measured cell with different extracellular solutions was achieved using a gravity flow microperfusion system at a rate of 200 μL/min. Excess fluid was removed continuously. Solutions containing the test compounds were made fresh before the experiments in ECS from 10 mM stock solutions stored at −20 °C. Stock solutions were prepared from powder dissolved in anhydrous DMSO (Sigma-Aldrich Hungary). The control solution was ECS with 0.5 % DMSO. ECS with a pH of 6.4 was used as a perfusion test for each cell. The reduction in the current amplitude and the prominent change in the current activation threshold were indicators of both the ion channel and the proper operation of the perfusion system.

For the recording of $K_V1.3$ currents, the ECS contained 145 mM NaCl, 5 mM KCl, 1 mM $MgCl_2$, 2.5 mM $CaCl_2$, 5.5 mM glucose, and 10 mM HEPES, pH 7.35 titrated with NaOH. The ICS in the pipette contained 140 mM kF, 2 mM $MgCl_2$, 1 mM $CaCl_2$, 10 mM HEPES, and 11 mM EGTA, pH 7.22 titrated with KOH.

For the recording of $Na_V1.5$ currents, the ECS contained 145 mM NaCl, 5 mM KCl, 1 mM $MgCl_2$, 2.5 mM $CaCl_2$, 5.5 mM glucose, and 10 mM HEPES, pH 7.35 titrated with NaOH. The ICS in the pipette contained 105 mM CsF, 10 mM NaCl, 10 mM HEPES and 10 mM EGTA, pH 7.2 titrated with CsOH.

Voltage Protocols. The current through hH_V1 was elicited by applying 1.0-s-long voltage ramps or steps to +60 mV from a V_h of −60 mV every 15 s. In the case of large currents local proton depletion may occur potentially changing the driving force and gating of H_V1, therefore drug application was only started after the current amplitude had stabilized. For recording $K_V1.3$ and $Na_V1.5$ currents, 15-ms-long voltage steps to +40 and 0 mV were used, respectively, from a holding potential of −100 mV.

Patch Clamp Data Analysis. The pClamp 10.7 software package (Molecular Devices Inc., Sunnyvale, CA, USA) and GraphPad Prism 8 (GraphPad, CA, USA) were used for data acquisition and analysis. Current recordings were evaluated as follows. First, the traces were filtered (lowpass boxcar, 3 smoothing points), and off-line leak correction was applied for H_V1.

K^+ and Na^+ currents were recorded using on-line P/n leak subtraction.

The inhibitory effect of the compounds at a given concentration was calculated as the remaining current fraction (RCF=I/I_0, where I_0 is the peak current in the absence of the compound, and I is the peak current at equilibrium inhibition at the given concentration of the compound). The data points (average of 3–4 individual recordings) in the dose–response curve were fitted with a two-parameter inhibitor vs. response model using the following formula

$$RCF = \frac{IC_{50}^{n_H}}{IC_{50}^{n_H} + c^{n_H}}$$

where c is the molar concentration of the compound, IC_{50} is the concentration of the compound that inhibits the channel current by 50 %, and n_H is the Hill coefficient. All data are expressed as mean ± SEM.

4.5. In vitro antiproliferative measurements

The antiproliferative activity of the selected compounds was evaluated in the human breast cancer cell line MCF-7 and the human monocytic leukaemia cell line THP-1 using the MTS assay. The assay was performed using the 3-(4,5-dimethylthiazol-2-yl)-5-(3-carboxymethoxyphenyl)-2-(4-sulfophenyl)-2H-tetrazolium (MTS) reagent (Promega, Madison, WI, USA). MCF-7 cells were maintained in DMEM – low glucose (Sigma – Aldrich, St. Louis, MO, USA) and THP-1 in Roswell Park Memorial Institute (RPMI) 1640 medium with HEPES (Sigma-Aldrich, St. Louis, MO, USA). Both culture media contained 10 % fetal bovine serum, 100 U/mL penicillin, 100 μg/mL streptomycin, and 2 mM L-glutamine. RPMI 1640 was additionally supplemented with 1 mM of sodium pyruvate. To perform the assays cells were seeded in 96-well plates at a density of 4000 cells per well for MCF-7 and 15,000 cells per well for THP-1 and incubated for 24 h prior to treatment. The cells were then treated with the test compounds. As negative and positive controls 0.5 % DMSO and 1 μM of PU-H71 were used, respectively. After a 72-h incubation period, 10 μL of CellTiter96 Aqueous One Solution Reagent (Promega, Madison, WI, USA) was added to each well and the cells were incubated for a further 3 h. Absorbance was measured using a Synergy 4 Hybrid microplate reader (BioTek, Winooski, VT, USA). Compounds were tested for inhibitory activity at concentrations ranging from 50 μM to 0.2 μM in two biological replications each performed in a triplicate. Statistical comparison between the compound activity normalised to DMSO in MCF-7 and THP-1 cells was performed using unpaired *t*-test with Welch's correction.

4.6. Determination of thermodynamic solubility

The thermodynamic solubility test was performed using a 50 mM

phosphate buffer (PB) with a pH of 7.4 as the dissolution medium. First, an appropriate amount of the test and control substances were accurately weighed and added to the lower chambers of the Whatman Mini-UniPrep™ vials. Next, 450 μL of the prepared phosphate buffer (pH 7.4) was added to each vial to create an oversaturated suspension. The samples were then vortexed for at least 2 min to ensure thorough mixing. After vortexing, the vials were placed on a shaker and incubated at room temperature (approximately 25 °C) at a speed of 800 rpm for 24 h to reach equilibrium. After incubation, the samples were centrifuged at 25 °C for 10 min at 4000 rpm to facilitate phase separation. The Mini-UniPrep™ syringeless filter devices were then compressed to obtain the filtrates, which were further diluted if necessary. The solubility of each sample was quantified by LC-UV and LC-MS/MS analysis. The Whatman Mini-UniPrepTM Syringeless Filter Device (PTFE filter media with polypropylene housing, pore size 0.45 μM) from Cytiva (Marlborough, MA, USA) was used for the study. The tests were performed by WuXi AppTec (Shanghai, China).

4.7. Determination of plasma protein binding

The assay was performed using an HT dialysis plate (model HTD 96 b) and a dialysis membrane from HT Dialysis LLC (Gales Ferry, CT). Plasma from male CD-1 mice (SPF Biotechnology, Beijing, China) with EDTA-K2 as anticoagulant was used. The plasma was thawed, centrifuged to remove clots and adjusted to pH 7.4. The dialysis membrane strips were hydrated and pre-treated before use. Working solutions of the test and control compounds (warfarin) at 400 μM were prepared by diluting 4 μL of a 10 mM stock solution in 96 μL DMSO, followed by a further dilution to 2 μM using a blank matrix. For the assay, 50 μL of the loading matrix containing test or control compounds was added in triplicate to a sample collection plate and mixed with 50 μL of PBS to obtain a final volume of 100 μL. Stop solution (500 μL) containing tolbutamide and labetalol was added to the T0 samples. The samples were sealed, shaken at 800 rpm for 10 min and stored at 2–8 °C until further processing. The dialysis instrument was set up and 100 μl of loading matrix containing the test or control compound was added to the donor side of each dialysis well and an equal volume of PBS was added to the receiver side. The plate was incubated at 37 °C with 5 % CO_2 and rotated at approximately 100 rpm for 4 h. After dialysis, 50 μL aliquots from both sides were transferred to a 96-well sample collection plate, mixed with an equal volume of the opposite blank matrix or PBS and treated with stop solution. The samples were vortexed, centrifuged and the supernatant was analysed by LC-MS/MS. The blanks were prepared following the same processing steps as the test samples. The percentage of unbound, bound and recovered compounds was calculated using standard equations based on the peak area ratios of the LC-MS/MS analysis. The tests were performed by WuXi AppTec (Shanghai, China).

4.8. Determination of distribution coefficient

The determination of the distribution coefficient (log D) was carried out using 1-octanol and phosphate buffer (PB, pH 7.4) as the partitioning phases. To prepare PB saturated with 1-octanol, 10 mL 1-octanol was mixed with 100 mL 100 mM PB (pH 7.4), shaken vigorously and allowed to stand overnight at room temperature. Similarly, PB-saturated 1-octanol was prepared by mixing 10 mL of 100 mM PB (pH 7.4) with 100 mL of 1-octanol, followed by the same shaking and standing procedure. For the assay, 2 μL of a 10 mM DMSO stock solution of the test compound was aliquoted into duplicate tubes. Then 149 μL PB-saturated 1-octanol and 149 μL 1-octanol-saturated PB were added to the corresponding tubes. The tubes were mixed vigorously for 2 min and shaken for 1 h at 800 rpm at room temperature. They were then centrifuged at 4000 rpm for 5 min at room temperature. Corresponding volumes of the buffer and 1-octanol layers were aliquoted, diluted and analysed by LC-MS/MS without calibration curve. The log D values were calculated from the peak area ratios of the LC-MS/MS analysis. The tests were performed by WuXi AppTec (Shanghai, China).

4.9. Determination of metabolic stability in human and mouse liver microsome

The microsomal stability tests were performed by WuXi AppTec (Shanghai, China) according to predefined protocols [55]. Stock solutions of the test and control compounds (testosterone, propafenone and diclofenac) were prepared at a concentration of 10 mM in DMSO and then diluted to 100 μM with acetonitrile. The test compounds or positive controls were incubated at a final concentration of 1 μM with human or mouse liver microsomes at 37 °C. The final protein concentration in the reaction mixture was 0.5 mg/mL. Prior to the reaction, the plates were pre-incubated at 37 °C for 10 min, followed by the addition of NADPH (β-nicotinamide adenine dinucleotide phosphate) to initiate metabolism. The incubation lasted 60 min at 37 °C. Aliquots (60 μL) were removed after 5, 15, 30, 45 and 60 min and placed in wells containing 180 μL of stop solution. The plates were then sealed, shaken for 10 min and centrifuged at 4000 rpm at 4 °C for 20 min. The supernatant was analysed by LC-MS/MS. The stability of the compounds was expressed as *in vitro* half-life ($t_{1/2}$) and as intrinsic clearance (CL_{int}). The microsomal intrinsic clearance ($CL_{int(mic)}$) was calculated using the following equation: $CL_{int(mic)} = 0.693/t_{1/2}$/mg microsomal protein per mL. *In vivo* intrinsic (hepatic) clearance ($CL_{int(liver)}$) was estimated from liver microsomal data using the following equation and appropriate scaling factors: $CL_{int(liver)} = CL_{int(mic)} \times$ (mg microsomal protein/g liver weight) $\times$ (g liver weight/kg body weight). The scaling factors used were: 45 mg microsomal protein per gram liver tissue and liver weights of 88 g/kg body weight (mouse) or 20 g/kg body weight (human).

4.10. Determination of bi-directional permeability across the Caco-2 cell monolayer

Caco-2 cells were purchased from ATCC and seeded on polycarbonate membranes with a pore size of 0.4 μm in 96-well Corning insert plates at a density of 3.5×10^4 cells/cm^2. The medium was refreshed every 4–5 days until day 21–28 to allow the formation of a confluent cell monolayer. Nadolol was used as a marker for low permeability, metoprolol as a marker for high permeability and digoxin as a positive control for the P-gp substrate. HBSS (Hanks Balanced Salt Solution) with 10.0 mM HEPES (pH 7.4) was used as transport buffer. The test compounds were tested at 2.00 μM in a bidirectional assay in duplicate. Digoxin was tested at 10.0 μM bidirectionally, while nadolol and metoprolol were tested at 2.00 μM in the apical to basolateral (A to B) direction, also in duplicate. The final DMSO concentration was maintained at less than 1.0 %. The plate was incubated at 37 °C in a CO_2 incubator with 5 % CO_2 and saturated humidity for 2 h without shaking. After incubation, all samples were mixed with a stop solution and centrifuged. The concentrations of the test and control compounds in all samples were quantified semi-quantitatively by LC-MS/MS based on the area ratio of analyte to internal standard. Following the transport test, the Lucifer yellow rejection test was performed to assess the integrity of the Caco-2 cell monolayer. Data analysis included calculation of the apparent permeability coefficient (P_{app}) using the following equation: $Papp = (dC_r/dt) \times V_r/(A \times C_0)$, where dC_r/dt is the cumulative concentration of the substance in the receiver chamber over time, V_r is the volume of the solution in the receiver chamber (0.0750 mL on the apical side and 0.250 mL on the basolateral side), A is the surface area of the monolayer (0.143 cm^2) and C_0 is the initial concentration in the donor chamber. The efflux ratio was determined using the following equation: Efflux Ratio $= P_{app}$ (B-A)/P_{app} (A-B). The percentage of solution recovery was calculated as follows: %Solution Recovery $= 100 \times [(V_r \times Cr) + (V_d \times C_d)]/(V_d \times C_0)$, where V_d is the volume in the donor chambers (0.0750 mL on the apical side and 0.250 mL on the basolateral side) and C_d and C_r correspond to the final concentrations of the transported compound in the donor and receiver chambers, respectively. The tests

were performed by WuXi AppTec (Shanghai, China).

4.11. Determination of membrane fluidity

The effect of the compounds on membrane fluidity was evaluated by measuring the fluorescence anisotropy of 4'-(trimethylammonio)-diphenylhexatriene (TMA-DPH, Sigma-Aldrich) by spectrofluorometry, as previously described [47–49]. Briefly, CHO control cells and cells treated with 10 μM of the compounds were labelled with 10 μM TMA-DPH for 10 min at room temperature. Fluorescence intensities were recorded without washing using a Fluorolog-3 spectrofluorometer (Horiba Jobin Yvon, Edison, NJ, United States) with the cuvette holder temperature maintained at 37 °C via a circulating water bath. TMA-DPH was excited at 352 nm and its emission was measured at 430 nm. The fluorescence anisotropy (r) was determined in L-format using the following formula: $r = (I_{VV}\text{-}GI_{VH})/(I_{VV}+2GI_{VH})$, where I_{VV} and I_{VH} represent the vertical and horizontal components of the fluorescence excited by vertically polarized light. The correction factor G, which takes into account the differences in sensitivity of the detection system to vertically and horizontally polarised light, was calculated as follows: $G = I_{HV}/I_{HH}$, where I_{HV} and I_{HH} correspond to the vertical and horizontal components of the fluorescence excited by horizontally polarized light, respectively.

CRediT authorship contribution statement

Martina Piga: Writing – review & editing, Writing – original draft, Visualization, Investigation, Formal analysis. **Geraldo Jorge Domingos:** Writing – review & editing, Investigation. **Adam Feher:** Investigation, Funding acquisition, Formal analysis. **Ferenc Papp:** Supervision, Formal analysis. **Kavya C. Bangera:** Investigation. **Zoltan Varga:** Writing – review & editing, Supervision, Project administration, Investigation, Funding acquisition, Formal analysis. **Florina Zakany:** Writing – review & editing, Investigation, Funding acquisition, Formal analysis. **Tamas Kovacs:** Writing – review & editing, Investigation, Funding acquisition, Formal analysis. **Jaka Dernovšek:** Writing – review & editing, Visualization, Investigation. **Tihomir Tomašič:** Writing – review & editing, Visualization, Investigation, Formal analysis. **Nace Zidar:** Writing – review & editing, Writing – original draft, Visualization, Supervision, Project administration, Investigation, Funding acquisition, Formal analysis.

Declaration of generative AI and AI-assisted technologies in the writing process

During the preparation of this work the author(s) used ChatGPT and Grok 3 in order to revise the grammar and writing style. After using this tool/service, the author(s) reviewed and edited the content as needed and take(s) full responsibility for the content of the publication.

Declaration of competing interest

The authors declare the following financial interests/personal relationships which may be considered as potential competing interests: Nace Zidar reports financial support was provided by Slovenian Research and Innovation Agency. Zoltan Varga, Florina Zakany, Tamas Kovacs, Adam Feher reports financial support was provided by National Research Development and Innovation Office. If there are other authors, they declare that they have no known competing financial interests or personal relationships that could have appeared to influence the work reported in this paper.

Acknowledgements

This work was supported by the Slovenian Research Agency (Grant No. P1-0208), the National Research Development and Innovation Office, Hungary, grants OTKA K132906 (Z.V.), OTKA FK146740 (F.Z.), OTKA FK143400 (T.K.), ÚNKP-23-3-II-DE-10 New National Excellence Program of the Ministry for Culture and Innovation from the source of the National Research, Development and Innovation Fund (A.F.) and PhD Excellence Scholarship from the Count István Tisza Foundation for the University of Debrecen (A.F.). We would like to thank Giulia Sulis, Zala Kulovec, Tina Benčina and Živa Mlakar for their help with chemical synthesis.

Abbreviations

2GBI, 2-guanidinobenzimidazole; CHO, Chinese hamster ovary cells; ClGBI, 5-chloro-2-guanidinobenzimidazole; DCM, dichloromethane; DMAP, 4-dimethylaminopyridine; DMF, *N*,*N*-dimethylformamide; DMSO, dimethyl sulfoxide; DRG, dorsal root ganglion neurons; ECS, extracellular (bath) solution; ESI, electrospray ionization; FBS, fetal bovine serum; HATU, 1-[bis(dimethylamino)methylene]-1*H*-1,2,3-triazolo[4,5-*b*]pyridinium 3-oxide hexafluorophosphate; MCF-7, breast cancer cell line; HIF, H_V1 inhibitor flexible; hH_V1, human voltage-gated proton channel 1; ICS, intracellular (pipette) solution; MTS, 3-(4,5-dimethylthiazol-2-yl)-5-(3-carboxymethoxyphenyl)-2-(4-sulfophenyl)-2*H*-tetrazolium; NADPH, nicotinamide adenine dinucleotide phosphate hydrogen; NOX2, NADPH oxidase 2; ROS, reactive oxygen species; rt, room temperature; TBTU, 1-[bis(dimethylamino)methylene]-1*H*-benzotriazolium 3-oxide tetrafluoroborate; TFA, trifluoroacetic acid; THP-1, human monocytic leukaemia cell line; THF, tetrahydrofuran; VSD, voltage-sensing domain.

Appendix A. Supplementary data

Supplementary data to this article can be found online at https://doi.org/10.1016/j.ejmech.2025.117936.

Data availability

Data will be made available on request.

References

[1] Y. Shen, et al., Role of the voltage-gated proton channel Hv1 in nervous systems, Neurosci. Bull. 39 (7) (2023) 1157–1172.
[2] Q. Zhang, et al., Inhibiting Hv1 channel in peripheral sensory neurons attenuates chronic inflammatory pain and opioid side effects, Cell Res. 32 (5) (2022) 461–476.
[3] T.E. DeCoursey, Voltage-gated proton channels: molecular biology, physiology, and pathophysiology of the H(V) family, Physiol. Rev. 93 (2) (2013) 599–652.
[4] G. Chaves, et al., Voltage-gated proton channels in the tree of life, Biomolecules 13 (7) (2023).
[5] P.V. Lishko, et al., The control of Male fertility by spermatozoan ion channels, Annu. Rev. Physiol. 74 (74) (2012) 453–475.
[6] L.M. Henderson, J.B. Chappell, O.T.G. Jones, The superoxide-generating NADPH oxidase of human neutrophils is electrogenic and associated with an H+ channel, Biochem. J. 246 (2) (1987) 325–329.
[7] T.E. Decoursey, D. Morgan, V.V. Cherny, The voltage dependence of NADPH oxidase reveals why phagocytes need proton channels, Nature 422 (6931) (2003) 531–534.
[8] A. El Chemaly, et al., VSOP/Hv1 proton channels sustain calcium entry, neutrophil migration, and superoxide production by limiting cell depolarization and acidification, J. Exp. Med. 207 (1) (2010) 129–139.
[9] Y. Okochi, Y. Okamura, Regulation of neutrophil functions by Hv1/VSOP voltage-gated proton channels, Int. J. Mol. Sci. 22 (5) (2021) 2620.
[10] T. Lazaridis, Proton paths in models of the Hv1 proton channel, J. Phys. Chem. B (2023).
[11] A.D. Geragotelis, et al., Voltage-dependent structural models of the human Hv1 proton channel from long-timescale molecular dynamics simulations, Proc. Natl. Acad. Sci. U. S. A. 117 (24) (2020) 13490–13498.
[12] A. Chamberlin, et al., Mapping the gating and permeation pathways in the voltage-gated proton channel Hv1, J. Mol. Biol. 427 (1) (2015) 131–145.
[13] C. Gonzalez, et al., Molecular mechanism of voltage sensing in voltage-gated proton channels, J. Gen. Physiol. 141 (3) (2013) 275–285.
[14] S. Cong, et al., Research progress on ion channels and their molecular regulatory mechanisms in the human sperm flagellum, FASEB J. 37 (7) (2023) e23052.

[15] R. Zhao, et al., Role of human Hv1 channels in sperm capacitation and white blood cell respiratory burst established by a designed peptide inhibitor, Proc. Natl. Acad. Sci. U. S. A. 115 (50) (2018) E11847–e11856.
[16] L. Ribeiro-Silva, et al., Voltage-gated proton channel in human glioblastoma multiforme cells, ACS Chem. Neurosci. 7 (7) (2016) 864–869.
[17] E. Hondares, et al., Enhanced activation of an amino-terminally truncated isoform of the voltage-gated proton channel HVCN1 enriched in malignant B cells, Proc. Natl. Acad. Sci. U. S. A. 111 (50) (2014) 18078–18083.
[18] Y. Wang, et al., Clinicopathological and biological significance of human voltage-gated proton channel Hv1 protein overexpression in breast cancer, J. Biol. Chem. 287 (17) (2012) 13877–13888.
[19] Y. Wang, et al., Human voltage-gated proton channel hv1: a new potential biomarker for diagnosis and prognosis of colorectal cancer, PLoS One 8 (8) (2013) e70550.
[20] D.J. Bare, et al., Expression and function of voltage gated proton channels (Hv1) in MDA-MB-231 cells, PLoS One 15 (5) (2020) e0227522.
[21] Y. Wang, et al., Specific expression of the human voltage-gated proton channel Hv1 in highly metastatic breast cancer cells, promotes tumor progression and metastasis, Biochem. Biophys. Res. Commun. 412 (2) (2011) 353–359.
[22] J.J. Alvear-Arias, et al., Role of voltage-gated proton channel (Hv1) in cancer biology, Front. Pharmacol. 14 (2023) 1175702.
[23] L.J. Wu, et al., The voltage-gated proton channel Hv1 enhances brain damage from ischemic stroke, Nat. Neurosci. 15 (4) (2012) 565–573.
[24] E. Boedtkjer, S.F. Pedersen, The acidic tumor microenvironment as a driver of cancer, Annu. Rev. Physiol. 82 (2020) 103–126.
[25] Z. Petho, et al., pH-Channeling in cancer: how pH-Dependence of cation channels shapes cancer pathophysiology, Cancers (Basel) 12 (9) (2020).
[26] M. Piga, et al., Identification of a novel structural class of Hv1 inhibitors by structure-based virtual screening, J. Chem. Inf. Model. 64 (12) (2024) 4850–4862.
[27] A. El Chemaly, et al., Discovery and validation of new Hv1 proton channel inhibitors with onco-therapeutic potential, Biochim. Biophys. Acta Mol. Cell Res. 1870 (3) (2023) 119415.
[28] F. Qiu, et al., *Molecular mechanism of Zn* 2+</sup> *inhibition of a voltage-gated proton channel*, Proc. Natl. Acad. Sci. 113 (40) (2016) E5962–E5971.
[29] G. Chaves, et al., Zinc modulation of proton currents in a new voltage-gated proton channel suggests a mechanism of inhibition, FEBS J. 287 (22) (2020) 4996–5018.
[30] L. Hong, et al., Voltage-sensing domain of voltage-gated proton channel Hv1 shares mechanism of block with pore domains, Neuron 77 (2) (2013) 274–287.
[31] L. Hong, I.H. Kim, F. Tombola, Molecular determinants of Hv1 proton channel inhibition by guanidine derivatives, Proc. Natl. Acad. Sci. U. S. A. 111 (27) (2014) 9971–9976.
[32] C. Zhao, et al., HIFs: new arginine mimic inhibitors of the Hv1 channel with improved VSD-Ligand interactions, J. Gen. Physiol. 153 (9) (2021).
[33] C. Zhao, et al., A novel Hv1 inhibitor reveals a new mechanism of inhibition of a voltage-sensing domain, J. Gen. Physiol. 153 (9) (2021).
[34] T.G. Szanto, et al., 5-Chloro-2-Guanidinobenzimidazole (ClGBI) is a non-selective inhibitor of the human H(V)1 channel, Pharmaceuticals (Basel) 16 (5) (2023).
[35] A. Pupo, C. Gonzalez León, In pursuit of an inhibitory drug for the proton channel, Proc. Natl. Acad. Sci. U. S. A. 111 (27) (2014) 9673–9674.
[36] D.S. Ermolat'ev, E.V.V.d. Eycken, A divergent synthesis of substituted 2-Aminoimidazoles from 2-Aminopyrimidines, J. Org. Chem. (17) (July 26, 2008) 73.
[37] O.P. Hamill, et al., Improved patch-clamp techniques for high-resolution current recording from cells and cell-free membrane patches, Pflügers Archiv 391 (2) (1981) 85–100.
[38] L. Hong, I.H. Kim, F. Tombola, Molecular determinants of Hv1 proton channel inhibition by guanidine derivatives, Proc. Natl. Acad. Sci. USA 111 (27) (2014) 9971–9976.
[39] T.E. DeCoursey, V.V. Cherny, Voltage-activated proton currents in human THP-1 monocytes, J. Membr. Biol. 152 (2) (1996) 131–140.
[40] T. Kovacs, et al., Inhibition of the H(V)1 voltage-gated proton channel compromises the viability of human polarized macrophages in a polarization- and ceramide-dependent manner, Front. Immunol. 15 (2024) 1487578.
[41] M.P. Thomas, et al., Ion channel blockade attenuates aggregated alpha synuclein induction of microglial reactive oxygen species: relevance for the pathogenesis of Parkinson's disease, J. Neurochem. 100 (2) (2007) 503–519.
[42] A. El Chemaly, et al., Hv1 proton channels differentially regulate the pH of neutrophil and macrophage phagosomes by sustaining the production of phagosomal ROS that inhibit the delivery of vacuolar ATPases, J. Leukoc. Biol. 95 (5) (2014) 827–839.
[43] L. Di, et al., Mechanistic insights from comparing intrinsic clearance values between human liver microsomes and hepatocytes to guide drug design, Eur. J. Med. Chem. 57 (2012) 441–448.
[44] K. Sloczynska, et al., Metabolic stability and its role in the discovery of new chemical entities, Acta Pharm. 69 (3) (2019) 345–361.
[45] F. Zakany, et al., Direct and indirect cholesterol effects on membrane proteins with special focus on potassium channels, Biochim. Biophys. Acta Mol. Cell Biol. Lipids 1865 (8) (2020) 158706.
[46] D.J.B. Orts, M. Arcisio-Miranda, Cell glycosaminoglycans content modulates human voltage-gated proton channel (H_V1) gating, FEBS J. 289 (9) (2022) 2593–2612.
[47] Z. Petho, et al., A synthetic flavonoid derivate in the plasma membrane transforms the voltage-clamp fluorometry signal of CiHv1, FEBS J. (2024).
[48] T. Kovacs, et al., Cyclodextrins exert a ligand-like current inhibitory effect on the Kv1.3 ion channel independent of membrane cholesterol extraction, Front. Mol. Biosci. 8 (2021).
[49] F. Zakany, et al., An ω-3, but not an ω-6 polyunsaturated fatty acid decreases membrane dipole potential and stimulates endo-lysosomal escape of penetratin, Front. Cell Dev. Biol. 9 (2021).
[50] G. Batta, et al., Alterations in the properties of the cell membrane due to glycosphingolipid accumulation in a model of Gaucher disease, Sci. Rep. 8 (1) (2018).
[51] B. Cs Szabo, et al., Novel insights into the modulation of the voltage-gated potassium channel KV1.3 activation gating by membrane ceramides, JLR (J. Lipid Res.) 65 (8) (2024) 100596.
[52] A.D. Geragotelis, et al., Voltage-dependent structural models of the human Hv1 proton channel from long-timescale molecular dynamics simulations, Proc. Natl. Acad. Sci. USA 117 (24) (2020) 13490–13498.
[53] K. Takeshita, et al., X-ray crystal structure of voltage-gated proton channel, Nat. Struct. Mol. Biol. 21 (4) (2014), 352-U170.
[54] J.C. Shelley, et al., Epik: a software program for pK a prediction and protonation state generation for drug-like molecules, J. Comput. Aided Mol. Des. 21 (12) (2007) 681–691.
[55] X. Zhang, et al., Design, synthesis, and mechanistic study of 2-piperazineone-bearing peptidomimetics as novel HIV capsid modulators, RSC Med. Chem. 14 (7) (2023) 1272–1295.